University of Yaoundé I

Dynamic of biological molecules and insect pest damages

by

NDJOMATCHOUA THOMAS FRANK

Registration number: 10W1506

Department of Physics,

Faculty of Science,

Postgraduate school of Science, Technology and Geosciences,

This dissertation is submitted for the degree of Doctor of Philosophy (Ph.D.) in

Physics and Applications,

option Mechanics, Materials and Structures

Under the supervision of

Tchawoua Clément

Full Professor

March, 2017

Dedications

I dedicate this thesis to my parents NDJOMATCHOUA Benoit and NGATCHAM YITABEN Hortense Clarisse, my siblings TIAKAM Marthe Irene, NDJOMATCHOUA Emilie Vanessa and NDJOMATCHOUA Kelly Cynthia. I would like also to dedicate this thesis to my uncle TIAKO YITABEN Mathurin and my cousin WEPANDJEU POUTIEU Arnaud.

Acknowledgements

The accomplishment of this thesis would not be possible without the assistance and the help of numerous individuals and institutions.

I would like to acknowledge the Professor Timoléon Crépin KOFANE, the head of Department of Physics and laboratory of Mechanics at the Faculty of Sciences at University of Yaoundé 1 for receiving me in his laboratory.

I thank Professor Clément TCHAWOUA at the University of Yaoundé 1 who directed every aspect related to nonlinear physics of this work. His goodwill toward me since my master thesis beyond purely academic matters is deeply acknowledged. I consider him not only as a supervisor but as a father who is always available to provide guidance and to share experience in any aspects of life.

I would like also the acknowledge Doctor Henri Edouard ZEFACK TONNANG at International Maize and Wheat Improvement Center (CYMMYT) for my initiation to ecological modeling and ecological theory. He has been as a mentor who taught me several scientific knowledge. My vision of the field has been deeply shaped through our interactions. He co-supervised this thesis as the ecological modeler.

I express my deepest gratitude Doctor Bruno Pierre LE RU at Institut de Recherche pour le Développement (IRD) who taught me the entomology of lepidopteran stem borer. He co-supervised this thesis in all biological aspects related to insect pests.

I would like to thank Professor Gerrit HOOGENBOOM at University of Florida (UF) for supervising me during my research visit at UF where I was developing coupling points between maize growth and, insect pest population dynamic in DSSAT. The guidance of his team on computer modeling and simulation of agricultural systems have been very benefiting for me.

The assistance from a multi-disciplinary supervisory team including a non-linear physicist (Professor Clément TCHAWOUA), an entomologist (Doctor Bruno Pierre LE RU), an ecological modeler (Doctor Henri Edouard ZEFACK TONNANG) and, a crop scientist (Professor Gerrit HOOGENBOOM) has been a great privilege. Despite their multiple

occupations, the scientific knowledge and rigor they have provided to me have been very enriching. Please find here the expression of my deep gratitude.

Beside my main supervisor and co-supervisors, I thank the Professor Francois-Marie MOUKAM KAKMENI at the University of Buea for its advice and his scientific help during his postdoctoral research in Nairobi, Kenya.

The assistance and advice from Doctor Sheila VAKHTANG in the handling of FORTRAN modules of DSSAT and Professor Kenneth J. BOOTE for the understanding of plant growth at UF are highly appreciated.

The advice and the initiation of Doctor Pedro Agustinho SANSAO at Universidade Eduardo Mondlane, Professor Jean Michel TCHUENCHE at Centre for Disease Control (CDC) in mathematical epidemiology are greatly acknowledged.

I am also grateful to Professor Volker GRIMM at Helmholtz Center for Environmental Research and Doctor Adrian TOMPKINS at the International Centre for Theoretical Physics for discussions about ecological systems, climate change, phenology and potential perspectives and collaborations related to this thesis.

The constant availability of Doctor Paul Andre CALATAYUD at Institut de Recherche pour le Développement (IRD) to explain the biology and the ecology of African lepidopteran stem borers to me is acknowledged. His patience during the transmission of such knowledge to a physicist was not an easy task.

I also acknowledge Professor Johnnie VAN DEN BERG at North-West University and Doctor George ONGAMO at the University of Nairobi, Doctor Eric SIAW NTIRI and Mrs Nancy KHADIOLY for sharing some knowledge, materials and experimental data used in this study.

I am very grateful for the lab technicians, interns, consultants and students who are team members of the Noctuid Stemborer Borer Biodiversity (NSBB) project at *icipe* for their technical assistance during data collections in the field, measurements, and insect species identification; especially Boaz MUSUYOKA, Anthony KIBE, Julius OBONYO and Gerphas OKUKU.

I also acknowledge Doctor Pascal CAMPAGNE at University of Liverpool and Doctor Christophe PLANTAMP at University Claude Bernard, Lyon 1 which collaborations in the biology and data used in this study yielded articles.

The help of Mrs Margaret OCHANDA, Mrs Lisa OMONDI, Mrs Lilian IGWETA, Mr AOSA and Doctor Robert SKILTON for handling administrative matters for foreigners students at the Capacity Building and Institutional Development (CBID) at the international research institute African Insect Science for Food and Health is appreciated.

My deep gratitude is addressed to CBID in providing travelling grants to make possible the visit of Professor Clément TCHAWOUA in Nairobi in order to facilitate interactions among the supervisory team and an easy track of the evolution of this work.

The help of Mrs Kraus June for solving administrative issues for my trip to UF is also acknowledged.

I would like to acknowledge all the scientists of *icipe* for the knowledge and the skill they provided to me during discussions, posters sessions, seminars and interviews. I am grateful for introductory classes to chemical ecology, geographical information systems, biostatistics and biosystematics organized by CBID and, the science club meeting organized by the *icipe* student association (ISCA) in which I have personally served as the PhD student representative in the executive board.

I am very grateful for the scholarship provided by the Deutsher Akademisher Austauschdienst (DAAD) in the African Regional Postgraduate Programme in Insect Sciences (ARPPIS) at the international research institute African Insect Science for Food and Health - *icipe*.

I acknowledge in advance the scientists who will accept to examine this thesis.

I would like to thank the student community at *icipe* as well as the association of Cameroonians of Nairobi to make fell as at home.

I cannot conclude this section without appreciating the encouragement and the various help from all my friends and fellow comrades that I encountered throughout this thesis.

Grants, fellowships and financial supports

1. Grant of excellence of the Head of State of Cameroon for Higher Degree students, 2011-2012
2. Grant of excellence of the Head of State of Cameroon for Higher Degree students, 2012-2013
3. ICITP student travel grant to attend the Regional Workshop on Climate Application for Food Security, Niamey, Niger. Organized by Centre Régional d'Agro-Hydro-Météorologie (AGRHYMET) and International Center of Theoretical Physics (ICTP), Trieste, Italy, in September 2015.
4. ICIPE travel grant to attend the International Society for Ecological Modelling (ISEM) Global Conference 2016 from 8th to 12th MAY 2016, at Townson university, Baltimore, Maryland state, USA.
5. ICIPE travel grant to attend the training program on the Decision Support System for Agrotechnology Transfer (DSSAT): Assessing crop production, nutrient management, climatic risk and environmental sustainability with simulation models, the University of Georgia, Griffin, Georgia, USA. In May 2015
6. The German Academic Exchange Service (DAAD) grant number 91560064//A1395231 in the African Regional Postgraduate Programme in Insect Sciences (ARPPIS) at the international research institute African Insect Science for Food and Health - *icipe*.
7. Travel grant from icipe/CBID-DAAD to finance my research visit at University of Florida 25 January 2016 - 25 July 2016 (06 months) at Institute for Sustainable Food Systems, Department of Agricultural, and Biological Engineering, University of Florida, USA.
8. The Grant provided by *icipe*, Institut de Recherche pour le Développement (IRD) and the Ministry of Foreign Affairs of Finland sponsorship through the

Climate Change Impacts of Ecosystem Services and Food Security in Eastern Africa (CHIESA) project at *icipe* for the data collected in this study.

List of abbreviations

a.s.l.: above the sea level
BF: Busseola fusca
CA: Cellular automata
CP: Chilo Partellus
CSM: Crop Simulation Model
CT: Cob tunneling
DH: Dead heart
DNLSE: Discrete nonlinear Schrödinger equation
EH: Exit hole
LD: Leaf damage
MT: Microtubule
SC: Sesamia calamistis
ST: Stem tunnelling

APSIM: **A**gricultural **P**roduction **S**ystems s**IM**ulator
CERES: **C**rop-**E**nvironment **RE**source **S**ynthesis
CIMMYT: **C**entro **I**nternacional de **M**ejoramiento de **M**aiz y **T**rigo
DAAD: **D**eutsher **A**kademisher **A**ustausch**D**ienst
DSSAT: **D**ecision **S**upport for **A**gro-technological **T**ransfer
FORTRAN: **FOR**mula **TRAN**slation
IPM: **I**ntegrated **P**est **M**anagement
ICIPE: **I**nternational **C**entre for **I**nsect **P**hysiology and **E**cology
MATLAB: **MAT**rix **LAB**oratory
SOYGRO: **SOY**bean crop **GRO**wth simulation model

Table of contents

Abstract

Alpha helix and microtubules and are two majors biological molecules involved in the majority of biological processes within insect and animals. The present thesis aims to understand some critical issues related to the dynamics of these bio-molecules and insect pest damages.

More specifically, an improvement of the Davydov's model for energy transfer in α-helix protein is proposed. Using hyperbolic cosine potential type to model hydrogen bond potential, we have obtained from the adiabatic approximation, a discrete nonlinear Schrödinger equation with inverse hyperbolic sine nonlinearity. Using the two-dimensional discrete map approach, we have found a linearly stable intrinsic localized mode of the corresponding developed equation. The mobility of the intrinsic localized mode was achieved by moving the local impurity hypothesized as the anomalous band energy. The reactivity of the discrete breather under thermal noise was studied numerically with the Langevin's approach. It was shown that the intrinsic localized mode in the developed model keeps its shape longer under the thermal bath.

Inspired by standard electrophysiological models of microtubules, a discrete nonlinear equation for ionic wave propagation that incorporates a negative nonlinear resistance is presented. The conditions for wave propagation in forbidden band gap are analyzed without and with nonlinear dissipation. The nonlinear response manifold method is used to determine the supratransmission threshold of the case of study without nonlinear dissipation. This threshold is found to be similar to the value obtained by analytical methods. With the dissipation, the monitoring of the accumulated energy is used to estimate the infratransmission threshold. It appears that the value of the supratransmission threshold can be lower than the value of the infratransmission threshold. The system is found to amplify significantly the amplitude of the input signal, thus confirming known experimental results.

The two previously mentioned biopolymers and involves in the survival and the behavior of insect and animals; they can adjust the neurological transmission in the brain while the organisms propagate for searching a place to host them and, they allow the energy transport through muscular contraction. Concerning the particular case of insect pest,

understand and predict the spatial propagation of their damage in the agricultural crop has always been a difficult task. An accurate knowledge on the formation of spatial and temporal patterns during the damage spread; as well as the modeling of damages is particularly relevant for small-scale farmers in order to apply adequately control measures. Thus, one of the main purpose of this study was to understand the spatio-temporal spread of the maize stem borer *Busseola fusca* (Fuller) (Lepidoptera: Noctuidae) in smallholder maize farms as well as to investigate injuriousness and yield losses due to this insect, which is one of the most important insect pests of maize in sub-Saharan Africa.

More explicitly, the analysis carried out allowed the establishment of complementary sampling scheme and analysis that can be applied to investigate the propagation of stem borer damages and extended to other insect pests. This approach requires consideration of all plants point locations, the knowledge on the level of damage and its characterization. Results showed that there was a two-week interval between the occurrence of the peaks of leaf damage and male adult moth abundance. The prior role of leaf damages in the farm infestation by *B. fusca* is revealed, and an estimate of the mean transition time between different damage types is provided. Furthermore, damaged plants exhibited a local spatial autocorrelation within a range of dependence of 0-10 meters; and the spatio-temporal pattern of *B. fusca* damage spread evolves as a spiral around an initial patch of damaged plants. By assuming a neighbor configuration of distribution of damaged plants nearby non-damaged, we showed that the inner plants are likely to become damaged within a time period of a week; thus, *B. fusca* infests farms in a systematic fashion. Overall, these results have useful implications for improving and optimizing existing field sampling methods for insect pest damages. The approaches used in carrying out the analysis further provided a deep understanding helpful to improve integrated pest management (IPM) strategies against stem borers and offer IPM practitioners' the opportunity to design, develop, and implement optimum control methods against *B. fusca*.

Secondly, a precise sampling scheme was applied to study the damage incidence in maize caused by this insect pest in selected small-scale farms in which pest control measures and fertilizer were not been applied. During the crop grow stages and harvest; plant and cob geometrical features were recorded as well as the length of tunnels bored by the insect. It is

demonstrated that cob mass is an adequate variable for understanding yield losses caused by this pest. The ensemble of maize plants with a combination of leaf damages and dead heart was the group with the lowest number of cob at harvest. Although the number of plants damaged characterized by stem tunnel was greater than those with cob tunnel, damages inflicted in ear have the most considerable impact on yield losses. The recorded yield losses ranged from 35.96% to 48.19% for corresponding quantities of 56.85 Kg/ha to 133.48 Kg/ha in term of average cob mass reduction. In general, the cob tunnel and the time of infestation were linearly correlated while cob tunnel length and cob biomass were linked by a cubic nonlinear function. The length of the stem tunnel and the cob mass seems to not follow a precise functional curve. The observed yield losses at harvest of the maize crop suggest that controls measures should be applied continuously throughout the whole growing season.

Thirdly, the spatial and temporal infestations dynamics were simulated using an integrated conceptual framework governed by cellular automata (CA) paradigm. The selection of cells sizes was based on the percolation theory, the creation of CA neighborhood applied fuzzy inference that reposed on the male adult abundance of *B. fusca* whereas, multi-fractal concept and correlation probes were used to compare the model output and collected field data. The study suggested that; instead of conducting systematic sampling within the entire field/farm, it may be adequate to conduct sampling at defined unit capable of easily capturing the spread of infestations. Owing to the fact that the developed model predicted with an accepted level of accuracy the geographical coordinates of the maize plant sequence of contagion week after week; integrated pest management (IPM) specialists could use the outcomes to design and develop efficient and more effective timing strategies to control stem borers in maize farms. For example, targeted and well specify pheromone traps can be placed at specific locations using this study outputs to optimize the reduction of maize pests in the fields.

Finally, we developed a generic method to couple crop growth simulation model and pest population dynamic. The method is designed to incorporate insect pest damages into crop system model (CSM). The widely used CSM called Decision Support System for Agrotechnology Transfer (DSSAT) simulates synergic and systemic interactions between the soil, plant crop, and atmosphere well, but do not generally consider the biotic constraints that

take places within the system. The software DSSAT is moved towards being an agroecological framework via an explicit integration of pest dynamic and damages. The maize and the insect pest lepidopteran stem borer are used as a case of study. In order to model plant-pest interaction, the fuzzy logic approach was used to take into account the effect of the plant maturation in the larvae biomass accumulation. The pest module developed in DSSAT is used to demonstrate how the developing lepidopteran population reduces the above ground biomass and green leaf area index. The simulation results show a gradual increase of yield losses due to stem borer damages and suggest that injury levels are generally underestimated. Furthermore, the model suggested that the plant compensates relatively well the leaf area index lost at the beginning of the growing season. Although the linkage of population models and CSMs increases the complexity of the simulation, a tool to explore biotic constraints within farming systems is provided.

Keywords : discrete Davydov's soliton, hydrogen bond potential, moving impurity, thermal stability, microtubule, electrical amplification, supratransmission, infratransmission, *Busseola fusca*, insect-plant interactions, Smallholder maize farms, Damage dynamic, yields losses, cellular automata, percolation theory, fuzzy sets theory, multifractals, crop dynamics, DSSAT

Résumé

L'hélice alpha et les microtubules et sont deux molécules majeures impliquées dans la majorité des processus biologiques chez les insectes et les animaux. La présente thèse a pour but de comprendre certains aspects critiques liés à la dynamique de ces biomolécules et dommages induits par les insectes dans les champs agricoles.

Plus précisément, une amélioration du modèle de Davydov pour le transfert d'énergie dans la protéine α-hélice est proposée. En utilisant un potentiel te type cosinus hyperbolique pour modéliser l'énergie potentielle de liaison hydrogène, nous avons obtenu à partir de l 'approximation adiabatique une équation de Schrödinger non linéaire discrète avec non linéarité sinus hyperbolique inverse. En utilisant l'approche de carte discrète bidimensionnelle, nous avons trouvé un mode intrinsèque localisé qui est linéairement stable. La mobilité du mode localisé intrinsèque a été obtenue par le déplacement de l'impureté locale considérée comme la bande d'énergie anormale détectée dans les protéines. La réactivité du mode localisé discret subissant l'influence d'un bruit thermique a été étudiée numériquement avec l'approche de Langevin. Il a été montré que le mode localisé intrinsèque dans le modèle propose dans cette étude conserve sa cohérence plus longtemps dans le bain thermique comparativement au model classique de Davydov.

Inspiré par les modèles électrophysiologiques standard des microtubules, une équation non linéaire discrète pour la propagation des ondes ioniques qui intègre une résistance non linéaire négative est présentée. Les conditions de propagation des ondes avec des fréquences dans la bande interdite sont analysées sans et avec dissipation non linéaire. La méthode de la variété de réponse non linéaire est utilisée pour déterminer le seuil de supratransmission du cas d'étude sans dissipation non linéaire. Ce seuil se révèle être similaire à la valeur obtenue par les méthodes analytiques. En considérant la dissipation non linéaire, le suivi de l'énergie accumulée est utilisée pour estimer le seuil d'infratransmission. Il vient que la valeur du seuil de supratransmission peut être inférieure à la valeur du seuil d'infratransmission. Dans le cadre du modèle développé dans cette thèse, le système amplifie significativement l'amplitude du signal d'entrée, confirmant ainsi les résultats expérimentaux connus.

Les deux biopolymères mentionnés précédemment sont impliqués dans la survie et le comportement des insectes et des animaux; ils peuvent ajuster la transmission neurologique dans le cerveau tandis que les organismes se propagent pour chercher un hôte et, ils permettent le transport d'énergie par contraction musculaire. En ce qui concerne le cas particulier de l'insecte nuisible, comprendre et prédire la propagation spatiale de leurs dommages dans la culture agricole a toujours été une tâche difficile. Une connaissance précise de la formation de motifs spatiaux et temporels pendant la propagation des dommages; ainsi que la modélisation de ces dommages, est particulièrement pertinente pour les petits exploitants agricoles afin d'appliquer des mesures de contrôle adéquates. Ainsi, l'un des principaux objectifs de cette étude était de comprendre la propagation spatio-temporelle des dégâts de l'insecte *Busseola fusca* (Fuller) (Lepidoptera: Noctuidae) dans les champs de maïs de petits exploitants, ainsi que l'étude des dommages causés par cet insecte. Cet insecte nuisible est l'un des plus menaçant du maïs en Afrique subsaharienne.

De façon plus explicite, l'analyse réalisée a permis d'établir un schéma d'échantillonnage et une analyse complémentaires qui peuvent être appliqués pour étudier la propagation des dommages causés par le foreur de tige et étendus à d'autres insectes nuisibles. Cette approche nécessite la prise en compte de tous les emplacements des plantes, la connaissance du niveau des dommages et de leur caractérisation. Les résultats ont montré qu'il y avait un intervalle de deux semaines entre l'apparition des pics de lésions foliaires et l'abondance des adultes mâles. Le rôle antérieur des dommages foliaires dans l'infestation de la ferme par *B. fusca* est révélé et une estimation du temps moyen de transition entre différents types de dommages est fournie. De plus, les plantes endommagées présentaient une autocorrélation spatiale locale dans une plage de 0 à 10 mètres; l'évolution spatio-temporel de la propagation des dommages de *B. fusca* évolue comme une spirale autour d'un ensemble initial de plantes endommagées. Nous avons démontré qu'en moyenne, si un ensemble de quatre plantes voisines endommagées repartie autour d'une plante non-endommagées alors les plantes internes sont susceptibles d'être endommagées dans une période de temps d'une semaine. Ainsi, *B. fusca* infeste les fermes de manière systématique. Dans l'ensemble, ces résultats ont des implications utiles pour l'amélioration et l'optimisation des méthodes existantes d'échantillonnage sur le terrain pour les dommages causés par les insectes nuisibles.

Les approches utilisées dans la réalisation de l'analyse ont également permis une compréhension approfondie utile pour améliorer les stratégies de lutte intégrée contre les foreurs de tiges et offrir aux praticiens de ce type the lutte la possibilité de concevoir, de développer et de mettre en œuvre des méthodes de control optimales contre *B. fusca.*

Un schéma d'échantillonnage précis a été appliqué pour étudier l'incidence des dommages causés sur le maïs par ce ravageur dans certaines exploitations de petite taille dans lesquelles des mesures de lutte contre les ravageurs et des engrais n'étaient pas appliquées. Pendant les phases de culture et de récolte; les caractéristiques géométriques de la plante et de l'épi ont été enregistrées ainsi que la longueur des tunnels creusés par l'insecte. Il est démontré que la masse de l'épi est une variable adéquate pour comprendre les pertes de rendement causées par ce parasite. L'ensemble des plants de maïs avec une combinaison d'endommagement des feuilles et de cœur mort était le groupe ayant le plus faible nombre d'épi au moment de la récolte. Bien que le nombre de plantes endommagées par la creusée de tunnel dans la tige ait été plus important que celui de la creusée de tunnel dans l'épi, les dommages infligés à l'épi ont le plus d'impact sur les pertes de rendement. Les pertes de rendement enregistrées varient de 35,96% à 48,19% pour les quantités correspondantes de 56,85 Kg/ha à 133,48 Kg/ha en terme de réduction moyenne de la masse de l'épi. En général, la creusée de tunnel dans l'épi et le temps d'infestation sont été linéairement corrélés tandis que la longueur du tunnel dans l'épi et la biomasse cob sont liées par une fonction non linéaire cubique. La longueur du tunnel dans la tige et la masse de l'épi ne semble pas suivre une courbe fonctionnelle précise. Les pertes de rendement observées à la récolte de la culture de maïs suggèrent que les mesures de contrôle devraient être appliquées en continu tout au long de la saison de croissance.

La dynamique des infestations spatiales et temporelles a été simulée à l'aide d'un cadre conceptuel intégré régi par des automates cellulaires (AC). La sélection de la taille des cellules a été faite sur la base de la théorie de la percolation, l'usage d'inférence floue reposant sur l'abondance adulte mâle de *B. fusca* a été appliquée pour modifier le voisinage de l'AC dans le temps, tandis que le concept de multi-fractale et de corrélation ont été utilisés pour comparer les résultats du modèle et les données collectées dans les champs. L'étude suggère qu'au lieu de procéder à un échantillonnage systématique dans l'ensemble du champ ou de l'exploitation,

il peut être approprié de procéder à un échantillonnage à une unité définie capable de representer facilement la propagation des infestations. En raison du fait que le modèle développé a prédit avec un niveau de précision acceptable les coordonnées de la contamination séquentielle des plantes de maïs semaine après semaine, les spécialistes de la lutte intégrée contre les ravageurs pourraient utiliser les résultats pour concevoir et mettre au point des stratégies efficaces de lutte contre les foreurs de tige dans les exploitations de maïs. Par exemple, des pièges à phéromones peuvent être placés à des endroits spécifiques en utilisant les résultats de cette étude pour optimiser la réduction de ce ravageur du maïs dans les champs.

Enfin, nous avons développé une méthode générique pour coupler le modèle de simulation de la croissance des cultures et la dynamique des populations d'insectes nuisibles. La méthode est conçue pour intégrer les dommages causés par les insectes nuisibles dans le modèle de système de culture (MSC). Le Système de Soutien à la Décision pour le Transfert d'Agrotechnologie (SSDTA) largement utilisé simule les interactions synergiques et systémiques entre le sol, les plantes cultivées et l'atmosphère, mais ne considère généralement pas les contraintes biotiques qui se produisent dans le système. Dans cette thèse, le logiciel SSDTA est orienté vers un cadre agro-écologique via une intégration explicite de la dynamique et des dommages des ravageurs. Le maïs et les lépidoptère foreurs de tige de maïs sont utilisés comme cas d'étude. Afin de modéliser l'interaction plante-parasite, la logique floue a été utilisée pour prendre en compte l'effet de la maturation des plantes dans l'accumulation de la biomasse dans des larves de cet insecte. Le module FORTRAN développé dans SSDTA est utilisé pour démontrer comment la population de lépidoptères en développement réduit la de biomasse du maïs et l'indice de surface des feuilles vertes. Les résultats de la simulation montrent une augmentation progressive des pertes de rendement dues aux dommages causés par les foreurs de tiges et suggèrent que les niveaux de dégâts sont généralement sous-estimés. En outre, le modèle suggère que la plante compense relativement bien l'indice de surface foliaire perdu au début de la saison de croissance. Bien que le couplage des modèles de population et des MSC augmente la complexité de la simulation, un outil pour explorer les contraintes biotiques dans les systèmes d'exploitation est fourni.

Mots-clés : Soliton discrèt de Davydov, potentiel de liaison hydrogène anharmonique, impureté mobile, stabilité thermique, microtubule, amplification électrique, supratransmission, infratransmission, *Busseola fusca*, interaction insectes-plante, fermes de maïs de petits exploitants, dommages dynamiques, pertes de rendement, automates cellulaires, théorie de la percolation, théorie des ensembles flous , multifractales, dynamique des cultures, DSSAT

List of tables

List of figures

General introduction

The Understanding of transport and propagation mechanisms has always been a paramount of science in general and physics in particular. Many technologic and scientific progress have been made by mastering the transport of energy in various systems such as semi-conductors [1], magnetic recording [2], or optical fibers [3]. The understanding of propagation process is also of a particular interest for nano-biological and ecological systems. Numerous biological phenomena require energy propagation; for instance, nervous influx transport [4], sodium-calcium pump [5], DNA replication [6], muscular contraction [7,8], and protein folding [9]. One of the focuses of the present study is on wave's propagation in alpha-helical protein and microtubules. The energy transport and transformation in bio-molecular systems is vital for living organism moving in their ecosystem; this is the reason why the damage spread propagation of insect pest in maize farm and forecast their induced crop yield losses will be one of the main focuses of this study.

In alpha-helical proteins, the transport of energy is principally initiated by the Adenosine Triphosphate (ATP) hydrolysis, which energy generated is carried along the protein chain. In the 70's, Aleksandr Sergeevich Davydov suggested a model for energy transport in biological in this biological molecule [10]. The mechanism has been applied in alpha-helical protein molecules which is ubiquitous in cells of living organisms of insects and animals [11]. In spite of the simplicity of this model compared to the real structure of a protein, it is able to provide a good qualitative description of the dynamic of this biopolymer. One of the main challenges of prediction of this model is the shorter lifetime of the excitation during energy transfer along the protein at the biological temperature [12]. This thesis aims to address this problem.

The microtubule (MT) is an interesting biopolymer involved in the electrical activities of cells [13]. Its potential implication in neurodegenerative disease makes them more interesting [14,15]. This biological complex system interacts with surrounding mediums and organizes depending on a supply of energy and its transformation. Various roles of MT in cellular and sub-cellular electrical signals have been demonstrated in development, physiology, regeneration, and pathology [16]. Therefore, the interest is growing in performing well-designed measurements and explaining the limited amount of reliable experimental results. Since the pioneering study work of Priel and Tuszyński [17], numerous nonlinear and

dynamical models have been suggested to mimic the electrical behaviour of MT [17–22]. Among the existing studies, none have been able to imitate electrical signal amplification and modulation due to calcium ions observed in experiments involving MT [23]. In this thesis, we attempted to develop a model to fill this knowledge gap.

These two biopolymers and involves in the survival and the behaviour of insect and animals [7,8]; they can adjust the neurological transmission to the brain while the insect propagate in order to search for host and, they allow the energy transport through muscle [24]. Concerning the particular case of insect pest, understand and predict the spatial propagation of their damage in the agricultural crop has always been a difficult task [25,26]. An accurate knowledge on the formation of spatial and temporal patterns during the damage spread is particularly relevant for small-scale farmers in order to apply adequately control measures. During several decades, physicists have used interesting methods such as percolation theory, cellular automata, fractals and fuzzy logic. To illustrate, percolation theory have been used in various physical circumstances such as the turbulent regimes of lines of electromagnetically forced vortices [27], high-mobility of electron system [28], the dynamic of site-diluted Josephson-Junction arrays [29], metal-insulator transition in GaS systems [30], charge transfer between superconductors [31], propagation of solitons in nonlinear optical fiber with a randomly distributed refractive index [32] and wave train propagation in a spatial predator-prey system [33]. Cellular automata has been suggested as a concept to study soliton's dynamics [34–37], to replicate the behaviour of reaction-diffusions systems [38,39], to study the infectious diseases [40], to model seismic elastodynamic [41], to simulate elastoplastic wave propagation [42], to model statistical mechanics of lattice gas, non equilibrium process [43], to simulate complex system such as fluid flows, fracture processes, road traffic models and pattern formation [44], and, to model networks of interacting sub-micrometer magnetic dots used to perform logic operations and to propagate information [45]. Fuzzy logic has been used to control chaotic systems [46,47] and to model noise in biological systems [48]. Fractals have been used as a mean to characterize the geometric complexity of chaotic attractors [49,50]. Although these concepts have been extensively used, they are yet to be adapted in an agroecological framework. This study aims to bridge and apply these

concepts in a practical case of insect named lepidopteran stem borer which is a major pest of maize crop in Africa [51]. The damages propagation will be simulated using these methods.

The ability of simulate yield losses due to insect pest and diseases in general and stem borer in particular is of a paramount importance. It can assist in mimicking in real-time the yield losses due to the pest in contrary to the purely empirical approaches which are limited to the specific conditions at which the data were collected [52]. Crop simulation models are emergent powerful tools to forecast yield gaps, to foresee the agricultural production and to analyze the effect of climate change [53]. Scientist are currently attempting to move toward an integration of a new set of functions different from their primary tasks such as the estimate yield losses due to pest and diseases [54]. One of the main challenges faced while coupling pest and crop is a "two-way" approach whereby the pest variable drive the crop model and vice versa [53]. The existing crop simulation models are still poorly efficient in this "two-way" approach" [55–59]. We will focus on the software Decision Support System for Agrotechnology Transfer (DSSAT) which is a broadly used modelling tool that comprises CSMs for over forty-two crops [57] and, it integrates CERES-Maize which is a simulation model for maize growth and development [60]. A conceptual approach based on fuzzy logic in order to couple pest and crop with a particular case of study of the lepidopteran maize stem borer, maize crop and the crop simulation model CERES-maize is proposed.

The choice of this thesis topic was deliberate and two-fold. First of all, models for the dynamic of wave biopolymer in the insect and animal are developed studied. Secondly, spatial and temporal model are developed and applied to comprehend and to predict spatial features of the patterns generated by an insect in the agricultural crop. Finally, a pest-crop coupling method is suggested.

The first part of this thesis is devoted to the Davydov's model. In this part, protein structure and function are briefly presented as well as the generalities on the model of Davydov and the problem related to this model. A modification of the original model is suggested. In addition, the methods used to construct discrete soliton, to study their stability, and to consider the effect of a biological temperature are presented.

In second part, the main focus is on will be the study of the electrical wave transmission and amplification in microtubule. First of all, the structure and the function of this bio-molecule is described. The existing models are reviewed and, the improvement intended in this study is presented. The electrical wave amplification by a microtubule excited by periodic waves is studied and the potential biological implications of obtained results are discussed.

In thirt part, the description of the spatial pattern generated by the insect pest called *Busseola fusca* while propagating in the maize farm are analyzed in order to assess the existence of simple law/rules of damage propagations with time. The potential yield losses due this insect pest using empirical data are done. The obtained results are discussed and pest managements actions are suggested.

In fourth part, a model that can mimic the spatial and temporal dispersion of the leaf damage in smallholder maize fields caused by *B. fusca* is developed. The model is based on a hybrid approach comprising of percolation, fuzzy logic, cellular automata, and multifractals. The spatial threshold for assessing the spread pattern of *B. fusca* infestation is estimated and, we tried to understand how rules governing the changes could lead to spatial patterns obtained during the subsequent of infestation of plants by the pest.

In fifth part, a generic approach for coupling pest and crop with stem borers and maize in order to simulate the potential yield losses due to insect pests is suggested. The process to included the pest module in DSSAT is described and, some results of simulations are shown as illustration.

Finally, a general conclusion summarizing the main finding and the futures directions are provided.

Chapter I: Literature review

I-1 Introduction

This chapter present a brief overview on the physical systems and physical phenomena studied in this thesis. It is organized as follows: section I-2 deals with the overview on Davydov's solitons, section I-3 is devoted to the overview of electrical waves in microtubules, in section I-4, the insect pest is briefly described, in section I-5 and insight on the modelling approaches for the insect pest damages spread are presented, in section I-6 generalities on coupling the pest dynamics and the crop growth simulations are provided. Finally, the last section conclude this chapter.

I-2 Overview on Davydov's soliton

I-2-1 Generalities on proteins

Proteins have been an intense object of study in the community of biologist. They are functional agents of cells and represent a considerable part of biological molecules. proteins are involved in a wide number of the fundamental process where they play a key role in structural and dynamical aspects of cells [7]. Proteins play a role in the growth of cell, muscular contraction; digestives enzymes, an antibody of the immunity system, hemoglobin and majority of hormones are proteins [7]. Chromosomes which transmits all hereditary characteristics under the form of genes are made of nucleic acids and proteins [7]. In other words, proteins are involved in the functioning of all living organisms [8].

Proteins are linear polymers of an amino acid linked by covalent peptide bonds. Proteins present in a living organism are formed by a set of twenty different amino acids. Each amino acids (Figure 1 (a)) has a carboxylic group $-COO^-$ and amine group NH^{+3}; both of them are linked with an atom of carbon named α linked with a lateral chain R characterizing the amino acid. For instance, Glycine (Gly), the lateral R is an atom of hydrogen, for Alanine (Ala), the lateral chain is the group $-CH_3$ etc. The complete sequence of amino acid residuals formed during the chemical reaction described in Figure 1(b) characterize each protein and determine its function; this sequence is the primary structure of the protein. A rotation around the link C-N (angle ϕ) and C-C (angle ψ) (Figure 1(c)) can generate a secondary structure called α -

helix stabilized by hydrogen bond (Figure 1(d)). Although the protein is able to organize spatially in more complex tri-dimensional structures, this chapter will focus on α -helix only.

In the vibratory point of view, the proteins are complex. These macromolecules have a high number of degrees of freedom implying a dense vibratory spectrum which is not fully understood nowadays because the interpretation of infrared measurements with the aims of identification of eigenmodes is difficult. Although each of the modes is a potential canal for energy storage, some appear to play a prominent role compared to others. In any proteins, it is always found a group CO-NH centered around the peptide link. This group has a set of noticeable vibratory characteristics called <<*amid*>> vibration which privileged modes because of their present along the whole structure. Their name and values are reported in **Table 1**. The transport of the vibrational energy is made via interactions with neighbours, for instances the C=O of the next neighbour. These couplings allow the delocalization of the vibrations. By combining effect of dispersion due to the lateral coupling and the nonlinearity Davydov predicted the emergence of soliton in proteins [10].

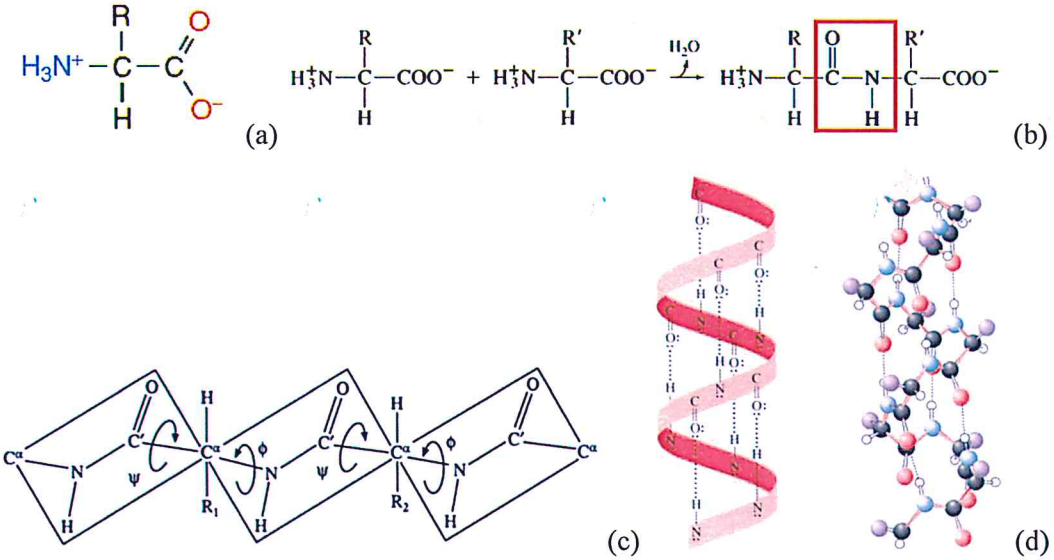

Figure 1: (a) General structure of an amino acid, amino group (in blue), a carboxyl group (red) and R the lateral group linked to the alpha-carbon. (b) The chemical reaction of two amino acids, the peptide linkage is highlighted in red. (c) Rotation angle (ϕ-ψ) around the peptide group. (d) The structure of alpha-helix; on the left , evidence of the helicoidal shape, on the

right, real shape with carbon (in black), oxygen (in red), nitrogen (in blue) and the lateral group (in purple) [7,8].

Mode	Link	Intensity in (eV)
amide-I	C=O stretching	$\simeq$ 0.1984
amide-II	N-H torsion + C-N stretching	$\simeq$ 0.1934
amide-III	N-H torsion	$\simeq$ 0.1637
amide IV to VII	Group CONH vibration outside the plan	$\simeq$ 0.0992
amide-A and amide-B	Resonance between N-H stretching and amide- II	Between 0.3719 and 0.4091

Table 1: Principal vibratory modes of a protein.

I-2-2 The mechanism of Davydov's

In 1973, a Soviet physicist Alexander Sergueïevitch Davydov suggested a mechanism based on the concept of soliton to model energy transfer in proteins [10]. He exploited the regularity of the structure of the α-helix, and; showed that a simplified model of this molecule can localize an energy under a form of a stable pulse soliton. This author illustrated that the amide-I vibratory energy associated to C=O stretching is present in each peptide group H-N-C=O along the alpha helix protein chain that carries the energy released by ATP hydrolysis under the form of a solitary wave. The nonlinear coupling between exciton (amide-I vibration) and acoustic phonon due to deformation of amino acids chain allows self-trapping of energy as soliton [11]. Experimental evidence of Davydov's soliton in acetanilide polymer has been done [61,62].

The mechanism suggested by Davydov start from adenosine triphosphate (ATP) hydrolysis. This chemical reaction produces approximately two quanta $\hbar\omega$ of the mode C=O. Thus, this vibration is a candidate for the storage of the energy hydrolysis of ATP. Moreover, the oxygen of the C=O is engaged in hydrogen bond contributing to the stability of the helix. Then, it seems realistic to think that the deformation of the helix (phonon modes) are coupled with C=O vibration which contributes to the distorting locally the helix. This distortion tends to slightly modify the frequency of vibration of excited C=O which stops to be resonant with the other C=O in the neighbourhood. This reduces the energy transfer rate toward C=O links and, maintain the ATP hydrolysis under a localized form. This progressive process of excitation

produces a stable nonlinear excitation called «*soliton*», and solution of the nonlinear Schrödinger equation derived from the usage of the Davydov's Hamiltonian [11].

I-2-3 Formulation of the Davydov's model

Let consider an infinite one-dimensional chain of hydrogen-bonded peptide group sequence (···*H*–*N*–*C*=*O*···*H*–*N*–*C*=*O*···*H*–*N*–*C*=*O*···), (*H*–*N*–*C*=*O*) are peptide groups and (···) represents the hydrogen bond. Each peptide group has a mass *m*. The excitation energy of each C=O bond is characterized by an energy ε_0=1666 Cm^{-1} [63]. Collective excitations are modelled by the quantum state vector [64]: $|\psi(t)\rangle = \sum_n a_n(t) B_n^+ |0\rangle$, with the normalization condition $\langle\psi(t)|\psi(t)\rangle = \sum_n |a_n(t)|^2 = 1$. The ket $|0\rangle$ stands for the ground state. The Function $|\psi\rangle$ satisfies the time-dependent Schrödinger equation:

$$i\hbar \frac{\partial |\psi\rangle}{\partial t} = \hat{H} |\psi\rangle. \tag{1}$$

The Davydov's Hamiltonian of the system is [64]:

$$\hat{H} = T + U + \sum_n \left[\varepsilon_0 B_n^+ B_n - J\left(B_{n+1}^+ B_n + B_n^+ B_{n+1}\right)\right] + \sum_n \chi\left(u_{n+1} - u_n\right) B_n^+ B_n, \tag{2}$$

where $B_n^+ \left(B_n\right)$ is the creation (annihilation) operator for amide I vibration excitation at n^{th} peptide group. The variable u_n is the displacement at n^{th} amino acid from its equilibrium position. J is the nearest neighbouring dipole-dipole interaction of amide I quanta. χ is the strength of the interaction between the exciton and the lattice distortion at site n. The Hamiltonian of lattice vibration is given by the relation:

$$T + U = \sum_n \left[\frac{p_n^2}{2m} + V(r_n) \right]. \tag{3}$$

where T is the kinetic and U the generalized hydrogen bond potential energies of the displacement of peptide groups from their equilibrium positions. The variable p_n is the

impulsion of the n^{th} group, $r_n = u_{n+1} - u_n$ and m is the mass of a lattice unit. The Hamilton's equations are:

$$i\hbar \frac{da_n}{dt} = (\varepsilon_0 + T + U)a_n - J(a_{n+1} + a_{n-1}) + \chi(u_{n+1} - u_n)a_n, \tag{4}$$

$$m\frac{d^2u_n}{dt^2} = V'(u_{n-1} - u_n) - V'(u_n - u_{n+1}) + \chi\left(|a_n|^2 - |a_{n-1}|^2\right), \tag{5}$$

where, $i^2 = -1$ and $\hbar = \frac{h}{2\pi}$, h is the Planck's constant. V can be a linear or a nonlinear potential. The prime in the exponent of V denotes the differentiation of the function V with respect to its argument. The gauge transform:

$$a_n \to a_n \exp\left[-\frac{i}{\hbar}(\varepsilon_0 - 2J + T + U)t\right] \tag{6}$$

modifies equation (4) into:

$$i\hbar \frac{da_n}{dt} = \chi(u_{n+1} - u_n)a_n - J(a_{n+1} - 2a_n + a_{n-1}), \tag{7}$$

The biological parameters of the model calculated in the reference [65] are: m= 5.7 10^{-25} **Kg**, J = 1.55 10^{-10} **pJ**, and χ = 34 **pN**. The potential V in linear approximation gives the elastic coupling constant K = (39 - 58.5) **N/m**. Upon defining the new dimensionless time variable $\tau = \frac{J}{\hbar}t$ and the dimensionless quantities $\phi_n = \frac{\chi}{\sqrt{JK}}a_n$, $\beta_n = \frac{\chi}{J}u_n$, the expressions (7) and (5) respectively became:

$$i\frac{d\phi_n}{d\tau} = (\beta_{n+1} - \beta_n)\phi_n - (\phi_{n+1} - 2\phi_n + \phi_{n-1}), \tag{8}$$

$$\Lambda\frac{d^2\beta_n}{d\tau^2} = V_1'(\beta_{n-1} - \beta_n) - V_1'(\beta_n - \beta_{n+1}) + |\phi_n|^2 - |\phi_{n-1}|^2, \tag{9}$$

where $\Lambda = J^2m/\hbar^2K$ takes numerical values between 0.021 and 0.032.

I-2-4 Problem statement

Some challenges related to the Davydov's model exist. For example, the bound states (exciton-phonon) was proposed to travel with subsonic velocity [65]. In addition, the lifetime of the soliton is very short at a biological temperature [12].

The issue related to the velocity has been substantially addressed by the correction of the linear hydrogen bond potential which links peptides. For instance, the cubic nonlinear potential was used to represent the energy of hydrogen bond that links peptide groups [66–68]. The major contribution of such modification was the possibility of introducing supersonic soliton velocity in continuum approximation for the soliton.

Pérez and Theodorakopoulos were among the first scientists to study the coupled Davydov's equations with nonlinear hydrogen bond potential under its fully discrete form [69]. They applied the full Lennard-Jones potential for modeling the hydrogen bond potential energy. After giving an arbitrary amplitude at specific sites for the waves, they assessed the stability during a collision between exciton and lattice distortion propagation. Recently, an intrinsic localized mode of nonlinear discrete saturable Schrödinger equation for modeling exciton dynamic of the Davydov's model was estimated [70]. The saturable nonlinearity arose from a higher order of exciton-phonon coupling. The first question that motivated this study is: what are the options to construct a discrete breather fitted for the Davydov's model with nonlinear hydrogen bond?

In proteins, amide-I vibration energy is not unique [71]. The N-H stretch energy has been found in α-helical molecules [72,73]. Furthermore, the anomalous band energy (ABE) very close to the amide-I energy was detected [63]. This energy was described as free exciton that is not affected by the nonlinear interaction with the phonon system [63]. The original Davydov's model takes only amide-I into account. However, the energetic impurity mode could modify the nonlinear dynamic of electronic excitations interacting with phonon in molecular chains. Such inhomogeneity is capable of triggering reflection, trapping and influencing the wave transmission [74,75]. This can also generate a dipole like excitation with spatiotemporal influence on the lattice [76]. Considering ABE as an impurity in the

Davydov's model, the second question to investigate in this study is: what can be the impact of free moving energy along the protein?

Numerical studies showed that Davydov's solitons are inhibited at physiological temperature [77–79]. Furthermore, it has been demonstrated that there is a critical velocity whereby the soliton is thermally unstable [80]. A soliton of the classical Davydov's model is more stable for values of exciton-phonon coupling parameter higher than experimental estimates [81]. A rigorous physical proof of the obtained results in this previously mentioned study has been done using multi-quanta states for deriving the relationship between the effective phonon-exciton coupling and temperature [82]. In reference [83], the authors demonstrated that the disorder in the sequence of amino acid masses has an influence on the thermal stability of Davydov's soliton. It was further proved that taking into account multi-quata amide-I vibrational states, reconsidering the usual formulation of the coupling between the acoustic amide-I and modifying the coherent states were possible ways for obtaining long living Davydov's solition at a biological temperature [84]. Using the Lindblad's formulation for Davydov-Scott monomer [85], it was showed that the high anharmonicity of hydrogen bond could regulate the specific heat of monomer in the biological thermal bath [86]. Discrete breathers submitted to stochastic noise have been reported to be stabilized and localized by hyperbolic cosine potential type in Hamiltonian lattices [87]. Therefore, the third preoccupation of the present study was: can thermal instability problem in the Davydov's model be tackled by a nonlinear hydrogen bond potential under the form of hyperbolic cosine function?

I-3 Overview on electrical waves in microtubules

I-3-1 Generalities on microtubules

Microtubules, the largest of the cytoskeletal elements, are hollow tubes about 25 nm in diameter, each composed of a ring of 13 protein proto-filaments (see Figure 2). Globular proteins consisting of dimers of α- and β-*tubulin* subunits polymerize to form the 13 protofilaments. The protofilaments are arrayed side by side around a central core, giving the

microtubule its characteristic tube shape [7]. In many cells, microtubules form from nucleation centers near the center of the cell and radiate toward the periphery. They are in a constant state of flux, continually polymerizing and depolymerizing [8]. The average half-life of a microtubule ranges from as long as 10 minutes in a non-dividing animal cell to as short as 20 seconds in a dividing animal cell. The ends of the microtubule are designated as plus (+) (away from the nucleation center) or minus (–) (toward the nucleation center) (see Figure 2) [7,8]. Along with facilitating cellular movement, microtubules organize the cytoplasm and are responsible for moving materials within the cell itself [88–90].

The endogenous electrical field can be generated in MTs; it plays a significant role in directing the transport of molecules and electrons [91]. The biological importance of MTs for electrical conduction and amplification in neurons include the following attributes: intracellular information processing, regulation of synaptic inputs, modulation of neural firing, regulation of developmental plasticity and mediation during transport of electrical signals [16]. In addition, the temporary presence of calcium ions on MTs could play a significant role in regulating the activity of dynein motors [20]. It is reported that the mechanical vibrations of MTs can be affected by electrical fields [92] and electrical pulses are able to re-organize the spatial disposition of MTs [93]. Disruption of cancer cell replication is possible by applying alternating electric field which affects mitosis spindle [94]; thus, electrical activities of MTs are very important in fighting some diseases.

Furthermore, MTs are involved in the facilitation of the electrical signal processing in neurons [95,96]. Neurological disorder and neurodegenerative diseases have been reported to be linked with serious cytoskeleton malfunctions [15]. Therefore, using MT-stabilizing-agents and MT-protective-agents are promising candidates for the treatment of neurodegenerative diseases, axonal transport failure and mitochondrial impairment [97–101]. Also, stimulation of neurons by the magnetic field is capable of attenuating motor signs of neurodegenerative diseases [102]. This effect could be explained by the neuroinflammatory response affected by the field [103], or the potentiation of neurite outgrowth in affected neurons [104]. Nevertheless, the exact physical mechanism underlying this effect is not completely understood [15].

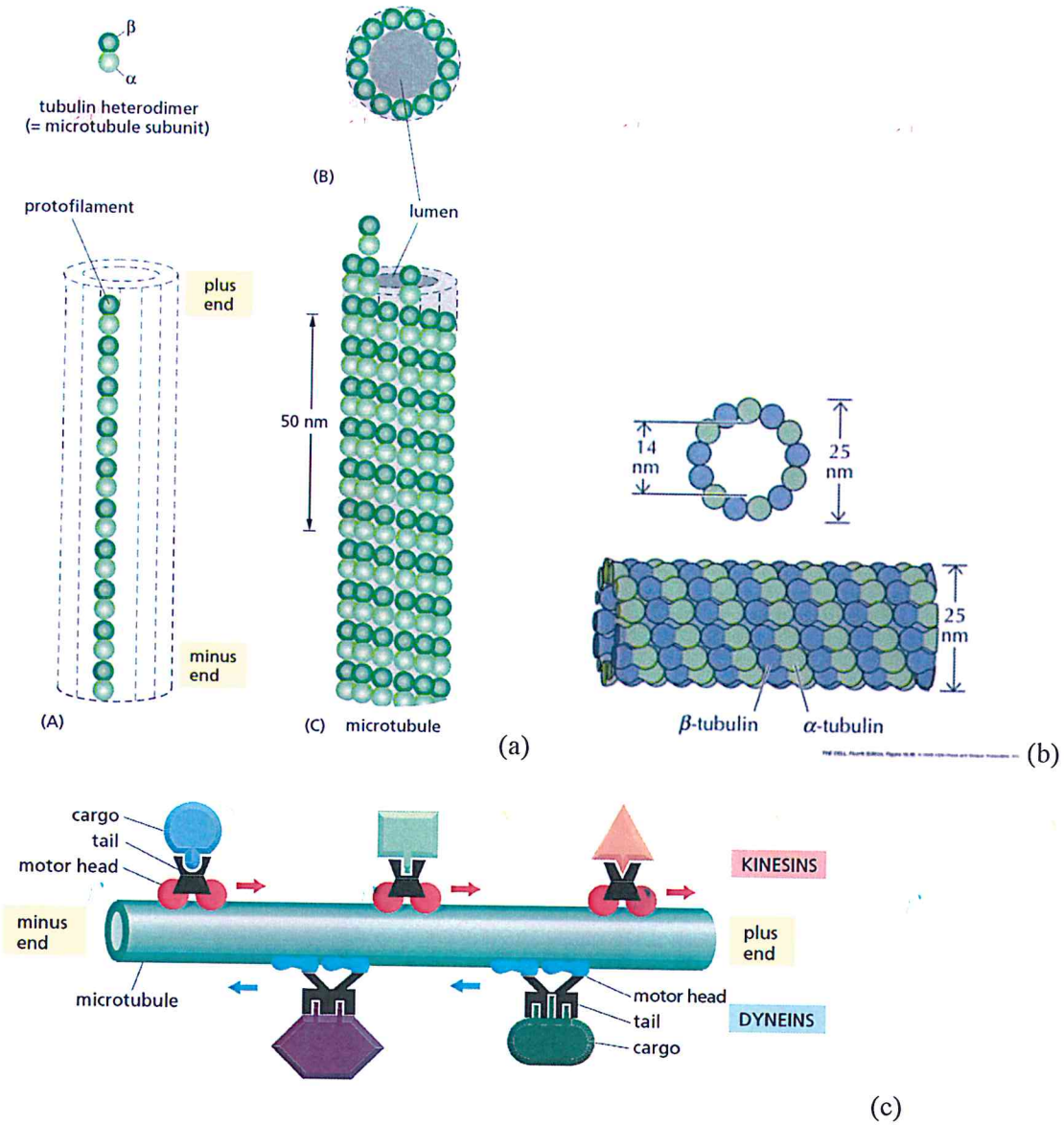

Figure 2: Representation of the structure of a Microtubules (MT). (a) illustration of the hollow and cylindrical shape of a MT, (b) the size of a MT (c) illustration of a cellular organelles transport [7,8]

I-3-2 Models mimicking the electrical properties of microtubules

MTs are also nanoscale biological systems, which play an important role in the electrical activities of cells. They are often modeled using electrical transmission line [13]. Models of the propagation of ionic waves in MTs that incorporated a nonlinear capacitance have been suggested [17,18,20]. The authors used anti-kink excitations to explain some of the known properties of MTs [105]. It has been suggested that the nanopores (NPs) of MTs could play a significant role in the transfer of ionic wave [19]. Inspired by this study [19], an electrical MTs model with a negative nonlinear conductance was proposed [21]. Furthermore, taking into account the oscillating tubulin tails (TTs) of MT dimmers and the linear conductance, Sekulic et al [22] suggested another model for the propagation of the electrical wave in MTs. In [21,22], the possibility of obtaining pulse solutions in MTs was investigated. It thus appeared that TTs and NPs could play a relevant role on self-focusing of the propagation of ionic wave in MTs [21,22]. The findings of [21,22] were corroborated by the experimental results reporting MT as an electrical signal amplifier [105].

I-3-3 Problem statement

Ionic current flow from cations through nano pores of MT was studied by Feedman et al. [106], their results displayed in two dimensions a nonlinear current-voltage curve which could be fitted by a cubic nonlinear function. The evidence of the existence of an electrical amplification property in MTs was provided by Priel et al. [105]. Through an experiment MT was isolated and electrical signals were infused to one end and received from the other end, meaning that this biological pipe (MT) is capable of transmitting signals [105]. Within the same experiment, it was observed that the output voltage pulse revealed a significant reduction in amplitude compared to the input voltage [105]. Thus MTs act both as transmitter and modulator of electrical signals; the later propriety offers them the name of biopolymer transistor. Identical experience with the addition of calcium ion demonstrated a considerable increase of energy transfer by MT [23]. It was also noted that an increase of ions concentration stimulates the reduction of the dissipative property of MT [23]. The authors concluded that the electrodynamical property of MTs could be modulated by the presence of

calcium ion. Unfortunately, majority of models found in the literature to mimic the electrical properties of MTs did not capture these important biological features of the system [17–22].

Infratransmission and supratransmission are among the existing phenomena observed during the propagation of the wave in nonlinear media [107–110]. In a linear system, it is well known that periodical excitation with a frequency within the allowed band propagates through a lattice [111]. In contrary, out of the allowed band, the wave is evanescent [111]. However, Geniet and Leon [107] demonstrated that in the nonlinear system a lattice driven at one of its extreme end by a periodical excitation could transport an energy event if its frequency lies inside the forbidden band gap. This property is due to the fact that in a nonlinear system, there is a certain value of the threshold for the driving amplitude, which can allow the propagation of a plane wave along the lattice with a frequency inside the forbidden frequency band gap [107]. The phenomenon is termed nonlinear supratransmission [107]. In opposition to supratransmission, there is a nonlinear infratransmission, for representing a phenomenon that usually takes place in nonlinear systems with linear dissipation [108–110]. In this context, the lattice becomes non-transmitting above a certain value of the amplitude threshold for the driving with a frequency inside the forbidden band gap [107–109]. The nonlinear supratransmision is a generic phenomenon in nonlinear systems. It has been investigated in different physic systems; coupled mechanical oscillators; optical wave guide arrays, Fermi-Pasta-Ulam (FPU) and in discrete electrical line with nonlinear capacitors [110,112–117]. The transmission of gap soliton has been proven to be also possible in electrical line by adding a noise in the driving source [118], by a frontal collision between waves [119] and via modulational instability [120]. Furthermore, another concept called the nonlinear response manifold (NLRM) [121] has revealed critical transmission amplitude in a nonlinear system driven by a time-periodical excitation [122,123]. Below or above the amplitude threshold predicted by the NLRM, the transmission can be strong or low [122]. Although these phenomena could probably explain why an exited MT from one of its extremity can conduct the electrical current and at which condition the electrical wave propagation is possible, they are yet to be investigated in electrical models mimicking the electrical behaviour of MTs [17–22].

I-4 Overview on stem borers and maize crop

I-4-1 Generalities

The relation between ecological processes (such as individual dispersal, habitat selection, and spatial damage distribution pattern) is of primary importance in ecology and in agro-ecological systems, to allow efficient control measures against insect pests [25,26]. Yield losses in crops are a consequence of the spatial and temporal dispersal of the insect pests [124–128]. Therefore, for decades, spatial and temporal dispersion information about these harmful organisms has gained great relevance for plant protection specialists and agricultural entomologists [129–147].

Maize (*Zea mays* L.) is the most important staple food in sub-Saharan Africa, particularly in East Africa [148,149]. However, biotic (stem borers, gray leaf spot, maize streak virus) and abiotic (drought, low soil fertility) factors constrain maize production [150]. Lepidopteran stem borers are considered to be the most damaging insect pests of maize in Africa [151]. In East Africa, the noctuid *Busseola fusca* (Fuller) is the most damaging in the high potential yield areas, which include the highland tropics and moist transitional zones [152,153]. Kenya is among the Sub-Saharan countries of Africa with a higher consumption rate of maize per person [154]. Cropping of this staple food in Kenya is significantly constrained by insect pests such as lepidopteran stem borers [152,155]. In high potential areas of Kenya, yield losses of maize due to stem borer infestations are estimated at between 12% to 50% of the total production, as a result of leaf feeding, dead heart, stem tunnelling, direct damage to grain, and secondary infection by stalk [51,155,156].

Assessment of yield losses in maize by stem borers is usually done by collecting data such as the mass of plant stem, cob or grains [157,158]. The relevance of the knowledge gained from the data depends on the resources available for sampling and, the accuracy needed for the purposes of assessment [52,158]. After obtaining different degrees of reduction of masses of maize grain, the yield losses can be assessed by comparing the features of un-attacked and attacked plants [52,158].

The injuriousness of *B. fusca* has been assessed by several authors since decades [159–170]. These studies emphasized that the destruction of the growing part of the plant (dead heart), the number of larvae per plant, stem tunnelling, ear damages and positions of the attack on the stem are major factors affecting yield losses.

Estimating the link between pest damages and yields losses at field scale by empirical models can be useful to predict and manage the pest [158,171–173]. Most of the relationships between the damage level caused by *B. fusca* and the yield are decreasing functions [160,163,170,174]. In addition to regression analysis, the estimate of overall percentage of yield losses can be useful to policy makers and farmers for a better perception of the incidence of pest damages [52,152,161,173,175–180].

I-4-2 The insect *Busseola fusca*

Adults emerge from pupae in the late afternoon and early in the evening and are active at night. During the day, they rest on plants and plant debris and are seldom seen unless disturbed, they fly briefly. Usually, the night of emergence the females release a pheromone to attract males and then mates [167,181–183]. The female lays several hundred of eggs in a batch of 30-100 inserted between the sheath and the stem [184]. Larvae hatch after one week and disperse over neighbouring plants by using silk strands [184]. After passing through five larvae instars in 30-45 days, eating leaves and stems, they pupate in tunnels inside the plant, often after first excavating emergence windows to facilitate the exit of adult moths [151]. Adults emerge 10-20 days after pupation. The life cycle is completed in 7-8 weeks. At the end of the rainy season, if the environmental conditions are unfavourable, larvae of the last generation enter into a facultative diapause in maize stubble. They pupate a few months later, just before the start of the following rainy season [151].

I-4-3 The damages

The severity of damages on maize plants varies greatly among ecological zones and season but also depending on crop growth age, a number of larvae feeding on the plant, environmental conditions , and agronomic practices. *B. fusca* at the early larval stage cause foliar damage during plant whorl stage [184]. During this stage, larvae feed by scraping off

the epidermal and parenchyma cells on one side of the leaf. Young larvae may also feed on the leaves of the intact whorl, which gives an array of small holes when unfolded. This damage is called leaf damage (LD). Stem tunnelling (ST) is caused by old larvae that bore into the stem. The destruction of the meristematic tissues causes death heart (DH) damage, which may cause the total death of maize. Stem tunnelling destroys the central pith and constructive tissues causing a reduction in nutrient uptake with interruption of grain filling [185]. Furthermore, stem borer may cause exit holes (EH) damage at the periphery of the stem. Those holes facilitate exits of adult moths but may create avenues for pathogens [184]. Damages caused by stem borers at the larval stage are ultimately stunting plant growth and plant death (D) [186] (see illustrations in Figure 3). The severity level is precisely the span of attack area on the leaves, the number of LD, the length of each tunnel, the number of DH, the number of death plants and the number of EH.

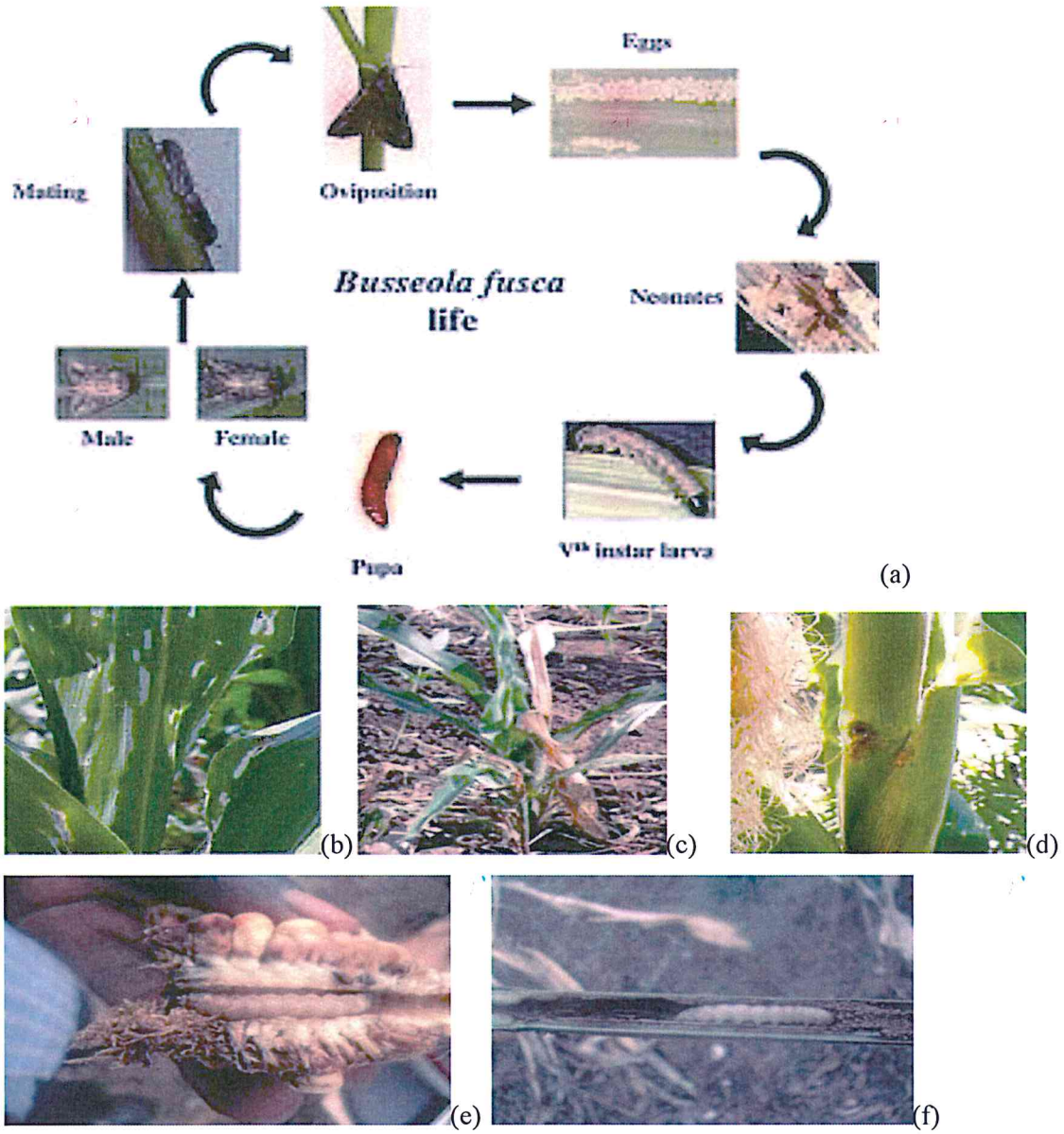

Figure 3: The life cycle of *B. fusca* [187]. Photo of different type of damages inflicted by the insect: (b) leaf damages, (c) dead heart, (d) exit hole, (e) cob tunnelling and (f) stem tunnelling (Photo (b)-(f) have been taken by Frank T. Ndjomatchoua in the field).

I-4-4 Problem statement

Several methodologies are usually employed to describe spatial and temporal pattern distribution of insect pest damages. The most commonly used approaches are the following: tracking evolution of the centroid of infestation distribution [133,134,188], analyzing the spatial autocorrelation of infestation [135,136,189,190], carrying out the spatial analysis by distance indices [137–139,191–195], conducting Markovian chains analysis [140], deploying geostatistical tools [141,143,146,188,196], usage of spatial mapping [144,147,197–199] and cluster analysis [145]. With these approaches, conclusions are only made on the type of spatial and temporal pattern which plant pests could adopt while colonizing/damaging cultivated areas. It has also be found that the spatial patterns generated by insects are random with either aggregated or regular structures [26,200]. Although some of the mentioned methodologies for spatial analysis were applied to various types of insect pests and crops [129–147,189,190,192,194–198,201], no studies have investigated the spatio-temporal damage patterns of lepidopteran stem borer using experimental data from smallholder maize farms.

Research on Lepidopteran stem borer pests, have been carried out in Sub-Saharan Africa since decades [155,184,187]. Although the biology and ecology of lepidopteran stem borers have been extensively studied during decades [155,184,187], available spatial information is related only to the regional distribution, agro-climatic preference and phylogeography over wide scales [151,153,184,202–207]. In particular, there are no downscaled studies obtained from smallholder maize farms to assess spatiotemporal infestation dynamic of *B. fusca*. Understanding the spatial and temporal dynamic of damages spread constitutes the basic information necessary for future development of appropriate pest management strategies. Most studies oriented towards smallholder farm scale focused on the density and rate of infestation at field level by selecting at random few plants per field and looking at the within-plant insect distribution, without any precise damage characterization and insect distribution inside the field [208–211]. Such sampling approach presents a considerable bias and cannot help to adequately understand/capture the spatial and temporal dynamic of infestation of an insect pest.

Whilst yield losses estimate are keys information used to manage stem borers, the estimate of yield losses in existing studies is ambiguous; on one hand, it seems to be overestimated in the other hand, the methods and techniques for the estimations are either not clear or unknown [155,184,187,212]. Links between the pest damages and the yield were established but their extrapolation is difficult because the studies are conducted by artificial infestations, on insecticide-protected fields or the data collected focuses on few samples randomly selected in the field [159–170]. Additionally, rigorous selection of plant physical traits used to study damage incidence and, associating ear mass to different damage types have not been done. Although African farmers perception of the impact of lepidopteran stem borers is still high [213–215], it is noticed that the values of yield losses due to *B. fusca* currently reported in literature are not updated [155,184,187,212].

I-5 Overview on modelling damage spread of insect pests

I-5-1 Generalities

Considerable research efforts have been made in studying insect pest population dynamics to better understand, predict and manage these pests on agriculture crops [216]. Because empirical approaches ignore the dynamics of crop–pest interactions and are limited to the specific conditions at which the data were collected, it has become valuable and important to employ advanced and robust predictive methods [54,217,218]. Therefore, ecological models have gained great relevance as tools for assisting in managing agricultural insect pests in the following areas: intercropping and trap cropping [219], resistance to pesticide [220] and *Bt*-transgenic crops [221,222], spatial distribution of host plants [223], infestation outbreaks [224,225], biological control strategies [226–228] and in integrated pest management dissemination programs [229,230]. Thus, the open problem of prediction of stem borer in maize farm gave us an excellent opportunities to develop new ecological modelling methods based on theories already applied in other context in physics.

Leaf damage was considered as the main parameter in this study since neonates begin to feed 7-8 days following the night when eggs were laid on the plant [167].Other damage types (exit hole, death heart, and plant death), which appear much later in a random fashion on

the plant and could not be directly connected to oviposition and flight dynamics of the pest at the adult stage were not considered during model development. In addition, it was reported that the impacts made by lepidopteran stem borers on young maize plants have the most significant effect on yield losses [155,231]. The current study focuses on the spatial and temporal propagation of leaf damage infestation, which is simulated using a combination of percolation theory, fuzzy logic, and multi-fractal methods integrated into a conceptual framework governed by cellular automata. In the following section, a brief background of each concept is described.

To survive, herbivore insect pest should spread to avoid unsuitable host conditions or overcrowding; however, the temporal and spatial dispersal of damages of insect pests in the agricultural landscape is complex and difficult to forecast [25,26]. In this context, a cellular automata (CA) method can mimic the dynamic of spatial infestation via a set of contagion rules coupled with an explicitly spatial approach. This technique has been applied to numerous type of insect pests and agro-ecological systems [232–239]; this led us to choose CA as the approach to simulate damages spread of *B. fusca* in maize farms. The percolation theory has been used for predicting infestation threshold in a framework of spatial epidemiology [240–244]; this theory has been adapted here for a proper estimate of the optimal cell size of CA for an improvement of computing speed during simulations. The fuzzy set theory can be used in a CA to incorporate a factor influencing the damaging process in models; especially when the exact link between the factor and the damages are imprecise or not well formulated mathematically [245–249]. This method will be used here to change dynamically the size of the CA neighbourhood and to integrate the effect of density of flying adult *B. fuca*. The multifractal dimension is a method that has been applied to characterize spatial pattern resulting from insect pest infestations in a landscape [250]; this method has been adapted here to assess the CA precision during the spatial and temporal simulation of *B. fusca* damage spread.

I-5-2 A brief background of each concept used in this section

The word Percolation is used to describe a phenomenon that is characterized by the formation of random and isolated patches of elements that can merge over time and space to generate of a giant cluster [251–255]. Such phenomenon is usually linked to the sluggish movement of liquid through a porous medium, with applications to the physical sciences [251–255]. Percolation theory has been used to predict the threshold distance of separation between different sites of contamination during propagation of fungi on substrates and soils [241,243,244], and to forecast the critical threshold of plague density during spatial infestation [242].

Cellular automata (CA) are spatially and temporally discrete systems characterized by local interactions and synchronous dynamical evolution [256–259]. This method was introduced in the 1950s by John von Neumann and Stanislaw Ulam to model self-replicating systems [260,261]. Typical CA consists of five main elements: (i) a grid of cells, (ii) cell states, (iii) neighbourhood, (iv) transition rules that determine how a cell change from one state to another, and (v) time step. During simulations, an individual cell is viewed in a given state.

This technique has been used particularly within an ecological framework for the following purposes: on the study of plant spatial ecology [262–265], modelling the dispersal of phytopathogenic fungi [232], mimicking the spatial propagation of insect pest infesting oak trees [233], measuring the spatial heterogeneity of damages caused by insects [237,266], estimating long-range dispersal of the insect pests and their damages in complex landscapes [234,235], assessing ecological risk due to insect pest population density on genetically modified crops [236] and natural disturbance of insects in forest ecosystems [237–239].

Although CA are alternative to partial differential equations [267], their basic features have to be extended to gain more accuracy in the ecological modelling framework [268]. To replicate natural phenomena propagation with a good precision, CA performance can be improved by coupling with Fuzzy logic inference system [245–249,269,270].

Fuzzy logic was firstly developed by [271] to model uncertain and imprecise knowledge [245]. It is a useful approach to model systems that cannot be very well

formalized mathematically. Fuzzy logic is used to represent the degree of accuracy also called truth level that is scaled between a probability threshold of 0 and 1. The fuzzy model works as follows: (i) identification of the input and output variables, (ii) construction of an appropriate membership function (iii) formulation of appropriate linguistic rules linking the output and the input variables [245,272]. Fuzzy logic has been applied to improve the performance of several ecological CA models. To illustrate, the impact of wind intensity on the spreading of insect vector causing citrus death [245], the suitability level of spatial grid points for invasive crayfish establishment [246], the susceptibility level of trees to insects attack [247], the concentration level of the chemical substances favouring the algal blooms spread [248], and the influence of habitat suitability on grasshopper occurrence and dispersal [249].

The term fractal is used for self-similarity that appears in an object under varying degrees of magnification [273]. Unlike a natural object with a dimension 1, 2, 3, a fractal object possesses a non-integer dimension [273]. However, fractal dimension only gives a global geometrical description without any indication of how constituents of the object are distributed spatially. This is why the application of multi-fractal is most often preferred than fractal analysis. An object is said to be multi-fractal if it has more than one fractal dimension [273].

Multi-fractal methodology is usually employed for measuring spatial repartition of living organisms [274–277]; it can also be used to provide proper characterization of patterns distribution resulting from disturbance of living organisms in complex landscapes [250,278]. Some of the most used multifractal dimensions are the following: information dimension (D_i), which gives the degree of repartition of elements inside a surface and the correlation dimension (D_C) that provides the degree of localization of elements by measuring the level of clustering [279,280].

I-5-3 Problem statement

Although several integrated pest management strategies have been developed for lepidopteran stem borers, the spatial and temporal spread of damages of these pests are yet to be properly accounted for [281–286]. No studies have so far attempted to build a model for

predicting the spatio-temporal damage patterns of lepidopteran stem borers applicable to smallholders maize farms in Africa.

A major challenge encountered while simulating spatial and temporal process with cellular automata (CA) is the computing speed and memory allocation. A choice of a higher spatial resolution is ideal but can be constrained by memory space available in a computer while in contrast a larger cell size could not give a good result because of the non-consideration of small-scale aspects thus, the proper selection of cell size of CA is a serious dilemma [240,287–292]. Trial and error approach has been developed to select the size of CA cell in a model simulating the spatial and temporal interaction of predators and preys [293]. Although spatial patterns generated by agricultural insect pest are scale-depended [294,295], it is noticed that the choice of the spatial resolution or unit cell size used to implement CA simulations of spread of insect pest infestation in agro-ecological systems is yet to be done [232,233,235,237,239,245–248,263–266,268,269]. In this study, a procedure to select a threshold scale is suggested. Since it is possible to predict invasive spread and infestation from a percolation threshold [241–244], this theory is adapted here to estimate the optimal cell size (not too small and not too large) of the CA to simulate *B. fusca* infestations.

The choice of the neighbourhood type is crucial for a CA model because the spatial pattern obtained is sensitive to its configuration [288–290]. The challenge is the choice of the appropriate configuration or how to make it dynamic. Solutions to this problem have been suggested in CA models developed for land use modelling by considering a dynamic neighbourhood configuration representing variable interactions among spatially distributed localities [296,297], and in computer science in order to increase computational speed via dynamical change of links between cells [298]. It is noticed that the neighbourhood used in CA ecological model for insect pest infestation in agro-ecological CA models is considered as fixed [232,233,235,237,239,245–248,263–266,268,269]. Although fuzzy set theory has been used to represent a parameter influencing the pest infestation spread in fuzzy-CA with fixed neighbourhood configuration and cell sizes [245–249,269,270], this theory is adapted here to make the neighbourhood configuration dynamic during infestation spread. It is done by inferring number of adults of *B. fusca* males to obtain fuzzy propagation index which

determining the type of neighbourhood of the CA with time. The spatial distribution estimate of the infested plants was done with the multi-fractal concept.

The accuracy of ecological CA simulation is sometimes evaluated quantitatively by the use of mean absolute error and root mean square error comparing the states of observed and predicted cells [245,299] or using confusion matrix and kappa index [300]. The present study adapts to multifractal concept initially developed to characterize the spatial distribution of spatial point data in a map in order to evaluate the precision of the developed CA model in this study. In clear, the multifractal dimension is used here for characterizing the spatial distribution of infested CA cells and measuring the precision of the CA model.

I-6 Overview on coupling insect pest dynamic and crop simulation models

I-6-1 Generalities

The majority of tropical countries and the sub-Saharan region, in particular, have an increasing population and consumption which imply a rising demand for food production while yield gaps due to biotic stresses remain a major problem [301]. Despite the existence of crop protection methods, the global yield losses induced by pests, also called bio-aggressors (weeds, insects, pathogens, etc.) remains a significant threat to the potential agricultural production [302]. The study of pest-crop interactions is therefore of a paramount importance for integrated pest management and sustainable agriculture [54,218]. In this particular context, preventing simultaneously crop yield losses and lower quality of food production via an efficient linkage between the forecast of plant growth dynamic and the prediction of pests and diseases impact is crucial. This can assist in mimicking in real-time the yield losses due to the pest in contrary to the purely empirical approaches which are limited to the specific conditions at which the data were collected [54,218].

Numerous authors developed dynamical models for specific insect pests and crops such as cereal leaf beetle [303], alfalfa weevil [304], cotton bollworm [305], oak leaf roller

[306], onion maggot [307], rice leaf folder [308], moth of olive orchards [309] and drosophila of berry fruits [310]. Moreover, a general mathematical modelling framework to study pest-plant interactions has been suggested [311,312]. These studies mostly used temperature as the only external driving variables for the pest, the crop, and the pest-crop interaction; however, crop simulation models (CSMs) are advanced tools using a system approach which integrate knowledge about soil, climate, crops, and management in order to understand, predict, manage and control agricultural production [53]. They are emergent powerful tools to forecast yield gaps, to foresee the agricultural production and to analyze the effect of climate change [53]. The scientific community is currently deploying significant efforts to take into consideration yield losses due to pest and diseases in CSMs [54]; to illustrate, some of the existing CSMs such as SOYGRO [56], CERES-rice [59], RICEPEST [313], DSSAT [57], InfoCrop [55], and APSIM-wheat [58] attempted to design a module able to predict the pest-crop dynamic and forecast potential reduction of the crop yield. These CSMs linked the pest and the crop with a linear/nonlinear functional plant response to a certain population level of the pest attacking different parts of the plant [55–59,313]. We will suggest a generic approach coupling pest and crop with stem borers and maize as a particular example.

I-6-2 A brief presentation of DSSAT

The decision support system for agrotechnology transfer (DSSAT) simulates growth, development, and yield of a crop [57]. The DSSAT-CSM is made up of a set of inter-linked modules coded in FORmula TRANslation (FORTRAN) programming language [57] (see also Figure 4). The latest version of this software with a personal license is available online upon a request to the development team (http://dssat.net/). This software has several CSMs including the CERES-Maize which focuses on the simulation of the basic growth process and phenological development of maize plants [60]. The subroutines, the functions and the link between states variables used to simulate the phenological development and the growth process is described in detail in references [57,60]. The model contains numerous differential equations representing the dynamic of soil water change, nitrogen variation, phosphorous dynamic, leaf area index and dry mass accumulation in plants that takes place under the

cropping system over time [57,60]. Here we just mention the equation modified during simulations which is the rate of change in total crop dry matter (W) in g/m^2 is described as:

$$\frac{dW}{dt} = W^* - S_L - S_S - S_R, \quad W^* = E^*(P_g - R_m) \tag{10}$$

Where today's new growth (W) is a function of photosynthesis (P_g), maintenance respiration (R_m) and the conversion efficiency (E), t is the time in days, S_L, S_S and S_R are the leaf senescence, stem senescence, and root senescence respectively. To be able to run the program for a particular experiment, a minimum data set is required for model development and testing. DSSAT needs a specific set of data such as weather data (daily maximum and minimum temperatures, precipitation, solar radiation, etc.), soil data (color, drainage, nitrogen, etc.), crop management data (crop, cultivar, planting date, row and plant spacing, etc.), just to name a few [57]. Once the data files are ready, primary modules (weather, management, soil, soil-plant-atmosphere, CROPGRO plant template and plant modules) and sub-routines are called by the main program to perform each step of processing in order to generate daily and seasonal outputs [57].

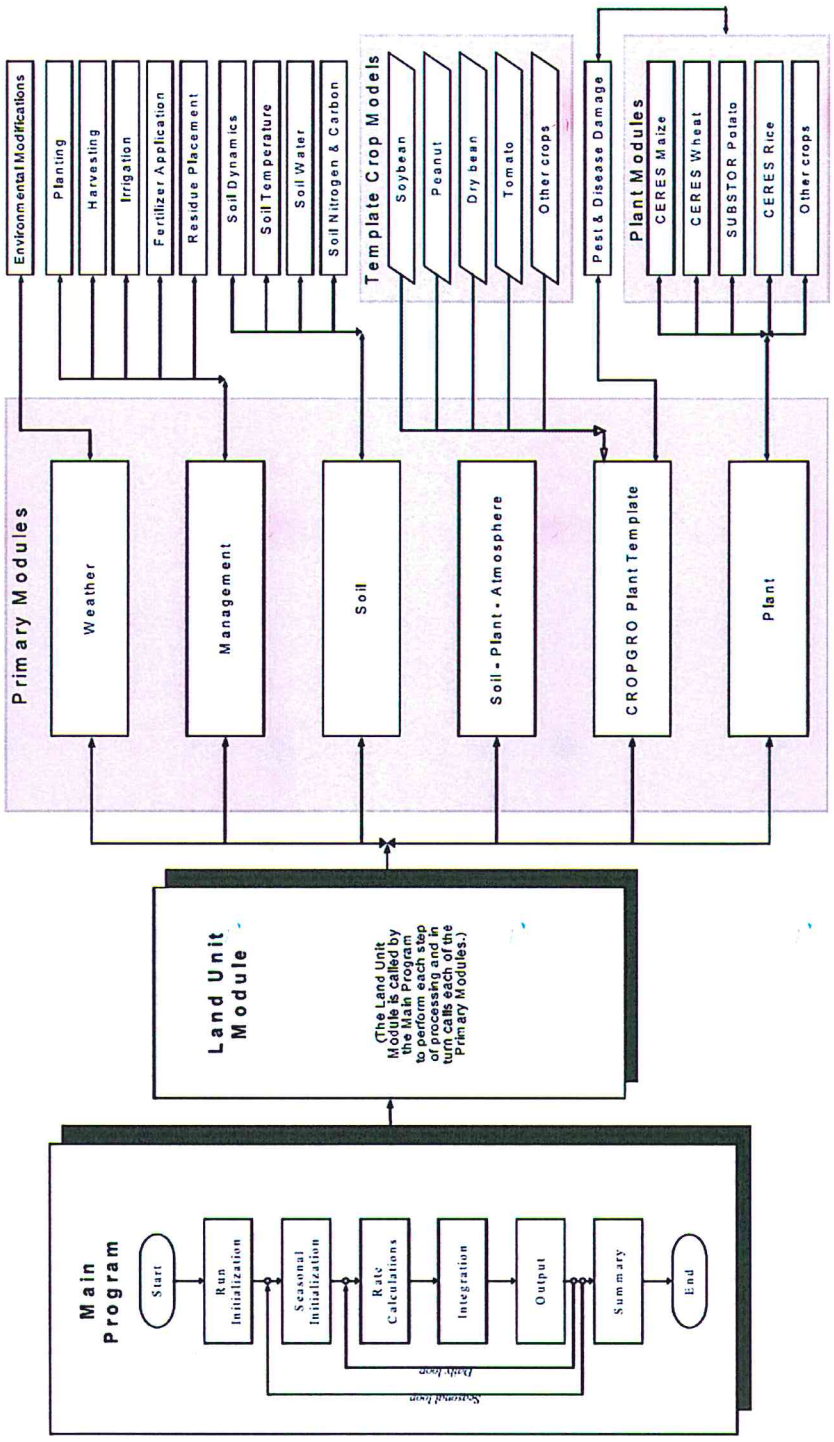

Figure 4: Representation of the components of DSSAT [57].

I-6-3 Problem statement

Simulation of the population dynamic of insect pest such as, the apple orchard pest *Cydia pomonella (L.)* [314], the fruit pest *Carposina sasakii* [315], *Bactrocera (Dacus) tyoni* [316] and tea pest, *Caloptilia theivora* [317] have been done mostly using dynamical equation with coefficients derived from experimental data. A plethora of experiments regarding the biology of *B. fusca* have been conducted in order to assess the effect of humidity, temperature, nutrients contained in maize plant but have never been exploited with the aim of modelling the population dynamic and the maize-insect interactions [318–320].

The pest attack does not always induce yield reduction because of the possible plant compensation of damages [321–324]; however, a proper representation of the feedback mechanism between the plant and the insect pest is a challenge because of absence of specific functional relationship between the biomass lost with time and the degree of pest attack [218]. This is among the major difficulties encountered while coupling pest and crop in a "two-way" approach whereby the pest and the crop model variables drives each other [53]. Despite the previously mentioned CSMs perform crop growth simulation, according to the best of our knowledge, none of them integrate the "two-way" concept as well as a dynamical model predicting pest population through its life cycle [55–59,313].

The present study attempted to fill this knowledge gap by improving the software Decision Support System for Agrotechnology Transfer (DSSAT) which is a broadly used modeling tool that comprises CSMs for over forty-two crops [57] and, integrates CERES-Maize which is a simulation model for maize growth and development [60]. The pest and the crop are coupled within DSSAT in this study via the fuzzy logic concept.

Fuzzy logic was developed with the aim of modelling uncertain and imprecise knowledge [271]. It is a useful approach for an abstractive representation for a system that cannot be very well formalized mathematically [271]. In contrast to the binary logic, the fuzzy logic is used to modify to original real variables into a corresponding number between 0 and 1 [272]. By means of a set of membership functions and, formulation of appropriate linguistic rules, the input and output variables of the system are connected [272]. Fuzzy logic

approach has been employed to handle the negative effect of abiotic stresses on maize plants such as the extreme wind speed effect in stalk lodging [325,326] and, the deficiency of nitrogen in the soil [327,328]. Since the exact functional link between the pest and the crop is usually unknown or, cannot be well formulated mathematically in general [218]; this approach was used here for coupling the stem borer damage and the maize plant growth.

I-7 Conclusion

In the end of this chapter, a brief overview of each physical description of the Davydov's model, its different limits and an highlight of our contributions have been provided. Furthermore, an overview of microtubules and the models mimicking the electrical behaviour as well as our potential contribution were highlighted. Moreover, we presented the insect pest its ecology, life cycle and damages in maize farm. The challenges related to the modelling of insect pest in general and the techniques that will be used in this study where presented. Finally, we highlighted the problems and challenges encountered in coupling the insect pest dynamic and crop simulation models. In the next section, we presented the different analytical, experimental and simulation approaches used to tackle these different problems in this study.

Chapter II: Materials and methods

II-1 Introduction

This chapter present a brief overview on the techniques used to solve the open problems stated in the chapter I are briefly presented. It is structured in three main parts: the discrete breather investigate in the modified Davydov's model, the criteria for electrical wave propagation in microtubules and finally, the analysis and modelling on insect pest damages in maize farm..

II-2 Anharmonic correction of the linear potential

A polynomial correction of the harmonic potential was introduced as follow:

$$V(z)=\frac{z^2}{2!}+\sum_{k=2}^{\infty}\frac{z^{2k}}{(2k)!}=\cosh(z)-1 \qquad (11)$$

The infinite summation in the right-hand side of the first equality represents an anharmonic correction of the harmonic potential. The nonlinear potential is: $V(r_n)=c\left(\cosh(br_n)-1\right)$.For convenience in the calculus, the following transformations were made: $c=\frac{KJ^2}{b\chi^2};b=\frac{\chi}{J}$. Introducing these dimensionless variables we obtained: $V_1(x_n)=\cosh(x_n)-1$, where $x_n=\beta_{n+1}-\beta_n$. The nonlinear hyperbolic cosine potential is a good approximation of harmonic potential around the minimum. This nonlinear potential gives the possibility of high vibratory energy amplitude for the very low value of displacements from equilibrium point. That is due to higher order terms in the infinite summation. It was also observed that hyperbolic cosine potential preserves the shape of harmonic potential from the original Davydov's model in spite of its nonlinearity. Phonon mass is larger than exciton one. Therefore, it is supposed to be very slow compared to exciton. Let apply Born-Oppenheimer or time adiabatic approximation [11] $\frac{d\beta_n}{d\tau}\to 0$, we obtained from (9) the identity $\beta_{n+1}-\beta_n=-\text{arsinh}\left(|\phi_n|^2\right)$. substituting this equation in the relation (8) we obtained:

$$i\frac{d\phi_n}{d\tau}+\phi_{n+1}-2\phi_n+\phi_{n-1}+\phi_n\operatorname{arsinh}\left(|\phi_n|^2\right)=0. \tag{12}$$

In the following section, we will show how to derive discrete breather of discrete nonlinear Schrödinger equation (DNLSE) (12) using a two-dimensional map approach.

II-3 Two dimensional map

To find the intrinsic localized mode we conducted the calculation as in the literature [329–335]. An estimate of the stationary breather for (12) was performed with the assumption that the solution has the following stationary form $\phi_n(\tau)=\eta_n\exp(i\omega\tau)$, where η_n is the stationary amplitude, and ω is the dimensionless frequency. By inserting this expression in (12) we have $-\omega\eta_n+\eta_{n+1}-2\eta_n+\eta_{n-1}+\eta_n\operatorname{arsinh}(\eta_n^2)=0$. By assuming $\theta_{n+1}=\eta_n$ we obtain the following two-dimensional (2D) map:

$$\mathbf{T}:\begin{bmatrix}\eta_n\\ \theta_n\end{bmatrix}\mapsto\begin{bmatrix}\eta_{n+1}\\ \theta_{n+1}\end{bmatrix}=\begin{bmatrix}(2+\omega)\eta_n-\eta_n\operatorname{arsinh}(\eta_n^2)-\theta_n\\ \eta_n\end{bmatrix}. \tag{13}$$

The nonlinear localized mode (pulse of kink) can be found obtained by searching homoclinic and heteroclinic tangles of this 2D map [335]. The fixed points of this map are given by $P_0=(0,0),P_{1,2}=(\pm\sqrt{\sinh(\omega)},\pm\sqrt{\sinh(\omega)})$. The eigenvalues of the Jacobian matrix:

$$\Xi=\begin{bmatrix}2+\omega-\operatorname{arsinh}(\eta_n^2)-\dfrac{2\eta_n^2}{\sqrt{1+\eta_n^4}} & -1\\ 1 & 0\end{bmatrix} \tag{14}$$

around the fixed point P_0 are:

$$\lambda_{\pm}=\frac{(2+\omega)\pm\sqrt{(2+\omega)^2-4}}{2}. \tag{15}$$

The fixed point P_0 is homoclinic if it is an unstable saddle point. This will happen if and only if the absolute value of one eigenvalue is greater than one and the absolute value of the second eigenvalue is less than one. Therefore, the trajectories of the nearby point in the direction of

corresponding stable eigenvalue will move toward this point, the nearby points in the direction of corresponding unstable eigenvalue will move outward from it [331,336]. To generate the unstable manifold, first, we have to find the eigenvectors corresponding to the unstable eigenvalue. Iterating the points, which are on the corresponding unstable vector and are close to the fixed point, through the map (13), then we can obtain the unstable manifold (W^u). We can also generate the stable (W^s) manifold by inverse map of the iteration (13) [331,336]. Once the unstable and stable manifold are generated, we can select the intersection as an initial condition for the 2D map. The backward and forward iterations will provide a pulse like profile $\eta_{-N} < \eta_{-N+1} < .... < \eta_0$, $\eta_0 > \eta_1 > .... > \eta_N$ which is corrected numerically with the iterative Newton-Raphson method.

II-4 Newton-Raphson method and linear stability

Let's consider the again the equation $-\omega\eta_n + \eta_{n+1} - 2\eta_n + \eta_{n-1} + \eta_n \text{arsinh}(\eta_n^2) = 0$, we are looking for the vector $\eta = (\eta_1, \eta_2, ..., \eta_n)^T$ solution of $f = (f_1, f_2, ..., f_n)^T = (0, 0, ..., 0)^T$ where:

$$f_n = -\omega\eta_n + \eta_{n+1} - 2\eta_n + \eta_{n-1} + \eta_n \text{arsinh}(\eta_n^2) \tag{16}$$

Let's define the Jacobian matrix **J** with the elements

$$J_{ij} = \frac{\partial f_i}{\partial \eta_j} \tag{17}$$

The iterative formula of Newton is given by:

$$\eta^{k+1} = \eta^k - J^{-1} \cdot f(\eta^k) \tag{18}$$

Where η^k is the value of η after *k*-iterations. The matrix **J** is a tridiagonal matrix with

$$\frac{\partial f_n}{\partial \eta_n}, \quad \frac{\partial f_n}{\partial \eta_{n+1}}, \quad \frac{\partial f_n}{\partial \eta_{n-1}}. \tag{19}$$

The first term of **J** is at the principal diagonal and at the two others are located at the off-diagonals of **J**. This matrix should be invertible and, the initial value $\eta^{initial}$ should be closer to the real solution to ensure a convergence of the iterative process. This is the reason why the initial guess is estimated first from the 2D map approach. The iterative process will stop if the following condition is satisfied [337]:

$$\| \eta^{k+1} - \eta^{k} \| \leq \varepsilon \tag{20}$$

ε has been chosen as 10^{-20}. After application of the Newton's method, we finally get an accurate stationary solution [338]. The linear stability of the obtained spatially localized mode have been investigated using the perturbation method [335]. By perturbing the stationary solution given by (12) we obtained:

$$\phi_n(\tau) = \left[\eta_n + \epsilon\left(a_n \exp(\sigma\tau) + b_n \exp(\bar{\sigma}\tau)\right)\right]\exp(i\omega\tau), \tag{21}$$

where a_n and b_n are complex parameters, ϵ is an infinitesimal parameter. Substituting equation (21) in (12) and keeping only linear terms in ϵ led to the following eigenvalue problem:

$$\frac{1}{i}\begin{bmatrix} \omega_n' - \Delta - f_n & -g_n \\ g_n & -\omega_n' + \Delta + g_n \end{bmatrix}\begin{bmatrix} a_n \\ \bar{b}_n \end{bmatrix} = \sigma\begin{bmatrix} a_n \\ \bar{b}_n \end{bmatrix}, \tag{22}$$

where σ is the eigenvalue of the spectral problem. Δ is a tridiagonal matrix with $\Delta_{n,n} = 2$, $\Delta_{n,n\pm1} = 1$, $g_n = \eta_n^2(1+\eta_n^4)^{-1/2}$, $\omega_n' = \omega - \text{arsinh}(\eta_n^2)$. The bar on top of b_n and σ represents the complex conjugate. The intrinsic localized mode is linearly unstable if at least one eigenvalue has a strictly positive real part. In the following paragraph, we explained how the impurity is used to achieve the mobility of the discrete breather and how the thermal bath was incorporated in the model.

II-5 Impurity and noise

In order to take into account the presence of an impurity, we reconsidered the original Davydov's model including the gauge transform (4) without the C=O stretching energy ε_0. The ABE energy ε_1 was added to the amide-I energy. Furthermore, a time adiabatic

approximation was performed. Moreover, we rescaled the impure vibrational mode ε_1 in the discrete nonlinear Schrödinger equation (12) by the gauge transform $\phi_n(\tau) \to \phi_n(\tau)\exp\left[i\left(\frac{\varepsilon_0}{J}(1+\gamma)+(1+\alpha_n)\right)\tau\right]$. This transformation introduced the amide-I and impurity energy of the original Davydov's model in non-dimensional form $(1+\alpha_n)$. It was assumed that the impurity impact is explicitly time and space dependent [76]. A similar gauge transforms have been used to introduce a stationary impurity in a discrete nonlinear Schrödinger equation [339]. The obtained dimensionless equation governing the exciton dynamic is:

$$i\frac{d\phi_n}{d\tau} - \left(1+\alpha_n(\tau)\right)\phi_n + \phi_{n+1} - 2\phi_n + \phi_{n-1} + \phi_n|\phi_n|^2 = 0, \tag{23}$$

where the dimensionless energy is given by: $\alpha_n(\tau) = \gamma\delta_{n,l(\tau)}$. The anomalous band energy (ABE) has a value $\varepsilon_1 = 1650\text{Cm}^{-1}$ [63]. Furthermore, $\gamma = \varepsilon_1/\varepsilon_0 \simeq 0.990$. Then, we derived a *representation* of ABE under a non-dimensional from $\gamma = 0.990$, symbol of Kronecker delta given by the following rules:

$$\gamma\delta_{n,l(\tau)} = \begin{cases} \gamma & \text{if } n = l(\tau), \\ 0 & \text{if } n \neq l(\tau). \end{cases} \tag{24}$$

Where $l(\tau)$ is the position of the impurity at the time τ. The pseudo-centre of breather is computed by the formula:

$$X(\tau) = \frac{\sum_n n|\phi_n(\tau)|^2}{\sum_n |\phi_n(\tau)|^2} \tag{25}$$

The dynamical position $l(\tau)$ of ε_1 on the lattice is determined by $E(\tau) - 100$. The function $E(\tau)$ rounds τ to the nearest integer less or equal to τ.

The Langevin's approach [340] is commonly used while taking into account thermal noise for Davydov's model [84,341,342]. The Langevin equation for the lattice is:

$$m\ddot{u}_n = V'(u_{n+1}-u_n) - V'(u_n - u_{n-1}) + \chi\left(|a_n|^2 - |a_{n-1}|^2\right) + \xi_n(t) - m\Gamma\dot{u}_n. \quad (26)$$

The variables $\xi_n(t)$ are random forces with a Gaussian distribution. The thermal noise satisfying fluctuation-dissipation relation is given by [342]:

$$\langle \xi_{n_1}(t_1)\xi_{n_2}(t_2)\rangle = \frac{2m\Gamma k_B T}{\Phi}\delta(n_2 - n_1)\delta(t_2 - t_1), \quad (27)$$

where k_B is the Boltzmann constant, T is the temperature, δ is the delta Dirac function, Φ is the noise correlation time and Γ the dissipation constant. The variables n_1 and n_2 are two distinct positions in the lattice. The noise temporal mean at a lattice point $\langle \xi_n(t)\rangle$ is considered null for the difference between two instants $t_2 - t_1 > \Phi$. Thus we considered Φ very small, given that the noise is assumed fluctuating quickly and the estimated lifetime of the Davydov's soliton at physiological temperature is in the order of few picoseconds [12,343]. Therefore, we have chosen $\Phi = \frac{\hbar}{J} \propto 10^{-12}$. Furthermore, Φ had been multiplied by the time step used during numerical simulations. This is quite similar to [342] whereby the Φ was chosen as a time step. To generate numerically a normalized stochastic and uniform Gaussian white noise, we applied the Box-Müller algorithm [344]. In the classical Davydov's model, we used initial conditions commonly used the literature for visualising impact of the thermal noise. In what follows, the methods used to study the second biological molecules which was the second focus of this study are provided.

II-6 Modified formulation of voltage dynamic in microtubule

A unit cell of the transmission line is depicted in Figure 5. The microtubule is assimilated to a succession of N adjacent unit cells. Each unit cell n of the lattice is made by a linear inductance L in series with a linear resistance r, shunted by a nonlinear capacitance $C(V_n)$ in parallel with a nonlinear resistance R_n.

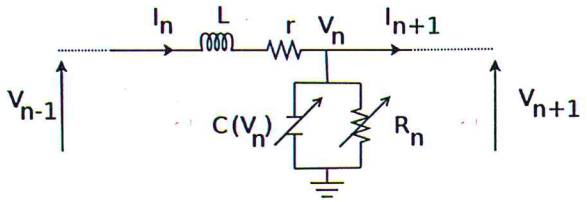

Figure 5: Description of the electrical analogy of the MT model.

In standards models, the nonlinear components are represented by a conductance and a capacitance [17–22]. Priel et al. [23] suggested that an ensemble MT-calcium ions could be represented by a transistor, in which MT is the core part and the flow of calcium ion ionic through the nanopores of MT constitute the base current of the transistor. The main difference between the present model and existing models [17–22] is the incorporation of a nonlinear resistance to capture the cation flow through nanopores within MTs. Our model is closer to the one recently developed and proposed by Sataric et al. [20]. They were inspired by the previous work of Freedman et al. [106] which indicated that $I(V)$ characteristic in the presence of the infiltration of cation ion through the nanopore of MTs was a nonlinear function. However, the model in [20] does not take into consideration the nonlinearity described by Freedman et al [106]. Thus we suggested adding a nonlinear resistance for modeling cation flow through nanopores of MT. In Figure 5, an arrow crossing the electrical component is used to represent the nonlinearity.

The nonlinear capacitance element $C(V_n)$, possess an electrical charge Q_n in the following form [345]: $Q_n = Q(V_n) = AC_0 \ln\left(1+\frac{V_n}{A}\right)$, where C_0 is the capacitance in the linear regime, A is a positive parameter. Such function is a good approximation of charge-voltage (C–V) curve [346–348]. It recovers the quadratic nonlinearity of capacitances in model used to mimic the electrical transmission properties of MT after asymptotic expansion with large parameter A ($A>>V_m$) [17–22]. The negative nonlinear resistance effects of ionic flow through nanopores is characterized by the following relation: $I^{R_n} = f(V_n) = B_1V_n^3 - B_2V_n$, where I^{R_n} is the current flowing through each negative nonlinear resistance R_n, $1/R_n = B_1V_n^2 - B_2$ where B_1, B_2 are positive parameters representing the nonlinear and linear

coefficients with the physical dimensions [Ohms^{-1}·Volts^{-2}] and [Ohms^{-1}] respectively. By applying Kirchhoff's Voltage laws in unit cell n of Figure 5 we have obtained the following expression:

$$\frac{LC_0}{1+\frac{V_n}{A}}\cdot\frac{d^2V_n}{dt^2}-\frac{LC_0}{A(1+\frac{V_n}{A})^2}\left(\frac{dV_n}{dt}\right)^2+\left(L\left(3B_1V_n^2-B_2\right)+\frac{rC_0}{1+\frac{V_n}{A}}\right)\frac{dV_n}{dt} \qquad (28)$$
$$+r\left(B_1V_n^3-B_2V_n\right)=V_{n+1}-2V_n+V_{n-1}$$

This equation represents the spatial and temporal evolution of the voltage $V_n(t)$. The terms containing B_1 and B_2 are the contribution of the ionic flow brought in by a nonlinear resistance. The terms with r represent the contribution of the linear resistance. The right-hand side of the Eq. (28) is the coupling entity between nearest neighbours $[n-1]-[n]-[n+1]$ of the system. Since we are in the presence of cationic current flow through MT, B_1, B_2 and r values are implicitly linked to ions concentration [17,106], hence they were considered as control parameters in the model. The remaining parameters were obtained from the literature, $C_0\simeq 0.1$ fF [20] and L$\simeq$1 fH [21]. In the following section, the analytical threshold for wave transmission in the forbidden band is derived.

II-7 Cut-off soliton

In this section, the main point of interest is the estimation of the critical amplitude that allows the wave to propagate with a frequency contained in the forbidden band gap of MTs. The MTs boundary is assumed to be excited with a periodical driving which frequency is inside the forbidden band gap. Equation (28) can be rewritten by assuming that the capacitor is linear ($A\gg V_n$) in a non-dimensional form as:

$$\ddot{V}_n+\omega_0\left(3LB_1V_n^2+(rC_0-LB_2)\right)\dot{V}_n+rB_1V_n^3-rB_2V_n=V_{n-1}-2V_n+V_{n+1}, \qquad (29)$$

where, $\omega_0 = \sqrt{1/LC_0}$ and the dot is the time derivative according to the non-dimensional time $\tau = \omega_0 t$. The boundary condition is chosen as $V_0(\tau) = U\cos(\omega\tau)$. It was observed in literature capacitors [110,112–117] that the analytical estimation of the transmission threshold for the boundary condition neglected the dissipation. In addition, the type of nonlinearity included in this section of the study has never been analyzed in this context. This justifies why we decided to study two cases: $f(\dot{V}_n) = \omega_0\left(3LB_1V_n^2 + (rC_0 - LB_2)\right)\dot{V}_n = 0$, and $f(\dot{V}_n) \neq 0$.

Case number 1: $f(\dot{V}_n) = 0$. By neglecting the contribution of the dissipative and nonlinear terms in equation (29), and assuming that $V_n(\tau) \propto \exp i(\omega\tau - qn)$, we obtained the linear dispersion relation:

$$\omega(q) = \sqrt{4\sin^2\left(\frac{q}{2}\right) - rB_2}. \tag{30}$$

The above relation is valid if the wave number satisfies the following condition: $q \geq q_c = 2\arcsin\sqrt{\frac{rB_2}{4}}$. The system is a low band pass filter with the allowed band defined by the frequency interval $[0\ \omega_c]$ where $\omega_c^2 = 4 - rB_2$ is the square of the upper cut-off frequency. Using the rotative wave approximation and the solution under the form:

$$V_n(\tau) \sim \epsilon\psi_n(\epsilon^2\tau)e^{i\theta_n(\tau)} + \epsilon\psi_n^*(\epsilon^2\tau)e^{-i\theta_n(\tau)} + O(\epsilon^2), \tag{31}$$

with

$$\theta_n(\tau) = \omega\tau - qn, \quad 0 < \epsilon \ll 1, \quad i^2 = -1, \tag{32}$$

we obtained the following terms in different orders of ϵ and $e^{i\theta_n(\tau)}$:

$$\epsilon e^{i\theta_n} : -(\omega^2 + rB_2)\psi_n - (\psi_{n-1}e^{-iq} - 2\psi_n + \psi_{n+1}e^{iq}), \tag{33}$$

$$\epsilon^3 e^{i\theta_n} : 2i\omega\dot{\psi}_n + 3rB_1\psi_n|\psi_n|^2. \tag{34}$$

By assuming that the wave number is at the edge of the first Brillouin's zone (q=π) we obtained the discrete form of the nonlinear Schrödinger equation:

$$2i\omega\dot{\psi}_n = (\omega^2 - \omega_c^2)\psi_n - (\psi_{n+1} - 2\psi_n + \psi_{n-1}) - 3rB_1\psi_n|\psi_n|^2. \quad (35)$$

The continuous approximation of equation (35), has the well known static pulse soliton solution given by:

$$\psi(x) = \sqrt{\frac{2(\omega^2 - \omega_c^2)}{3rB_1}}\,\mathrm{sec}\,h\left(\sqrt{\omega^2 - \omega_c^2}(x - x_0)\right). \quad (36)$$

The approximative maximal value of $V_n(\tau)$ at the boundary called the supratransmission threshold is then given by the expression [107]:

$$U_{th} = \sqrt{\frac{8(\omega^2 - \omega_c^2)}{3rB_1}}. \quad (37)$$

In order to insure that the threshold (37) is correct we used the nonlinear response manifold (NLRM) for numerical a estimate [121–123]. The stationary and periodic wave approximation $V_n(\tau) \sim a_n \cos(\sigma\tau)$ applied in equation (29) provided the backward two-dimensional (2D) discrete map $\mathbf{T}: a_{n-1} \mapsto a_n$:

$$\mathbf{T}: \begin{bmatrix} \eta_n \\ \chi_n \end{bmatrix} \mapsto \begin{bmatrix} \eta_{n-1} \\ \chi_{n-1} \end{bmatrix} = \begin{bmatrix} \left(2 - \sigma^2 - rB_2 + \frac{3rB_1}{4}\eta_n^2\right)\eta_n - \chi_n \\ \eta_n \end{bmatrix}, \quad (38)$$

where $\eta_n = a_n$, $\chi_n = a_{n+1}$ and $\sigma > \omega_c$. This discrete formulation is used to map the infinitesimal boundary condition at a_N for approximating the value of a_1 belonging to the unstable manifold of application (38). The critical value of the driving amplitude is obtained by identifying the turning point in the plane (V_1, U). Where V_1 is the voltage amplitude at the first cell and U is the value of the driving amplitude.

Case number 2: $f(\dot{V}_n) \neq 0$. The supratransmission is well known as a generic feature for nonlinear systems. However, it is noticed that most of the studies did not explicitly included the dissipation during the determination of the analytical supratransmission threshold [108,109,120,349]. Considering the nonlinear dissipative term and using the rotative wave

approximation described in the preceding subsection we obtained at different order of ϵ and $e^{i\theta_n(\tau)}$:

$$\begin{aligned}\epsilon e^{i\theta_n} &: -(\omega^2 + rB_2)\psi_n + i\omega_0(rC_0 - LB_2)\psi_n - (\psi_{n-1}e^{-iq} - 2\psi_n + \psi_{n+1}e^{iq}),\\ \epsilon^3 e^{i\theta_n} &: \left[\omega_0(rC_0 - LB_2) + 2i\omega\right]\dot{\psi}_n + 3B_1(r + iL\omega\omega_0)\psi_n|\psi_n|^2 .\end{aligned} \tag{39}$$

For $q=\pi$ we obtained the discrete cubic complex Ginzburg-Landau equation:

$$\dot{\phi}_n = R_r\phi_n + D(\phi_{n-1} - 2\phi_n + \phi_n) + \beta\phi_n|\phi_n|^2, \tag{40}$$

where $\psi_n(\tau) = \phi_n(\tau)\exp(iR_i\tau)$, $D = D_r + iD_i$, $\beta = \beta_r + i\beta_i$, $R = R_r + iR_i$, $\omega = \omega_c$ (the expressions of the coefficients D, β and R are given in Appendix 1). The analytical solution of equation (40) in the continuum approximation is assumed to be under the form $\phi(x,\tau) = u(\xi)\exp i(\theta(\xi) + \nu\tau)$, $\xi = x - \vartheta\tau$, ϑ is the velocity and ν is a frequency [350]. The *stationary* ($\vartheta = 0$) Pereira-Stenflo soliton solution is given by [350,351]:

$$\psi(x,\tau) = z\Gamma(\tau)\sec h(p(x - x_0))\exp -i\frac{q}{p}\ln\sec h(p(x - x_0)), \tag{41}$$

where $\Gamma(\tau) = \exp i(\nu + R_i)\tau$. (for the expression of z, p and q see the Appendix 1). In this subsection, we are interested only in the maximum value of the amplitude for the solution (41) centered at the origin boundary [109]. The supratransmission threshold and the frequency of the approximate stationary solution $V_n(\tau)$ are given by:

$$U_{th} = 2z = \sqrt{\Upsilon\cdot\left(\omega_c + R_i - \Omega - \frac{1}{1+\Phi}\right)} \tag{42}$$

where Υ and Φ are provided in the appendix, $\Omega = \omega_c + R_i + \nu$. Since $\Omega > \omega_c$, the parameter ν should satisfy the condition $\nu > -R_i$. In this subsection, Ω has been considered as the boundary driving frequency. The procedure for estimating the infratransmission threshold in reference [109], is used here. For that purpose, the system has been excited at its first boundary cell by the driving amplitude $\Lambda(\tau)\cos(\Omega\tau)$ where $\Lambda(\tau)$ is given by: $\Lambda(\tau) = U_{th}(1 - e^{-\tau/\tau_1}) + (U_0 - U_{th})(1 - e^{-\tau/\tau_2}), \tau_2 \gg \tau_1$. For several values of the parameter U_0

we computed the total energy of the system including the coupling energy at the boundary conditions of the system:

$$E=\sum_{n=1}^{N}\left[\frac{1}{2}(\dot{V}_n^2+(V_{n+1}-V_n)^2)+\frac{rB_1}{4}V_n^4-\frac{rB_2}{2}V_n^2\right]+\frac{1}{2}(V_1-V_0)^2 \quad (43)$$

The infratransmission threshold corresponds to the amplitude for which the accumulated energy drastically changes. In the following section, we explained how the electrical wave amplification is realised.

II-8 Simulating electrical wave amplification

According to Satarić et al. [352,353], an endogenous sinusoidal electrical field in living cells plays an important role in MT dynamics. Thus sinusoidal input voltage stimulus is usually a good candidate for boundary driving. Both experimental studies [23,105] used pulse function as an input signal. We also opted for the same, making our sinusoidal input have a secant hyperbolic function as amplitude. The analytical form of the input is considered as: $V_0=V_{in}(t)=V_m\sec h\left(\frac{V_g t}{L_s}\right)\cos(\omega t)$, where V_m is the maximal amplitude, V_g is the group velocity of the wave packet and L_s is the width of the pulse. An arbitrary value was chosen for the pulse L_s=18 cell, V_g=3240.41 cell/ps, and for the driving pulsation ω=2.04 rad/fs which belongs to the allowed band estimated in the previous section. The parameters were chosen following analysis of the preceding section to ensure signal coherence without any resistance. This is to minimize other factors influencing the amplitude and shape change during signal propagation [346]. We have also chosen V_m and $1/A$ to satisfy the condition ($A \gg V_m$).

In what follows, the data collection protocol, the preliminary analysis and the modelling related the insect pest damages in maize farm are presented.

II-9 Study sites and sampling procedures

II-9-1 First data collection

The farms selected for the study are located in Naivasha, in the Rift Valley region, Northwest of Nairobi. The geographical coordinates are: latitude 0°43′00″ S, longitude 36°26′09″ E, 2086 m a.s.l. *Busseola fusca* is the predominant lepidopteran maize stem borer at this elevation [153]. The study was carried out on private land, after the owners gave permission to conduct the study on these sites. Six maize plots (see Table 2) with monoculture planting style were selected. The maize plants were planted at regular row and within row space intervals, to facilitate counting. The planting date and crop management practices were identical in all selected plots. Data collection consisted of visual checking of all plants damaged by *B. fusca*, and was conducted weekly during 13 weeks, from the 23 November 2010 to the 10 February 2011. Coordinates of all sampled maize plants with/without damages were recorded. Four plant damage types were considered: LD, DH, EH and D. Furthermore, we placed two pheromone insect traps around each field to follow the flight dynamic of *B. fusca* males. For each plant, we assigned an ordinal number ranging from 1 to the total number of plants within the field. In addition, for each of the 4 damage types, we assigned for each plant an integer value indicating the week of the observed damage. If there was no *B. fusca* damage observed during the collection period, the value given was 0.

Plot	Row length (m)	Row spacing (m)	Dimensions (m)	Total number of maize plants	GPS coordinates Latitude , longitude (in degrees)
1	55.00	0.81	51.03×53.93	6547	-0.7701, 36.4959
2	31.54	1.86	150.66 × 31.57	3914	-0.7747, 36.4786
3	53.10	1.56	123.24 × 52.14	8146	-0.7819, 36.4711
4	30.50	1.49	120.69 × 30.50	4974	-0.7713, 36.4766
5	46.80	1.40	74.20 × 46.80	4884	-0.7826, 36.4704
6	27.82	1.05	153.30 × 27.82	7314	-0.7765, 36.4791

Table 2: Description of plots used for the first experiment. The dimensions are the maximal repartition range of plants inside the plot. The six plots

II-9-2 Second data collection

The second trial was conducted at Murang'a (00° 43' 00" S, 37° 09' 00" E and 1255 meters above sea level) in Kenya. A commercial maize variety DUMA-4 commonly grown by Kenyan farmers in mid-altitude areas was used throughout this study. The seed provided to farmers were planted in four plots described in Table 3. The plots were submitted to identical management and exposed to natural infestation by *B. fusca*; no control measures and fertilizers were applied during the whole plant grow period. Planting was conducted on 3rd March 2014 and the harvest occurred during the month of July 2014. The data collection started on 16th April 2014 and ended on 25th July 2014.

Data collection protocol was identical for all plots. In each plot, all plants were monitored weekly in order to detect infested maize plants. The incidence of damages was determined by visual observation of the plant within the plot. Infected plants were tagged with colored plastic materials having a unique set of number and letters which served as an identifier. The types of damages assessed were leaf damage, exit hole, and dead heart. Observations were done in one-week interval beginning 16th April 2014. Plants were examined *in situ* without uprooting. Damage level, taken as the tunnel length bored in the stem and the ear by *B. fusca* individuals that successfully colonized the plants was assessed at harvest. This was conducted by dissecting (opening by vertical split) ears and stems of infested plants.

During harvest, all infested plants were uprooted for proper inspection. Furthermore, each plot was divided into four quadrats of equal size and 25 non-infested plants were randomly harvested per quadrate. Plants features such as stem length, stem diameters, plant dry mass (leaves and stem without the cob) were recorded. Physical characteristics of unshelled maize cob with removed corn silk and husk were collected. Cob length, masses, and diameters from both infested and non-infested plants were also recorded.

Plots	Row length (m)	Row spacing (m)	Dimensions (Length×Width) (m)	GPS coordinates	
				Latitude (in degrees)	Longitude (in degrees)
1	21.00	0.60	21.00×17.17	0.922244964	37.15198829
2	21.00	0.60	21.00×17.17	0.922477751	37.15234651
3	18.60	0.60	23.40×20.70	0.923219997	37.14361341
4	18.60	0.60	18.60×10.80	0.919620737	37.13853050

Plots	Total number of rows	Total number of plants per row	Space between plants in row	Total number of quadrats during sampling at harvest	Total number of maize plants
1	36	60	0.30	4	2160
2	36	60	0.30	4	2160
3	40	70	0.30	4	2800
4	32	37	0.30	4	1184

Table 3: Description of the plots. Each dimension is given in meter. The plots were located within an area having a radius of 0.708 Kilometers.

II-10 Preliminary analyses I: exploration of emergent patterns

II-10-1 Observation of infestation rate variation and insect trap catches

To get the weekly variation of LD rate, the differences between numbers of damaged plants during two consecutive weeks were evaluated in each plot. Results were normalized so that the associated values ranged from 0 to 1. As well, the weekly mean values of adult *B. fusca* males caught in insect traps were computed and then, the temporal dynamics of LD rate and the abundance of adult males were compared.

II-10-2 Conditional probability for plant infestation

Because maize was planted at regular row/within row space and the planting date and crop management were identical as well as the date of data collection, we decided to compute the probability that a randomly selected plant is found dead (D) once damage i has occurred,

where i = LD, EH or DH. Next, the conditional probability that D occurs once i has occurred was computed.

II-10-3 Mean time transition between infestation types

The estimation of the average time span between damage types was done. First, for plant P we recorded the damage type i (i= LD, EH, DH or D), and the corresponding week of observation. Second, we checked and recorded the week of occurrence for other different damage from i, which we called j. Third, we computed the difference between the two weeks to get the time duration for the transition $P_i \rightarrow P_j$. Fourth, we repeated the same process for other maize plants to obtain a mean time transition from a damage type to another.

II-11 Preliminary analyses II: Spatial distribution

II-11-1 Spatial autocorrelation

Observations of damage in plants with different geographical coordinates may not be uncorrelated. Spatial autocorrelation may be positive or negative symbolizing how similar or dissimilar damage occurs close by. The farm in this context had a lattice structure made of discontinuous spatial repartition of maize plants. The first step in this analysis was to define the Euclidean distance matrix from x- and y-coordinates of two individual plants i and j (d_{ij}). Secondly, the spatial relationship between damaged plants was quantified using the spatial weight matrix **W** in which elements represent the strength of the spatial structure between units [354,355]. This matrix was used to evaluate the level of spatial autocorrelation. There are various ways to define **W** and the choice of a particular method to other is subjective. The easiest option is to construct a binary contiguity matrix (made of 0 and 1) by specifying the units that are adjacent (1) and those that are not (0) [356]. Therefore, the spatial weight matrix w_{ij}^r is equal to 1 for d_{ij} less than a certain critical distance r and, it is equal to 0 otherwise. The variable r is the radius of proximity. The Moran's I coefficient I^r is used to quantify the degree of spatial correlation between neighbouring infested plants. The formula used to calculate Moran's I can be found in the literature [135,357–359]. In this analysis, the value

assigned to each plant is a binary index of LD, EH, DH or D (0 for non-infested and 1 for infested plants). The interpretation of Moran's I is similar to the correlation coefficient [359]. If the Moran's I is null, then the spatial link between infested plants at distant locations is null, and there is no spatial autocorrelation (SA). If the Moran's I is positive, then the contagiousness of infested plants at distinct locations is considerable, and the SA is positive. If the Moran's I is negative, then the majority of the infested plants are not next to each other, and the SA is negative. The graphical representation of the Moran's I function of r is called variogram (or correlogram). For the Moran's I computation, data were reorganized as follow: for each maize plant we recorded the spatial coordinates. Values of LD, EH, DH and D, were 0 or 1 (1 is for infested and 0 for non-infested). The process was repeated cumulatively for subsequent weeks to obtain a temporal variogram.

II-11-2 Tracking the centre of plant infestation

Observing directly the spatial and temporal evolution of plant infestation is difficult in a maize farm having a considerable number of stems; thus we opted to compute the iso-barycentre (IB) coordinates of each occurring damage type. First, we selected the coordinates of plants with leaf damage, and then we calculated the coordinates of the weekly IB without taking into account results obtained from the previous week's computations. We obtained the IB coordinates by averaging x- and y-coordinates corresponding to the set of newly infested plants observed at each week, which allowed us to track the position of the center of patches formed by infested plants with time.

II-11-3 Model-based cluster analysis: spatial clustering

To follow the evolution of the initial shape, density and number of clusters of infested plants formed with time the model-based cluster analysis was used. For a spatial classification of clusters, the following procedure was adopted: (i) positions of damaged plants were assumed implicitly generated by a mixture of probability distribution function in which different components represent groups or clusters; (ii) based on the framework developed in [360], we used Gaussian and non-Gaussian probability density (PDF) functions for the clustering. In addition, orientation, volume, and shape of the cluster were determined using the

models summarized in Table 4 [361]. These three features are characteristics of the bottom of the two-dimensional PDF. The likelihood of each model is estimated via the expectation-maximization algorithm [362], which allows us to assign a Bayesian information criterion (BIC) [363,364] for selecting the best model. This section of the analysis was carried out using the statistical package "mclust" of the software R [365] .

II-11-4 Spatial and temporal contagion patterns: identification of cellular automata rules for the propagation of infestation

Cellular automata (CA) are spatially and temporally discrete system characterized by local interaction and synchronous dynamical evolution [366]. Usually, CA is used as a modeling approach to mimic the behaviour and pattern of the spread of an infestation. However, our objective was to find the likely geometrical configuration (rule) of the spread of infestation to uninfested maize plants by considering each maize plant as an element, which is attributed a state (infested/non-infested), which was assumed to change depending on the plant's state and the states of the plants in its vicinity. Hence, CA is useful for investigating the spatial pattern of the nearest neighbouring plants around a safe central plant that is most likely the source of the contagion. The minimal neighbourhood for the CA is estimated via the application of the algorithm described in [366]. The methodology was structured as follows: (i) the state of each plant and its neighbours are collected in a maximal neighbourhood radius (initially fixed), then the primary neighbourhood of a plant is formed by 24 maize plants (Figure 6); (ii) the initial neighbourhood was reduced by selecting the configuration that minimized the variance between the CA results and the data; (iii) in the obtained neighbourhood, the plants without any effect on the state of the central plant are removed; (iv) the BIC is used to determine the neighbouring configuration that has the most significant impact on the change of state of the central maize plant. This approach was implemented in Matrix Laboratory [367].

Model identifier	distribution
EII	Spherical
VII	Spherical
EEI	Diagonal
VEI	Diagonal
EVI	Diagonal
VVI	Diagonal
EEE	Ellipsoidal
EEV	Ellipsoidal
VEV	Ellipsoidal
VVV	Ellipsoidal

Table 4: Model identifiers use three letters encoding the geometric characteristics: Volume-Shape-Orientation. E means equal, V means varying across clusters and I refers to identical orientation [361].

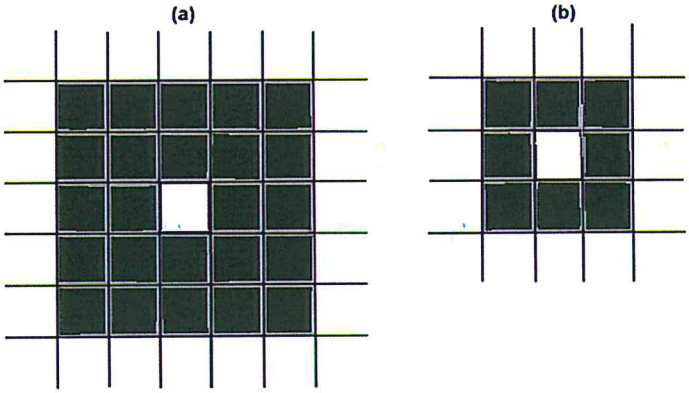

Figure 6: Neighbourhood plant configurations (black colour) around the central plant (white colour). (a) Representation of the extended Moore neighbourhood types the central plant possessing the label number 1 the rest are labelled randomly from 2 to 25. (b) Representation of the Moore neighbourhood type. We consider the central plant possessing the label number 1, the rest are labelled randomly from 2 to 9.

II-12 Preliminary analyses III: Yield losses analysis

Data were subjected to one sample Kolmogorov-Smirnov (K-S) normality test [368,369]. The means values of physical features of stems and ears from both non-infested and infested plants were compared using Welch's two sample Student t-test for pairs of normally distributed data [370,371] and, the Wilcoxon's two samples test was used for pairs non-normally distributed data [372]. The Fligner-Killeen (F-K) test was used to assess variance homogeneity between plots [373,374]. All the statistical tests were considered as less significant for p-values equal or greater than 0.05.

To determine yield loss, only the cob masses were considered [160,163,165,375]. Yield loss is frequently expressed as the fraction (percentage) of the attainable yield gone because of pest injuries [152,173,175]. It is then called relative yield loss (*RYL*), and is computed as: $RYL=100\times[(Y-Y_i)/Y]$ [52,152,161,173,175–180]. Yield loss was expressed as a difference of mean cob masses between the un-infested (Y) and infested plants (Y_i). In addition, the total losses per hectare were estimated by summing the difference between the average value cob masse from non-infested plants and individual value of cob masses from infested cob, then the result is divided by the plot surface value and expressed in hectare.

The estimate of the parameters of the damage functions which links *B. fusca* tunnel length and corresponding cob masses was conducted through nonlinear least square using Levenberg-Marquardt method [376,377]. The goodness of fit and selection of the candidate nonlinear functions was operated with the Akaike Information Criteria (AIC) [363] and, the R-squared. The linear link between the evaluation of yield losses and the mean cob tunnelling were done by using the Person's correlation coefficient (PCC) [378]. All analyzes were conducted with the statistical software R [365].

II-13 Modelling infestation spread

II-13-1 Critical percolation scale

Two scales (critical and non-critical) of leaf damage spread caused by *B. fusca* were distinguished. Using the percolation theory, the critical threshold scale of spatial resolution necessary to representing farm infestation is estimated. The estimate is operated from the temporal trends of the number of infested and isolated clusters of plants; derived from the spatial and temporal infestation of collected data. A cluster is set of infested adjacent cells (or one cell) that are (is) isolated from other infested cells by non-infested cells. To determine the percolation threshold the following procedures were taken: (i) a scale to visualize the infestation spread was selected, (ii) an isolated clusters formed by infested and isolated patches of maize plants were counted using cluster labelling techniques [379,380] and (iii) the number of clusters was plotted as a function of the number of sampling weeks. The three steps above were repeated for different scales until the final scale of the percolation threshold was obtained. This corresponds to the dimension that allows the observation of the number of isolated cluster of infested plants at a certain time to start decreasing (see the Figure 7 for a comprehensive diagram summarizing procedures for the percolation threshold estimate).

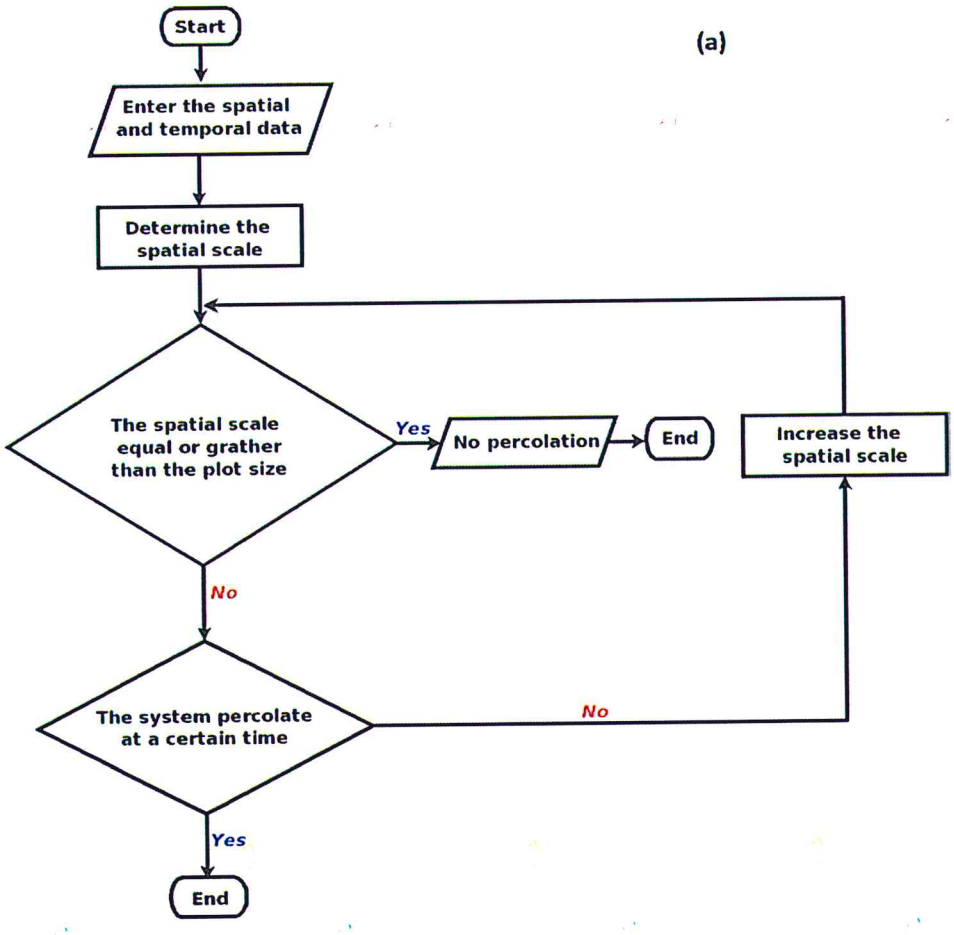
(a)
Start
Enter the spatial and temporal data
Determine the spatial scale
The spatial scale equal or grather than the plot size
Yes
No percolation
End
Increase the spatial scale
No
The system percolate at a certain time
No
Yes
End

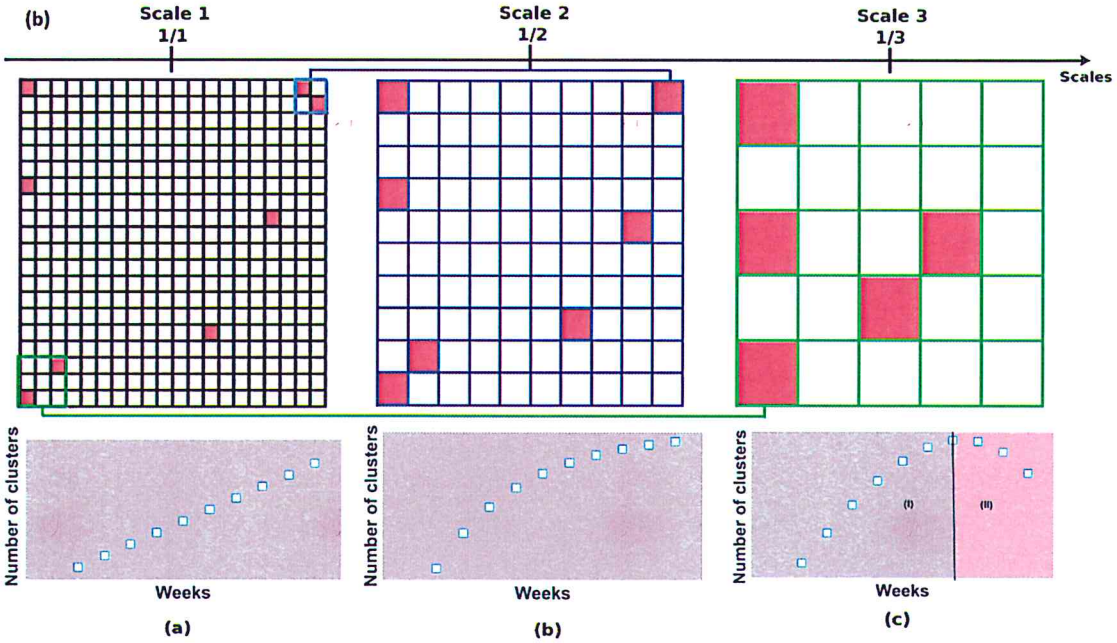

Figure 7: (a) Process for the spatial percolation threshold estimate before starting the CA simulations. (b) Graphical illustration of the overall process for varying the scale and detecting percolation threshold value. The lattice grid in sub-figures depicts a typical spatial and temporal data at a fixed week. The red cells in (a) are the infested maize plants. In sub-figures (b) and (c) the initial scale of observation for infestation dynamic (represented in sub-figure (a)) is reduced to 1/2 (2 cells × 2 cells) and 1/3 (3 cells × 3 cells) respectively. If at least one cell of the spatial lattice in (a) are present in the unit cell of the re-scaled map in (b) or (c), then that new unit cell is also assumed to be infested. The spatial resolution threshold is obtained when the temporal pattern depicted bellow the lattice grid in (c) is obtained. The temporal trend in (c) allows to distinguish two phases: in the left portion colored in gray (I) the isolation phase which correspond to the increase of the total number of infested clusters and in the right portion colored in pink (II) the connection phase which is the reduction of the total number of infested clusters (subsequent connection of isolated and infested clusters) with time. The maximum number of the curve represent the creation of the *first* connection among isolated and infested clusters of the lattice.

II-13-2 Cellular automata set up

The cell size selected for CA simulations was identical to the critical scale obtained for the percolation threshold. The CA cell was assumed to have only two states: infested and non-infested. Once a cell is infested, it never recovers. The temporal step of CA was fixed at 1 week; which corresponds to the time interval during data collection. The model assumed that the central cell is contaminated by others cells in the neighbourhood following the rule of type Moore (Figure 6). The edge effects were represented by fixed boundary conditions [381]. The central cell was considered to be changing state if a certain number of cells were infested in the neighbourhood.

II-13-3 Fuzzy scattering

The fuzzy rules applied in this work consist of 1 input, 1 output and fuzzy rules of the form "IF-THEN". The statement: "*number of flying adults is a decisive factor for the damage dispersion*" is imprecise. It was assumed that; if the infestation propagation is boosted by the abundance of adults, then the neighbourhood of infestation spreading can be augmented based on a propagation index (p), which is related to the number of adult (Na). So the neighbourhood is extended/shrank at a rate p. We considered that $p = p(Na)$. However, this dependence is only partially known by means of rules of the type: "*higher the value of Na, the higher p will be*". According to entomologists and crop protection experts, if the number of adult catches by pheromone-baited trap is higher, the damage incidence is higher thus infestation propagation could also be higher [382–390]. Expert knowledge about the link between the adult abundance in insect trap and the damage spread is imprecise and not well formulated mathematically. With this expertise on the dependence of p with respect to Na, we formulated the following rules translated by fuzzy inference system:

Rule 1: if (Na is very small) then (p is very weak)

Rule 2: if (Na is small) then (p is weak)

Rule 3: if (Na is medium) then (p is moderate)

Rule 4: if (Na is big) then (p is strong)

Rule 5: if (Na is very big) then (p is very strong)

If one rule is applied, the others can still be applied, too. The implication rule developed by [391] was further applied to link the input to the output. The real values of the fuzzy system output were computed using central-gravity-defuzzification formulae proposed by [392]:

$$\bar{z} = \frac{\int z \cdot \mu(z) dz}{\int \mu(z) dz} \tag{44}$$

Where $\mu(z)$ is the membership function, z the fuzzy variable and $\bar{z}$ the real value associated to fuzzy variable z. The triangular membership functions are represented in (Figure 8) (see appendix for more details about the methodology). We assumed that if the real value of the output $\bar{p}$is in the interval [0 0.25] then the index is weak and the corresponding neighbourhood is Moore-1. If $\bar{p}$ is in the interval]0.25 0.75] then $p$is moderate and the neighborhood is Moore-2. If $\bar{p}$ is in the interval]0.75 1] then p is strong and the neighbourhood is Moore-3. The index $\bar{p}$ taking effect on a precise week corresponds to the values computed in the previous two weeks. This assumption is based on the fact that the leaf damage from *B. fusca* larvae is only noticeable approximately two weeks after egg laying.

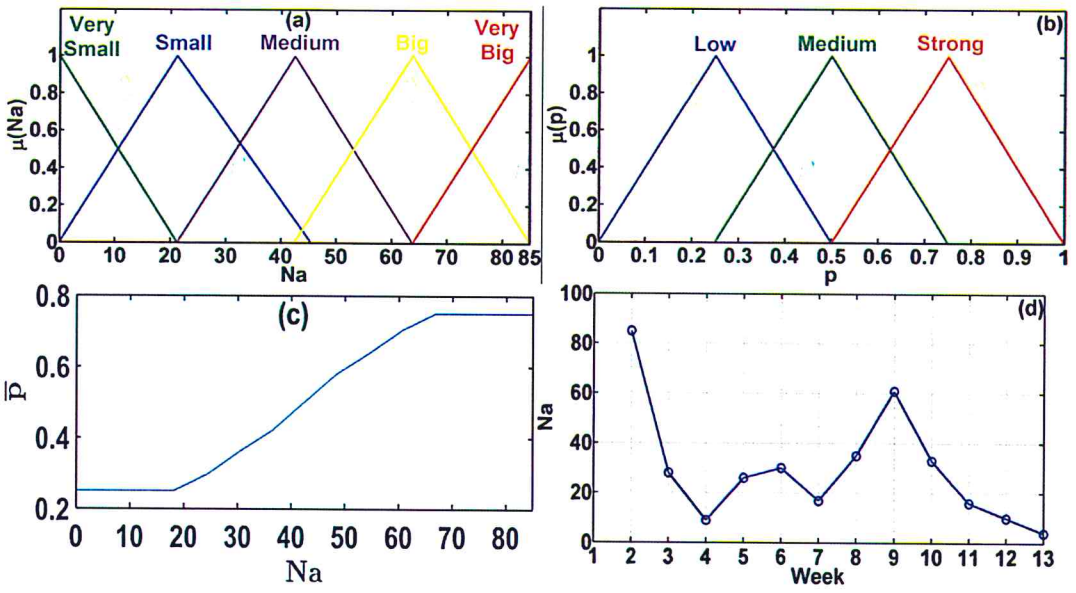

Figure 8: Representation of the fuzzy processing of data. In the upper panels, membership functions of the input variable number of adults (*Na*) and the output variable propagation

index ($\overline{p}$). In the lower left panel, the solution given by the fuzzy inference system. In the lower right panel, the collected data from the field are represented.

II-13-4 The complete model

The CA modelling was implemented as follow: (i) The minimal cell size for capturing the percolation phenomena was estimated (ii) The minimal possible neighbourhood for spatial and temporal contagion was assumed to be the Moore-1 (iii) Through fuzzy inference system (FIS), the propagation index was selected and the neighbourhood was changed. Finally, after a succession of trials and errors, the best number of infested cells in the neighbourhood of the central cell was selected [393–397]. Let's take a symbol δ as the threshold number of infested cells in the neighbourhood provoking infestation of the inner safe cell at week $n+1$. Depending on the type of selected neighbourhood, there are three possible threshold numbers of infested cells named $\delta_1, \delta_2, and\ \delta_3$ corresponding to Moore-1, Moore-2, and Moore-3 respectively. The operation $\sum State$ is the summation of all the cell states in the neighborhood. The summation is for 9 cells (Moore-1), 24 cells (Moore-2) or 48 cells (Moore-3). If this summation is strictly greater than δ, then the inner cell becomes infested during the following week. The model with each component is summarized in a flow chart (

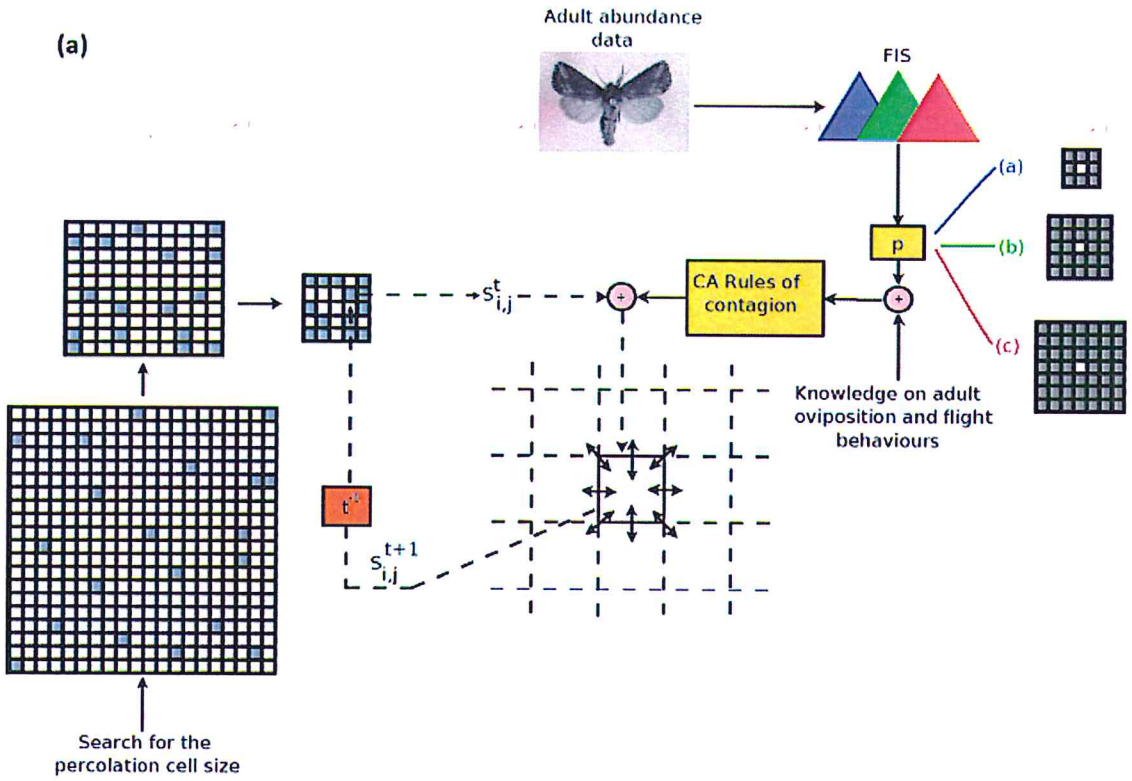
(a)
Adult abundance data
FIS
(a)
(b)
(c)
p
CA Rules of contagion
Knowledge on adult oviposition and flight behaviours
Search for the percolation cell size

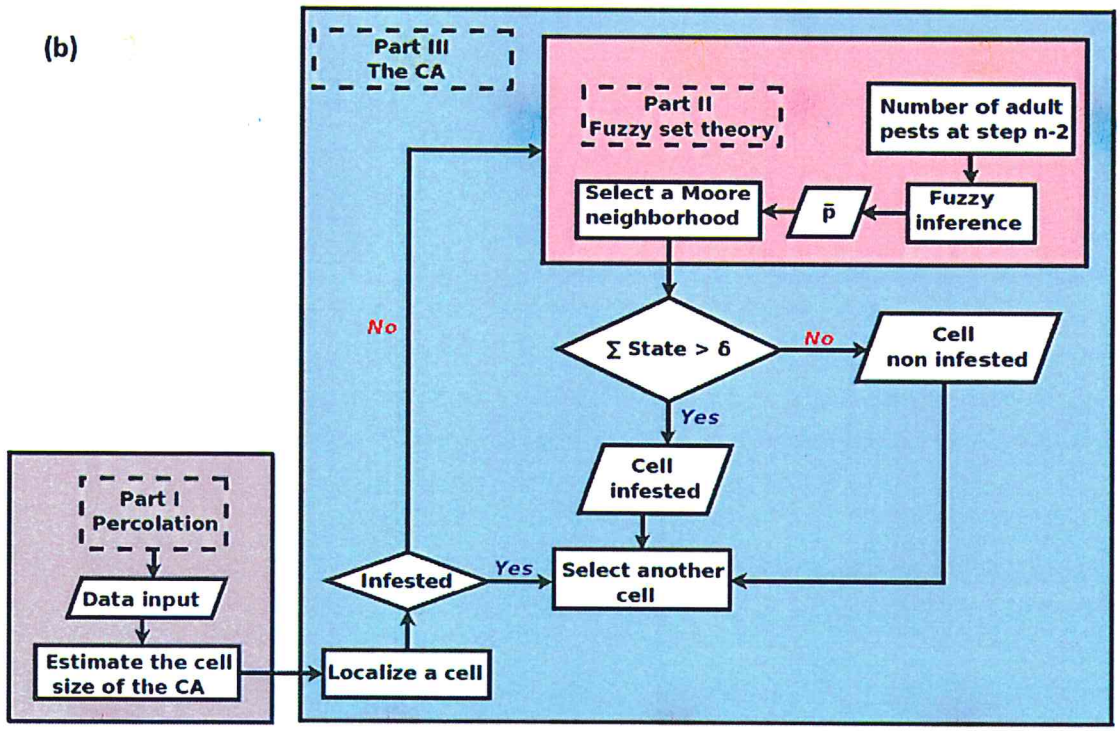
(b)
Part III The CA
Part II Fuzzy set theory
Number of adult pests at step n-2
Select a Moore neighborhood
p̄
Fuzzy inference
No
Σ State > δ
No
Cell non infested
Yes
Cell infested
Part I Percolation
Data input
Estimate the cell size of the CA
Infested
Yes
Select another cell
Localize a cell

Figure 9).

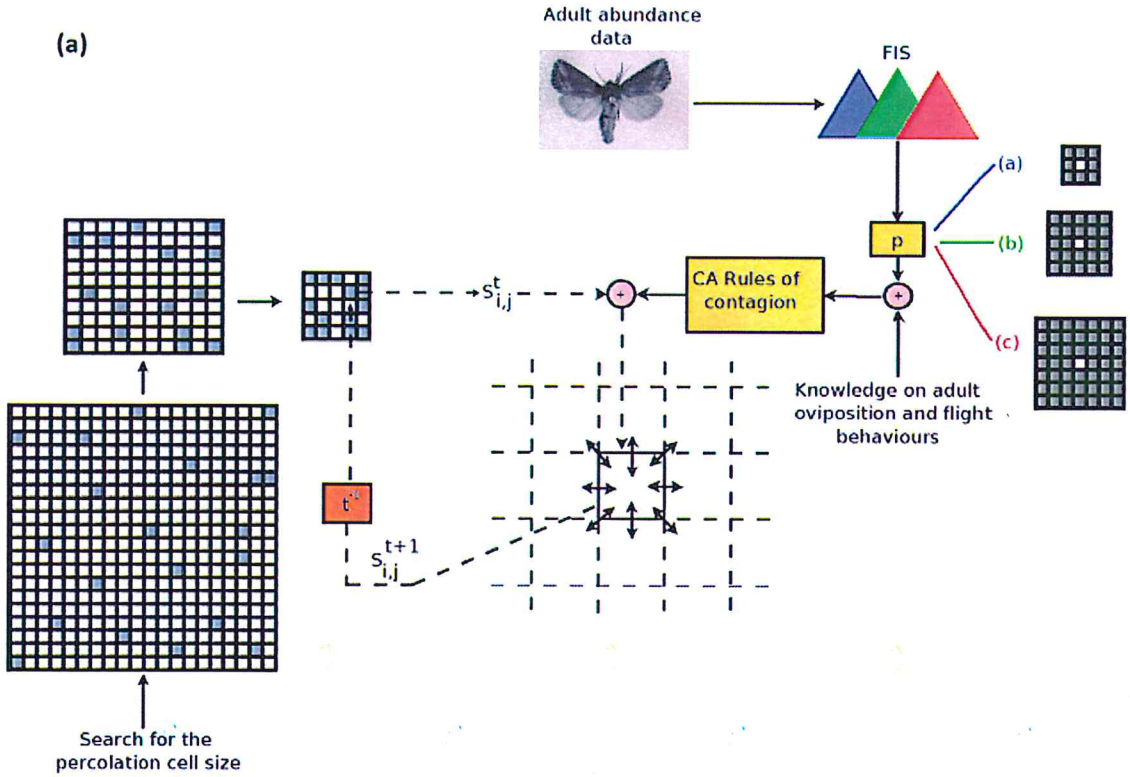
(a)
Adult abundance data
FIS
(a)
(b)
(c)
p
CA Rules of contagion
Knowledge on adult oviposition and flight behaviours
Search for the percolation cell size

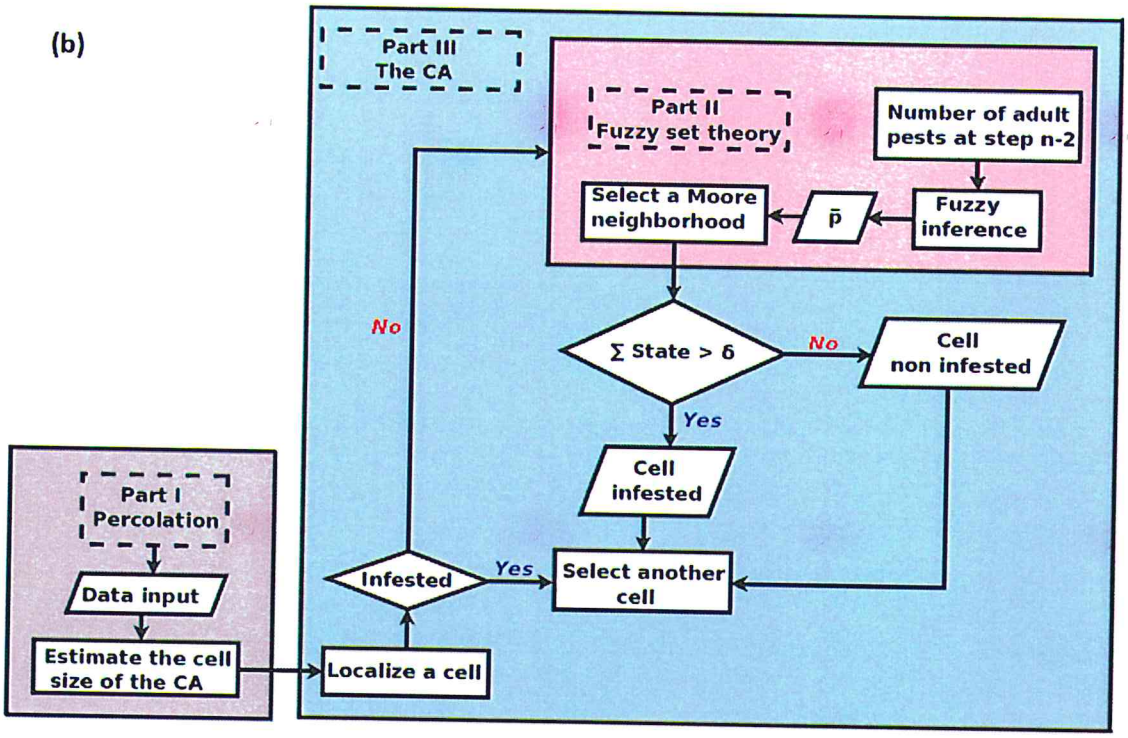

Figure 9: (a) Diagram summarizing the approach for modelling in field condition the leaf damages spread caused by *B. fusca* larvae. The grid cells are abstractive representations of the maize field quadrates. The approach is based on the combined application of cellular automata (CA), fuzzy logic systems and percolation. The three type of Moore neighbourhood selected after fuzzy calculus are represented: (a) Moore-1: the central cell surrounded by 8 cells, (b) Moore-2: the central cell surrounded by 24 cells and (c) Moore-3: the central cell surrounded by 48 cells. Where FIS = fuzzy inference system, S=state, (i,j) = coordinates, p = propagation index and t=time. (b) Overview of the model and the sub-models. The model is made of three sub-components: the part I estimating the cell size during all the simulations, the part II inferring the adults *B. fusca* abundance via the fuzzy sets theory and the part III determining the state of a cell at a week $n+1$ based on its current state and those of all its neighbours at week n. Part I is not involved in the change of states and rules of the CA, reason why it is drawn aside. In contrast, the fuzzy logic is applied during the whole simulation. We recall that the cell has only two states: infested (1) or non-infested (0).

II-13-5 Model validation, testing and uncertainty assessment

To measure the performance of the developed model using field data; cells infested at the initial stage were assumed to remain the same as observed during the first week of infestation [245], and subsequent state of other infested cells was predicted using CA simulations. Correlation coefficient between observed and predicted binary pixel image matrices was computed using two-dimensional correlation formulation [398]:

$$\rho = \frac{\sum_j \sum_i (A_{ij} - \bar{A})(B_{ij} - \bar{B})}{\sqrt{(\sum_j \sum_i (A_{ij} - \bar{A})^2)(\sum_j \sum_i (B_{ij} - \bar{B})^2)}} \quad (45)$$

where A_{ij} and B_{ij} are the observed value during the data collection and the predicted value at the cell (i, j) respectively, $\bar{A}$ and $\bar{B}$ are the average numbers of infested cells inside the plot. When ρ is close to 1, the level of agreement between the model predictions and field data is greater.

The cellular automata modelling framework also provides an additional feature; the information fractal dimension (D_i). D_i was evaluated using the methodology proposed by [399]. If the value of $D_i$is closer to 2, the highest is the probability of infested patches to recover their initial surface [276]. In the contrary, if the value of D_i is very weak, the patches are much clumped and the gaps between patches are more important [276]. To assess the level of agreement between the spatial distributions of infested cells obtained from model prediction and the data, the multifractal dimension of the observed and the predicted maps were compared. The error was evaluated by estimating the absolute value of the difference between D_i of the predicted map and observed map. In addition, the coefficient of determination (r^2) was evaluated to assess the goodness of fit of the multifractal dimension estimate [400–403].

II-13-6 Sensitivity analysis

The aforementioned CA modelling approaches help us understand how specific rules governing change lead to certain types of spatial patterns. Analysis of CA sensitivity consisted

of; fixing the threshold number of infested cells in the neighborhood (δ) to provoke infestation at the following week and then compute the output taken here as the mean correlation coefficient ($\bar{\rho}$) estimated by averaging the different correlation coefficients obtained while comparing all the model outputs and the observed data at each week. A multi-linear regression liking the values of this mean correlation as response variable controlled by the threshold number of cell for infestation was formulated as follow:

$$\bar{\rho} = \sum_i \alpha_i \delta_i + \varepsilon, \tag{46}$$

where δ_i threshold number of infested cells in the neighbourhood i, α_i are the slope of the regression quantifying the contribution of each neighborhood configurations and ε is the intercept. Coefficients α_i are considered significant for a P-value less than 0.05. Significance implicates that changes in the slopes values are significantly associated to the change of $\bar{\rho}$ and demonstrate potential impact of each neighborhood configurations on the accuracy level of the CA. The ability of the linear model (3) to explain all the variability of $\bar{\rho}$ around its mean has been done by calculating the r^2. In order to assess the model performance, the combination of threshold values for infestationδ_i providing the maximal $\bar{\rho}$ are selected. Furthermore, the running time (in seconds) are recorded after simulations of damages spread with different scales and previously estimated thresholds. Only the scales less or equal to the percolation threshold values were considered.

II-14 Coupling the pest dynamic and the CSM

In order to explore the effect of the pest on the plant, the data collected during in an experimental study conducted at Gainesville at the University of Florida in the USA have been used [53]. The maize cultivar McCurdy 84aa was planted the 26th February 1982 in a row spacing 61.0cm and 7.2 plant/m2. The application of the nitrogen fertilizer was very low and, the field was rainfed. The soil was loamy and silicate. The daily solar radiation, minimum temperature, maximum temperature, rainfall and wind speed were collected near to the field by instruments located at latitude 29.630m, longitude -82.370m and 10 meters above the ground [53]. This geographical location present a typical

In general, insect develops slower or faster if the temperature is low or high; thus it is a vital factor regulating the life history of insects [404]. In this study, the phenology restricted to the temperature as the key driver have been used here to simulate the fecundity, development, and mortality of *B. fusca*. The female oviposit about 90% of its eggs during the first 3 nights [183]. In the model, it is assumed that the proportion of the laid eggs (ϕ) eggs depend on the age of the adult females (α):

$$\phi(\alpha) = \frac{a_1}{1 + b_1 \exp(c_1 \alpha)} \tag{47}$$

where a_1, b_1 and c_1 are equal to 0.6, 0.0031 and 0.5085 respectively. In a controlled experiment, the total number of eggs laid increased between 15^{O}C and 20^{O}C then decreased with the following function [320]:

$$\psi(T) = \exp(-3.7017 + 0.8449T - 0.0188T^2) \tag{48}$$

where T is the temperature. The mean sex ratio between males and females is 1:1.1 [187,405]; then an average of 60% of the female is assumed to emerge from laid eggs; thus total number of eggs laid per day by an adult was estimated as $F = 0.6\phi(\alpha)\psi(T)$. The temperature dependent mortality rate at immature life stages are defined by the following functions [320]:

$$\begin{aligned} \mu_E(T) &= \exp(5.0138 - 0.4869T + 0.0100T^2), \\ \mu_L(T) &= \exp(3.8718 - 0.3872T + 0.0078T^2), \\ \mu_P(T) &= \exp(7.6441 - 0.7716T + 0.0175T^2), \end{aligned} \tag{49}$$

The functions $\mu_E(T)$, $\mu_L(T)$, $\mu_P(T)$ represent the mortality rate for eggs, larvae and pupae respectively. Following the method in reference [308], the mortality rates have been put in the inverse power or the longest development period ($(\mu_L(T)^{\frac{1}{\eta}}$, $\mu_E(T)^{\frac{1}{t_e}}$, $\mu_P(T)^{\frac{1}{t_p}}$), where t_e, t_l and t_p are 20 days, 168 days and 37 days respectively [320]. The developmental rate and ageing rate of the insect at each immature life stages and adult stage respectively are estimated as follows:

$$D_{1\to n} = \sum_{day=1}^{day=n} \left[\int_{0h}^{24h} R_x(T^{day}(h))dh \right], \quad x = E \to L, L \to P \; or \; P \to A \tag{50}$$

$$S_{1\to n} = \sum_{day=1}^{day=n} \left[\int_{0h}^{24h} SR(T^{day}(h))dh \right], \tag{51}$$

where R_x (in day-1) is the daily developmental rate with E, L, P and A representing eggs, larvae, pupae, and adult respectively. The equation (8) has been used to estimate the ageing rate where the symbol SR represent the senescence rate for the adult. The variable h is the hourly temperature of the insect estimated via the sine-wave approach [406–408]:

$$T_h(h) = \frac{T_{\max} - T_{\min}}{2} \sin\left(\frac{2\pi h}{24}\right) + \frac{T_{\max} + T_{\min}}{2}. \tag{52}$$

The variables T_{min} and T_{max} are the daily maximum and minimum temperature respectively. The functions R_x and SR (see the Appendix 1) are estimated from data in the literature [320]. The eggs laid by females at each day constitute a new cohort which population dynamic is simulated with the following set of coupled differential equations:

$$\begin{aligned} \frac{dE}{dt} &= FE - (\mu_E + \sigma_E)E, \\ \frac{dL}{dt} &= \sigma_E E - (\mu_L + \sigma_L)L, \\ \frac{dP}{dt} &= \sigma_L L - (\mu_P + \sigma_P)P, \\ \frac{dA}{dt} &= \sigma_P P - \mu_A A. \end{aligned} \tag{53}$$

If $D_{1\to n}$ is equal to 1, the development at the corresponding immature life stage is completed, then σ is equal to one, μ_A have been arbitral fixed at 10%. If $S_{1\to n}$ is equal to 1 all the survivor adults die due to ageing. The relative growth rate (RGR) according to the temperature is given by [319,409]:

$$RGR(T) = -0.0011T^3 + 0.1382T^2 - 4.6218T + 49.870 \tag{54}$$

The qualitative change of food during the maturity of the plant can induce diapause in some tropical insect and in *B. fusca* in particular [318,410]. The *B. fusca* larvae are most likely to start a diapause when the nutrient quality provided by maize plant becomes lower [318].

Moreover, the quality decreases with the age of the maize plant, which indirectly force the larvae to stop feeding itself. The link between the plant maturity and the regulation of the mass accumulation by the larvae (symbolized by k) has been formulated the following set fuzzy rules:

Rule 1: if (the plant is very young) then (k is low)

Rule 2: if (the plant is young) then (k is low)

Rule 3: if (the plant is old) then (k is moderate)

Rule 4: if (the plant is moderately old) then (k is high)

Rule 5: if (the plant is very old) then (k is high)

The process of fuzzification of the age of the maize plant in weeks given by: very young (6-9 weeks), young (8-11 weeks), old (10-13 weeks), very old (12-15 weeks) [318]. The details of the methodology are provided in the appendix. The symbol k represents the feedback and, $(1-k)RGR(T)$ is the mass assimilated/consumed by the *B. fusca* larvae. It is assumed that the consumption is done in 99% stem boring and 1% in leaf feeding. This has been done in the program by subtracting these percentages in the equation (1). The *RGR* estimated from the data of Ntri et al. [319,409] allow us to estimate the dynamic of the larvae mass (M_L) by the differential equation:

$$\frac{1}{M_L} \times \frac{dM_L}{dt} = (1-k)RGR(T), M_L(t=0) = 0.0 \quad (55)$$

In order to assess the effect of the insect on the plant, we will only focus on the accumulated biomass above the ground and the leaf area index. The leaf area index is a ratio between the surface covered by the plant canopy and the ground surface [411]. It is a very important variable that characterizes the ability of the plant to intercept light for photosynthesis [411].

II-15 Conclusion

In conclusion, different techniques to generate discrete breather, to investigate the linear stability and the noise effect in a modified Davydov's model were presented. The estimate of the supratransmission and infratransmission threshold foe electrical wave in microtubules were estimated. Furthermore, the techniques used to analyse data, and to

subsequently design a model based on these data were presented. In what follows we will present the obtained results and discuss them subsequently.

Chapter III: Results and discussions

III-1 Introduction

This chapter present the main results obtained in this thesis. It is subdivided in five parts dealing with the anharmonic and noise effects on Davydovs solitons, the electrical waves transmissions in microtubules, the analysis of *B. fusca* damages, the spatial and temporal modelling of *B. fusca* damages and finally the coupling between pest population dynamic and maize crop growth dynamics.

III-2 Discrete Davyvov's soliton in alpha-helical proteins with anharmonic bond and thermal noise

III-2-1 Results

The representation of the eigenvalue (15) as a function of the frequency is depicted in Figure 10(a). For a positive value of ω we have both 1D unstable and stable manifolds $W^u(W^s)$ given by $\eta = \lambda_+\theta$ $(\eta = \lambda_-\theta)$ around the saddle point P_0. In Figure 10(b), the homoclinic crossing of stable (gray) and unstable (black) are calculated. The localized mode emerging from tangles are plotted in Figure 10(c) and Figure 10(d). exciton has the pulse

shape while the phonon amplitude has the shape of a kink. These forms of both excitations are the same generated by the classical model of Davydov in the continuous approximation. After a perturbation of the stationary solution, the localized mode is linearly stable (Figure 10(e)); this is confirmed by the numerical simulations (Figure 10(f)). However, the wave has to be mobile to carry information through the protein.

The mobility of the ABE is represented in Figure 11(a). The numerical simulation of the original model of Davydov including an impurity (23) with an approximate stationary pulse solution as initial condition is depicted in Figure 11(b). The solitary wave has an amplitude that increases during the collision at $\tau = 100$ with radiations losses. It can be noticed that moving breather is created after the collision and the mobile portion moves in the same direction of ABE propagation. Referring to Figure 11(c), breather oscillates spatially with a low amplitude in order of 10^{-16} around the position initial solution. This is an effect of the Pierl-Nabaro barrier [335]. By considering the obtained DNLSE (12) with inverse hyperbolic nonlinearity (Figure 11(d)), there a splitting of the wave in three parts. Two of them move in the opposite direction than the impurity and, one of them in the same direction. The portion of the wave heading toward the impurity direction possess a low amplitude and moves relatively quickly, in the contrary, these moving in the opposite direction are slower and the amplitude of the middle waves is relatively high.

Numerical Simulation of Davydov's soliton in a thermal biological bath is displayed in Figure 12(a) and Figure 12(b). Solitary wave became more and more incoherent with time. However, in our model, the breather of 2D map is strongly localized and damped (Figure 12(c) and Figure 12(d)), with the presence of little radiations.

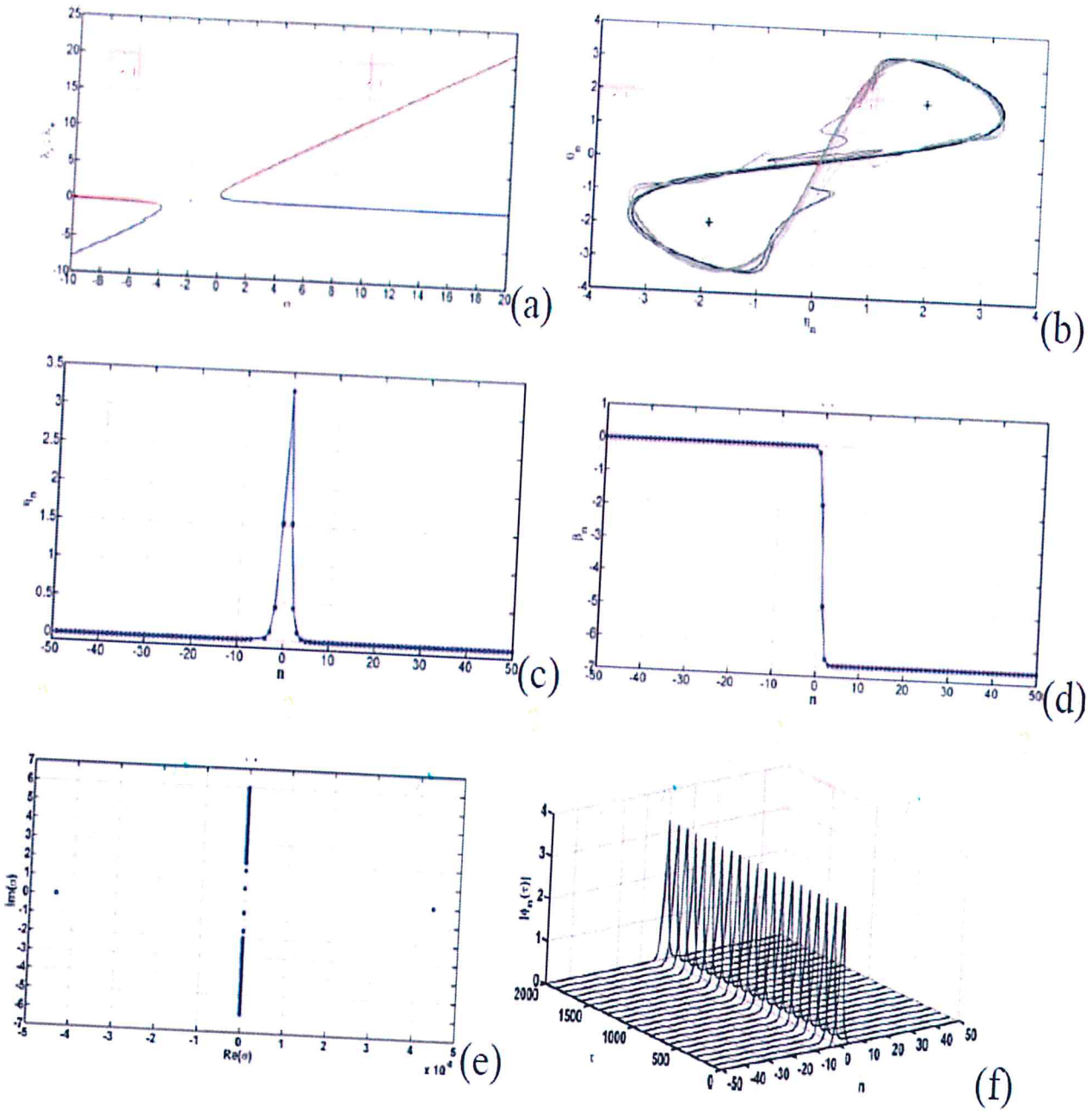

Figure 10: (a) Eigenvalues as a function of ω, λ_+ (red), λ_- (blue). For $\omega>0$ we obtain unstable and stable manifold around the origin. (b) Homoclinic tangles formed by stable and unstable manifolds (W^s and W^u). Unstable manifold in black, and stable manifold in gray. The

Saddle point P_0 is in red, and the fixed points $P_{1,2}$ are black cross. ω=2. (c)Localized modes centered in one site for the exciton amplitude η_n deduced from the 2D map. (d) The stationary amplitude of phonons β_n derived from the discrete equation. $\beta_{n+1} - \beta_n = -\text{arsinh}\left(|\phi_n|^2\right)$ (e)Eigenvalue spectrum for the linear stability analysis of the perturbed stationary exciton obtained from the homoclinic tangles of the 2D map. The complex eigenvalues are plotted in the complex plane under the form of dots (Im stands for imaginary parts and Re for the real part). (f) Numerical simulation of the nonlinear Schrodinger equation with the pulse 1(c) as an initial condition.

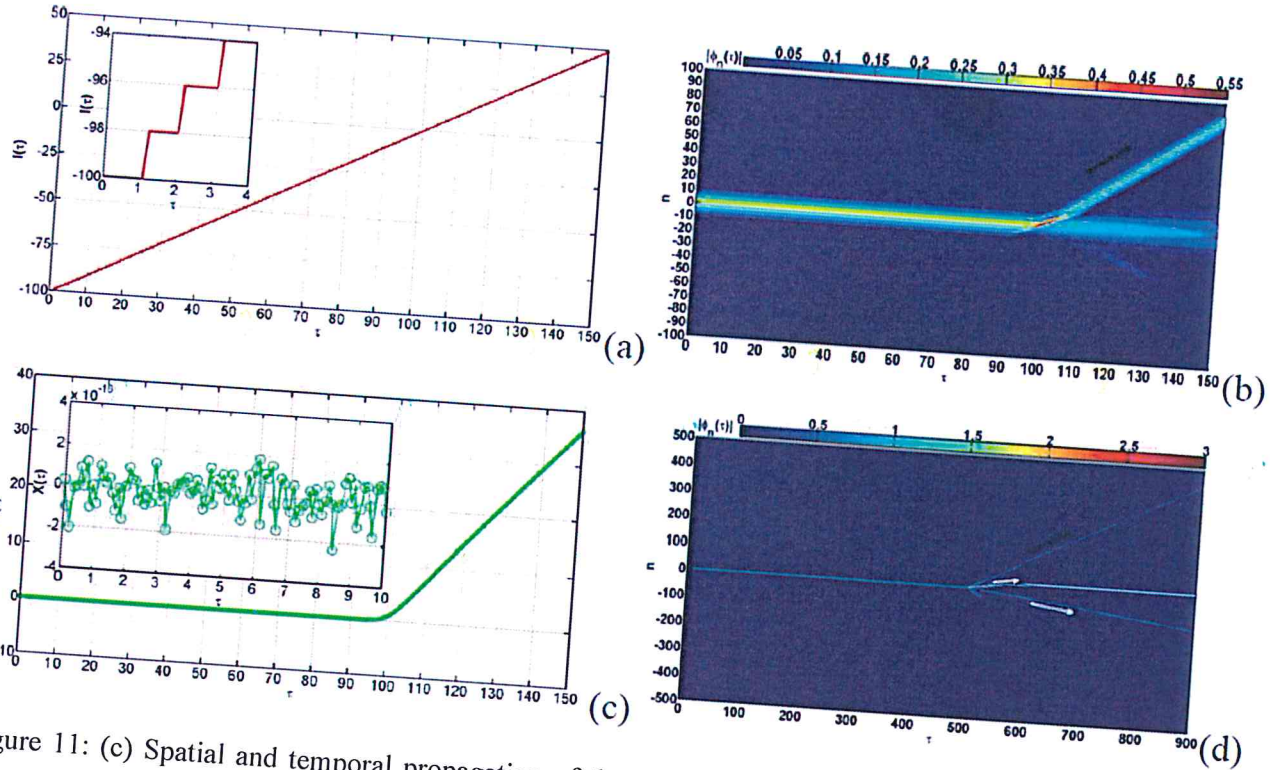

Figure 11: (c) Spatial and temporal propagation of the ABE vibratory energy. ABE collides Amide-I excitation at n=0 at $\tau = 100$. (b) Numerical simulation of the DNLSE with the cubic nonlinearity with the normalized pulse initial condition $\sqrt{1/8}\,\text{sec}\,h(n/4)$ [11] with null fixed boundary conditions. The black arrow indicates the portion of the wave moving toward the same direction than the impurity. (c) Plotting of the evolution of the soliton center in figure

11(b). (d) Numerical simulation of the DNLSE with the inverse hyperbolic nonlinearity. The initial condition is provided by the 2D map. Null fixed boundary conditions are used. The black arrow indicates the portion of the wave moving toward the same direction than the impurity. The lattice length has been taken larger than the case in (b) with the aim to assess possible collision between the middle hump and the upper one during a longer time period.

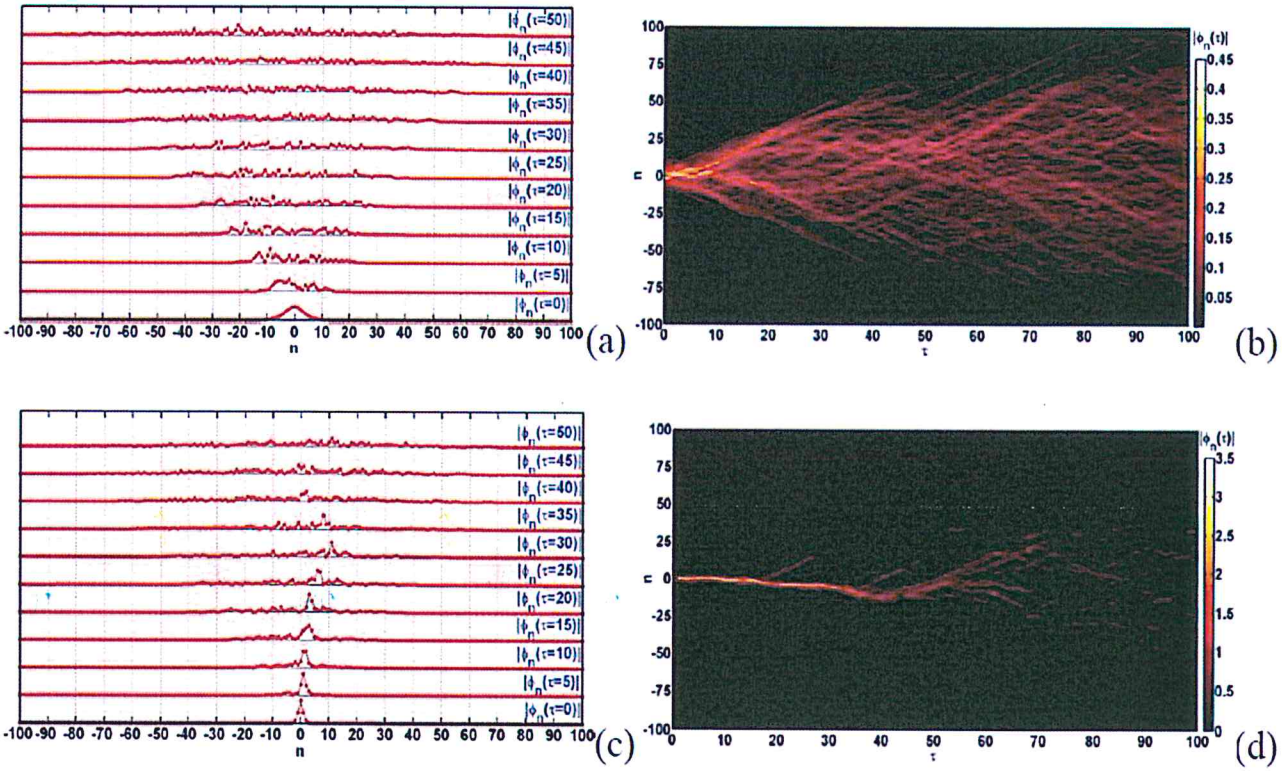

Figure 12: On the left side, the temporal snapshots of the exciton amplitude are represented ($|\phi_n(\tau=0)|$ *(bottom)* *to* $|\phi_n(\tau=50)|$ *(top)*), on the right side, the density plot are depicted. In (a) and (b), simulation of the coupled Davydov's equations with the initial conditions $\phi_n(\tau=0)=\sqrt{1/8}\,\mathrm{sec}\,h(n/4)$, $\beta_n(\tau=0)$, T=310K and Γ=2.406 $10^{12}s^{-1}$ [342]. In graphs (c) and (d), the same conditions are used with the exception of the pulse which is estimated from the 2D map.

III-2-2 Discussions

Some nonlinear potentials such as cubic [66–68] or Lennard-Jones [69] has been used to correct anharmonicaly the original Davydov's model. With the cubic potential [66–68], the initial conditions of the fully discrete model were derived from continuous approximation. This method assumes that the values of the physical quantity vary slightly from one lattice point to another. Thus making the equation to lose its discrete form and becomes continuous with partial differential terms. Such method can lead to neglecting higher other terms during Taylor's development, yielding a loss of accuracy in the final results. In Jones [69], the authors simulated numerically the fully discrete model with arbitrary localized initial values and the exciton-phonon collision was slightly stable. With the intention of getting more closer to the reality, we have chosen to use two-dimensional map approaches for finding intrinsic localized mode. The advantage of this method is the possibility of finding a solution by keeping the system discrete as much as possible.

The discrete nonlinear Schrödinger equation with inverse sine hyperbolic nonlinearity is very difficult to solve. According to our knowledge, it does not have an analytical solution. In this study, it was possible to find discrete intrinsic localized modes using 2D map approach as in DNLSE with various type of nonlinearities [329–335]. The original DNLSE of harmonic Davydov's equation has a cubic nonlinearity and it can be obtained from the DNLSE with inverse hyperbolic sine nonlinearity at very low amplitude by Taylor development around zero of the nonlinear term. Thus, biologically this equation could model production of high vibratory energy of amino acid during ATP hydrolysis.

The amide-I vibratory mode is most often the only excitation considered in Davydov's model for energy transport in alpha helix protein [11]. It is well known that many other excitations including the ABE were detected [63,72,73]. Moreover, the ABE was reported as not affected by the coupling with phonon and recognized as free exciton [63]. This was assumed to be an impurity and has been introduced in the DNLSE by a gauge transform [74,75,339]. In order to take into consideration, the effect of moving ABE along the protein, a version of an impurity with spatial and temporal impact was proposed. Although the effect of

the impurity was studied in molecular excitons, these type homogeneities did not trigger the mobility of the localized exciton [74–76]. In this work, a different version of spatiotemporal impurity was proposed and it achieved the mobility of localized mode.

Discrete breathers have a propensity to be strongly localized [412]. Many techniques can be used to move breathers. Some of the classical techniques are discrete Fourier transform [413] and energy kick [414]. For the Davydov's model particularly, mobility of the static soliton was achieved by kicking the initial stationary condition in the form of the analytical solution in the continuum limit [84], kicking the arbitrary discrete chosen initial condition for the exciton [343] , kicking the discrete initial condition [329] derived from numerical map method [415,416] or kicking the initial multi-peaked discrete breather [70]. We were able to realize the mobility of the discrete breather by using a hypothesized mobile ABE impurity as mediator. Such approach is different to previous works which consist to multiply (kick or apply a phase gradient perturbation) the stationary initial condition with an exponential function [65,70,84,329].

In the Davydov's model, the soliton is generated via ATP hydrolysis, which energy is transduced into the amide-I vibration that propagates along the protein chain, coupled with lattice distortion. The transport of the energy can be under the form of a single hump [84,343] or multihump solitons as described by analytical and numerical approximations [70,417–419]. Considering ABE vibration as an impurity which propagates along the lattice provided the mobility of static breather to the harmonic Davydov's model. In the anharmonic case, we observed a splitting of the stationary wave into multi-hump excitation which parts are moving in different directions. According to our knowledge this dynamical impact of the impurity is quite different from others inhomogeneity influences that were observed in DNLSE [335,339,420,421] and the multi-hump formation mechanism in Davydov's model [70,417–419]. Such mechanism in addition to the hyperbolic cosine potential for hydrogen bond might induce energy transport in more than one direction. It may be interesting in biological explications of transporting energy in multi-direction instead of a uni-directional case. Another biophysical significance could be the control of the movement of localized excitations on the polypeptide chains.

The problem of thermal instability of Davydov's soliton in a harmonic hydrogen bond potential has been investigated numerically [77–79]. Later, this instability was found due to: critical velocity of the soliton [80], the value of the nonlinear coupling between phonon and exciton [81,82], the disorder in the sequences of masses of amino acid [83] and multi-quanta state of the amide-I vibration [84]. Furthermore, most of the anharmonic Davydov's models did not include the noise impact [64,67,68,342]. Hamiltonian lattice with hard hyperbolic cosine type on-site potential was modeled [87]. Such potential shown the ability to regulate energy flow through the chain by accumulating energy of nonlinear localized mode in the presence of thermal noise [87]. Using the same type of potential for coupled Davydov's equations whereby the lattice equation is coupled with a Schrödinger equation has revealed that exciton keeps its shape longer in our proposed model than in the classical Davydov's equations. The present result is corroborated by the work on the anharmonic oscillation effect on the Davydov-Scott monomer in the thermal bath [86]. This work emphasized the importance of the nonlinear potential for controlling thermal noise which was not mentioned in studies [64,67,68,342].

III-3 Waves transmission and amplification in an electrical model of microtubules

III-3-1 Results

The numerical and analytical values are compared in Figure 13. for different values of the nonlinear coefficient B_1 and the forbidden band gap frequency ω. There is a good agreement between the analytical and numerical values of the thresholds. Using several numerical

simulations (

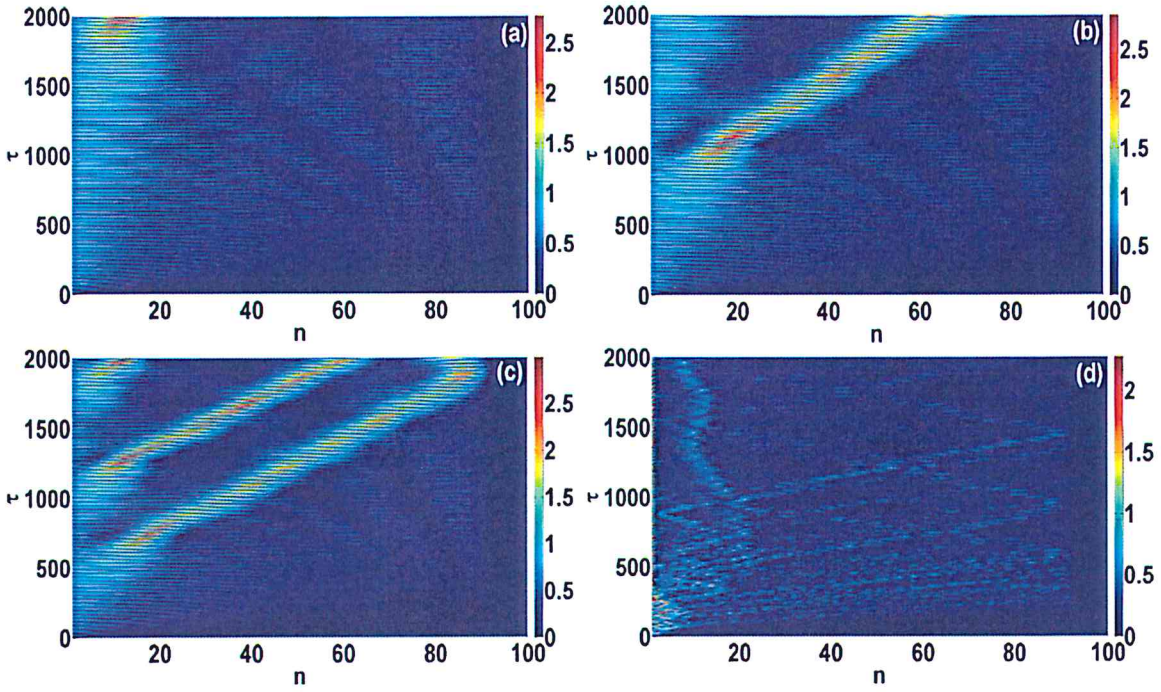

Figure 14), we assessed the validity of the value of the supratransmission threshold. If the value of the amplitude of the periodic driving is below the threshold, the wave does not reach remote sites whereas the solitons are generated if the value of the amplitude is slightly above the threshold. We further noticed that for very high values of amplitudes the wave is still transmitted but the soliton loses its coherence quickly. In Figure 15, two types of trends are depicted: when the value of B_2 is very low, the threshold amplitude decreases with r (Figure 15 (a)), while in contrast, the threshold amplitude increases with the augmentation of r when B_2 in high (Figure 15 (b)). In Figure 16, we made several numerical simulations for different values of the driving amplitude with a frequency inside the forbidden band gap. We noticed also that if the value of the amplitude is around or above the value of the analytical threshold, the wave is attenuated quicker than waves with amplitude very low compared to the value of the threshold amplitude. In Figure 17 we attempted to estimate the infratransmission threshold and obtained a value near 0.022.

Figure 18 (a) displays the results of the numerical simulations in the absence of the nonlinear resistance. Observed diminution on the amplitude of the stimulus due to the absence of negative nonlinear resistance is a phenomenon that has been reported in the literature [105]. By taking into consideration the effect of the negative nonlinear resistance, a significant amplification of the amplitude of the pulse voltage is observed (Figure 18 (b)). This result was also found in an experimental study using calcium ion [23] and it is of particular relevance in the potential use of MTs as nano-technological device, in which negative nonlinear resistance can be introduced into the system to capture the amplification of the signal. In order to identify the regions in the parameter space (B_1,B_2) where the amplification take place, we plotted in Figure 18 (c) the ability of the negative nonlinear resistance to amplify the input signal. The system (with the nonlinear resistance and the nonlinear capacitance) was simulated with the boundary condition V_{in} for a given value the parameters B_1 and B_2. If $\max_{1\leq n\leq N}(V_n(\tau=5))>V_m$ then the signal increases for the couple (B_1,B_2). The point in the space parameter is plotted with a black dot. Otherwise, The blank area represents the value of the coupling parameter that decreases input signal amplitude.

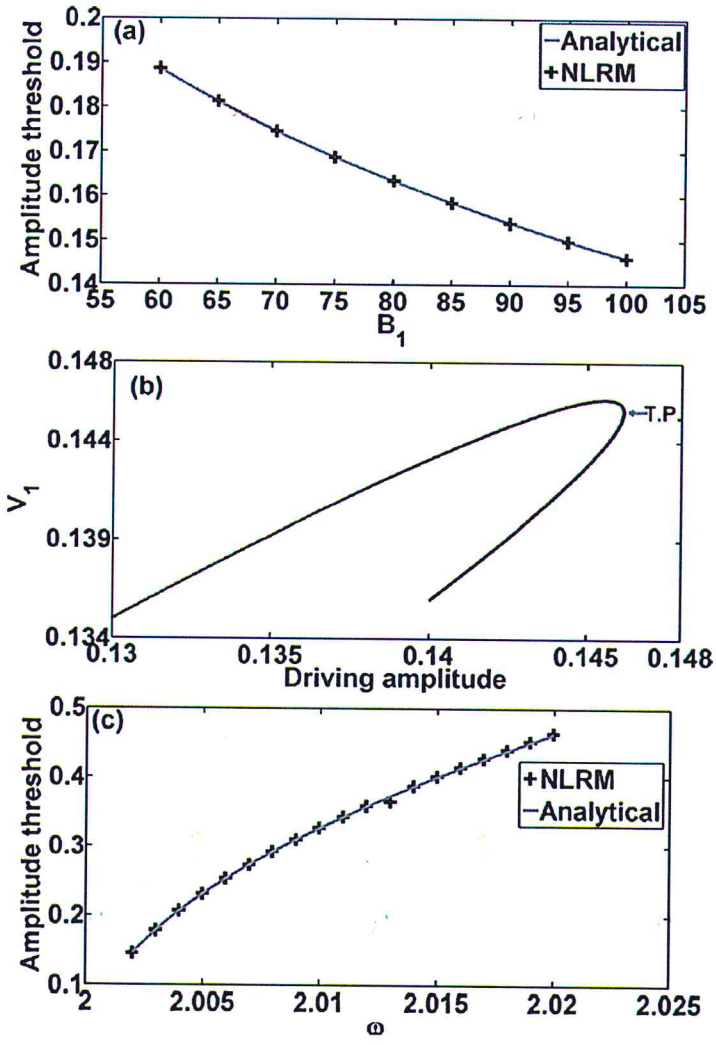

Figure 13: (a) Representation of the supratransmission threshold. The gray line is obtained using the analytical expression of the nonlinear supratransmission. The black cross is the numerical values of the threshold obtained by the NLRM projection. The values of the parameters are r=0.01, B_2=0.01, $\omega=\omega_c(1+0.1/100)$. (b) Display of the NLRM projection for the same set of the parameter used in (a) and B_1=100, $\sigma=\omega_c(1+0.1/100)$. The small gray arrow is pointing the turning point (T.P.) of the curve which represents the numerical value of the threshold driving amplitude (U). (c) Different values for the threshold according to different driving frequencies.

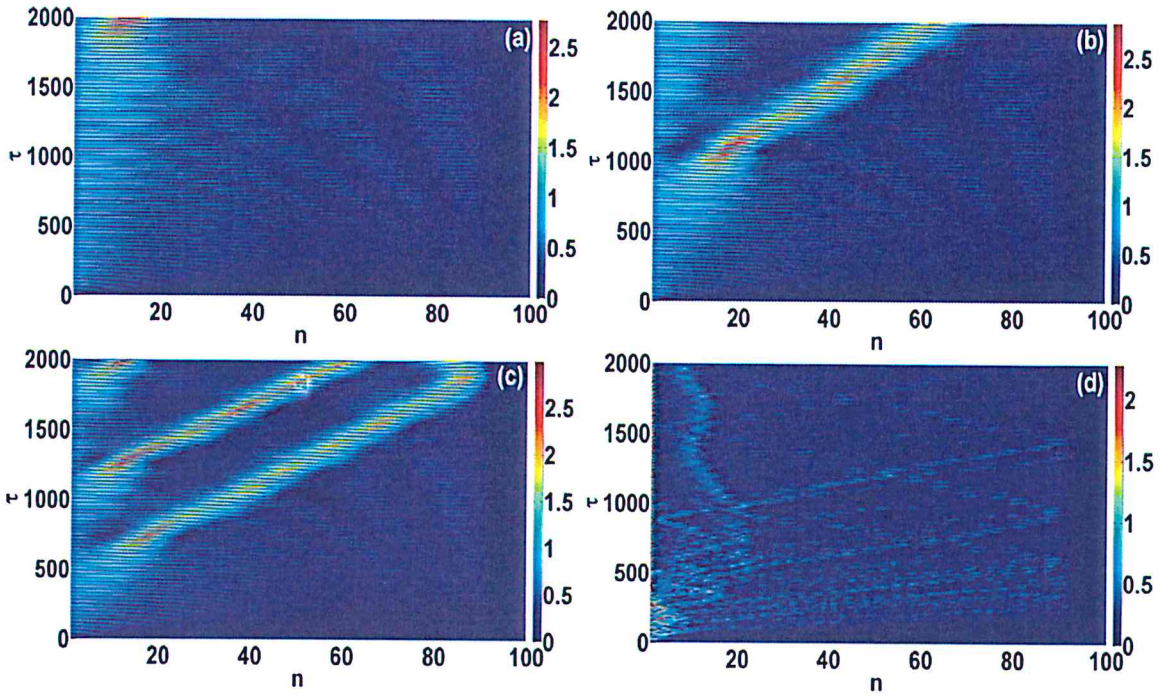

Figure 14: : Spatio-temporal evolution of the voltage through the lattice with the boundary condition $V_0(\tau)=U\exp(1-\tau/\tau_1)\cos(\omega\tau)$ with r=0.01, B_2=0.01, B_1=100, τ_1=10 , $\omega=\omega_c(1+0.1/100)$ and U_{th}=0.1461. The color bar at the right represents $|V_n(\tau)|/U$. (a) $U=U_{th}(1-10/100)$, (b) $U=U_{th}(1+10/100)$, (c) $U=U_{th}(1+30/100)$, and (d) $U=10U_{th}$.

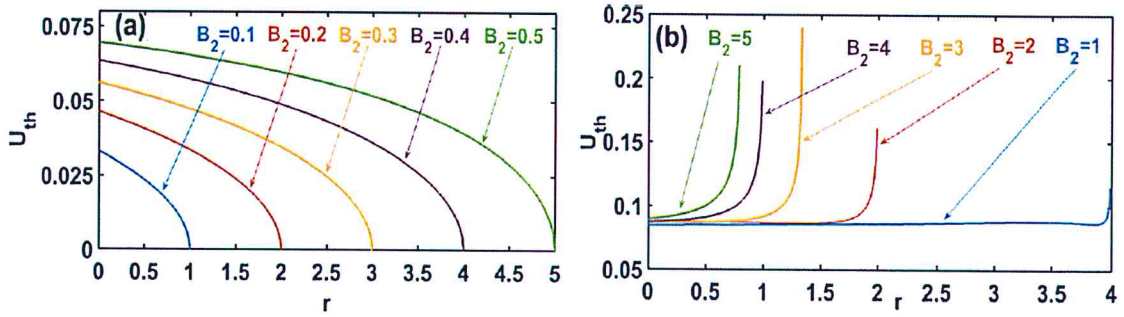

Figure 15: Variation of the estimated supratransmission threshold with the master equation containing the first order derivative of the voltage in respect to several values of r and B_2. The values assigned to B_1 and ν are 100 and 0.1 respectively. When the values of B_1 and B_2 are changed, only the threshold amplitude varies, and the obtained patterns remain unchanged.

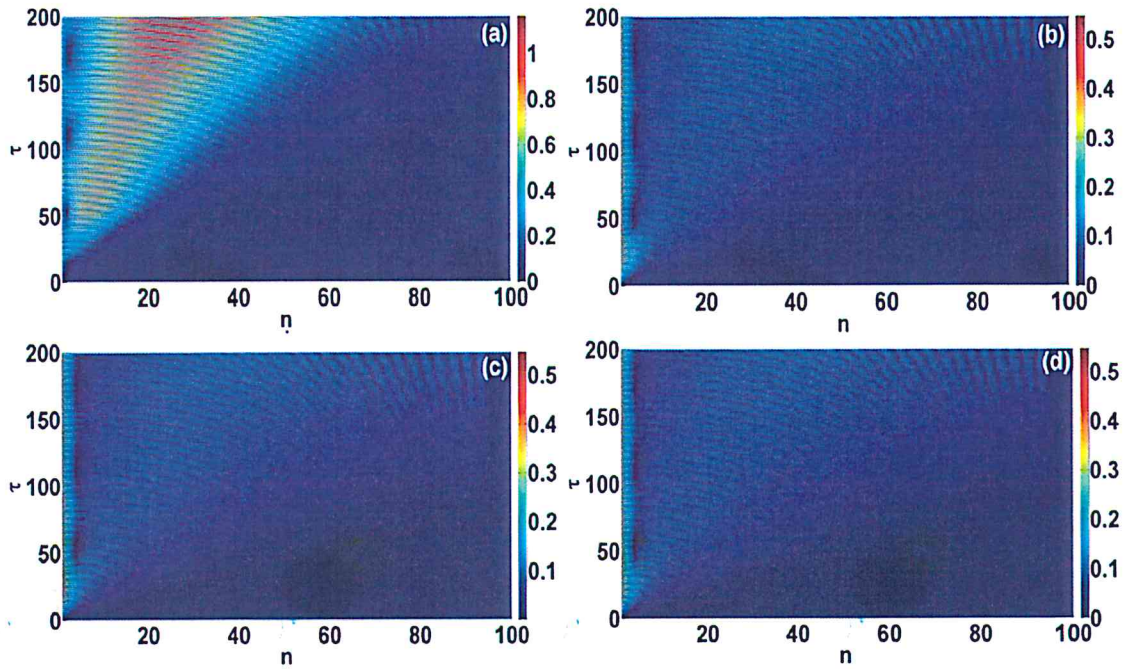

Figure 16: Spatio-temporal evolution of the lattice with the boundary condition $V_0(\tau)=U\exp(1-\tau/\tau_1)\cos(\Omega\tau)$ with r=0.01, B_2=0.005, B_1=10, ν=0.1, τ_1=10 , ω_c=2, Ω=2.1 and U_{th}=0.0210. The color bar at the right represents$|V_n(\tau)|/U$. (a)U=0.001, (b)U=0.02, (c)U=0.03, (d)U=0.04.

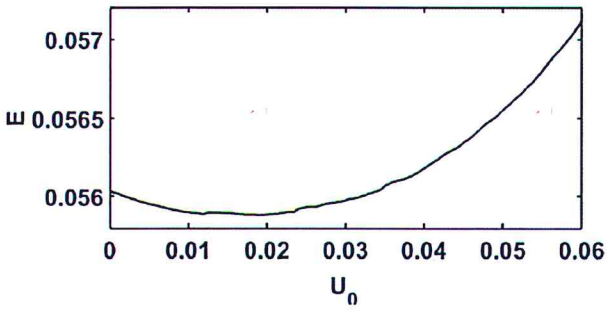

Figure 17: Total energy of the lattice without nonlinear dissipation. The lattice has 100 electrical cell, Ω=2.1, r=0.01, B_2=0.005, B_1=10, ν=0.1, τ_1=10, τ_2=100. The accumulated energy is extracted at τ=1000.

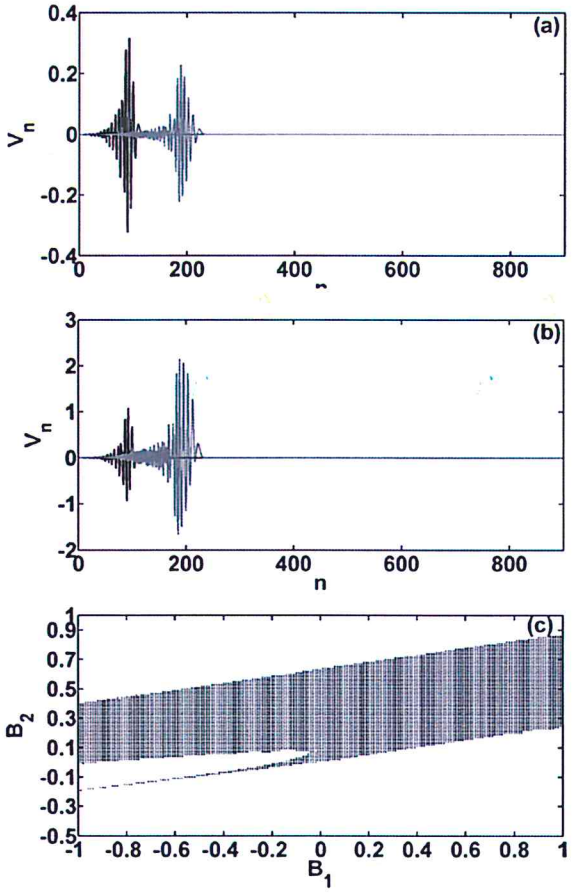

Figure 18: Results of numerical simulations of the developed model (with the nonlinear resistance and the nonlinear capacitance) with 900 units cells. The pulse was applied on the

first lattice cell. Firstly the absence of calcium ions was considered which is mathematically translated by $B_1=B_2=0$ (a). Secondly, in (b) the presence of calcium ion was considered with $B_1=10^{-3}$, $B_2=0.1$, $1/A=0.1$, $r=0.01$. The temporal snapshot of pulse propagation is depicted at $\tau=100$ (black), $\tau=200$ (Gray). The boundary driving amplitude is $V_m=0.50$, this value decreases progressively from 0.3167 at $\tau=100$ to 0.2288 at $\tau=200$ (a). In the graph (b) it increases from 1.084 at $\tau=100$ to 2.157 at $\tau=200$. τ is the dimensionless time obtained by the relation $\tau=\omega t$. In figure (c) we displayed the ability of the nonlinear resistance to amplify the input signal. The black doted region represents a couple of parameters (B_1,B_2) which allow voltage amplification.

III-3-2 Discussions

In the models to mimic the electrical transmission in MTs [17–22], the reason raised to explain the decrease of the amplitude of the input signal is the contribution of the resistance that dissipates the energy. However, the observation of such phenomenon could also be linked to the frequency of the stimulus outside the allowed band.

For the numerical confirmation of the value of the analytical threshold, the monitoring of the average flux of energy as a function of the driving amplitude have been employed [115]. Another rough estimation can be done by monitoring the value of the energy for several amplitudes of the driving [107]. However, these methods are computationally intensive because the system evolution has to be numerically simulated for each value of the driving amplitude. Moreover, another method like the NLRM can be used to detect critical amplitude(s) in a nonlinear system driven by a periodic excitation [121–123]. The obtained critical amplitude(s) from the NLRM is related to a transmission threshold in driven and disordered systems [123]; it seems that this quantity has not been explicitly compared with the analytical value of the nonlinear supratrasmission threshold. However, in the present study, it was noticed that the critical value of the amplitude obtained numerically by the NLRM is equal to the analytical value of the supratransmission threshold. It is important to note that such comparison is operated when the assigned value to the gap frequencies is slightly above the critical frequency [115].

In cases without dissipation with Klein-Gordon type of nonlinearity [422,423]; the system is a frequency filter of band pass type and the supratransmission is only possible below the lower cut-off frequency. Above the upper cut-off, the derivation of the analytical threshold is not possible because the expression for the solution is a kink. Thus the supratransmission threshold cannot be derived because the maximal amplitude is an infinite number. In our context, the model is a low band pass type and the nonlinear supratransmission occurred above the upper cut-off frequency.

Several studies have shown that nonlinear system with a linear dissipation could exhibit infratransmission phenomenon [108–110,349]; in addition, the obtained threshold is usually lower than the supratransmission threshold. Herein is was found that the supratransmission threshold can be lower than the infratransmission threshold in nonlinear dissipative system. However, both values of the threshold amplitudes are very close in the dissipative case. This could be the reason why we observed very weak wave propagation above the estimated supratransmission threshold.

High frequency and repetitive transcranial magnetic stimulation have an attenuating effect on motor signs in Parkinson's disease [15,102]. However, the exact mechanisms of this effect are not clearly understood [15]. The theoretical results obtained in the present study suggest that the infratransmission phenomenon could contribute to that observed effect. The primary motor signs of the Parkinson's disease are originated form electrical signal generated by excessively firing nerve cells. If the axonal MTs are stimulated with the high frequency they could undergo infratransmission phenomenon. Thus, the intensity of message flows could be attenuated. In addition to documented electrical behavior of MTs [15,16], Cytoskeletal elements of the axon of neuronal system, which contain excited MTs, could possibly influence ionic conduction within neurons by infratransmission.

Standards models for representing the ionic waves propagation in MT are often studied using the method of approximation with continuous limits [17–22] . This method assumes that the values of the physical quantities vary slightly from one lattice point to another. Such approach is well known to be appropriate only when looking for analytical solutions. However, these methods can lead to disregard of higher order terms during Taylor's development, yielding a loss of accuracy in the final results. Furthermore, it was reported that

accounting for individual MT subunits is important for modeling the behavior of that molecule [424]. In addition, at nanoscale, the discreteness effects are non-negligible. Considering these pitfalls and following the preceding section, it was found advantageous to solve wave propagation equation directly in fully discrete form, which in our sense is physically more realistic. The numerical scheme used for direct integration of our developed fully discrete equation is the Runge-Kutta algorithm [337]. The external excitation V_{in} was applied to the first cell of the discrete electrical line.

Existing models to mimic the electrical behavior of MTs [17–22], only emphasized on the ability of the system to decrease the input signal as in the experiment [105]. The biophysical model of this paper presents two outcomes. In the absence of the negative nonlinear resistance the signal is reducing, making our finding closer to the results reported in [105]; whereas, in the presence of the nonlinear resistance the signal considerably increases [23], meaning that nonlinear resistance plays the role of the calcium ion confirming its ability to induce the amplification of pulse signal [23].

It is well known that negative nonlinear resistances are able to amplify the electrical signal, however, numerical simulations that we conducted showed that even when the resistance is negative, the signal can still decrease. This is due to the interplay between the linear resistance r and the nonlinear resistance $R_n(V_n)$. This study also showed that for a signal to be amplified the linear coefficient B_2 must be positive. Because the negative value of the coefficient B_2 induces an additional dissipation of the voltage in the system.

Optimal electrical amplification requires a specific level of calcium ion concentration, and any departure from this level and the interactions of calcium ion with MT decreases the efficiency of both the amplification of electrical signal and mechanism of amplification [23]. Since electrical models are more appealing in their manipulations, the proposed circuit can be used at the initial stage to find the optimal value of the concentration of calcium ion that can be used as a modulator of signals for biological processes.

III-4 Investigation of damages spread and yield losses due to lepidopteran stem borer in a maize farm

III-4-1 Results

First data collection

Due to climatic conditions in Naivasha, *B. fusca* was the exclusive lepidopteran maize stem borer found during the survey periods. Subsequently the results presented here only focus on this specie.

Variation of the number of damaged plants and damage types per week for each plot are shown in Figure 19. It is observed that the phenomenon is not linear. A detailed observation of LD in plots 3, 5 and 6, displayed two notable phases of the occurrence of damages, especially around weeks 4-5 and weeks 7-8. During weeks 4 to 5 a sudden increase of damaged plants in plots 3, 5 and 6 is detected although no damage was previously noticed. At weeks 7 and 8, another sudden peak of damage is noted before starting to gradually decrease, as the maturity of the plants approached. In Figure 20, we showed the variation of the average number of insects caught and the number of LD in the six plots. Two peaks of male flying activities can be clearly seen during weeks 2 and 6. Subsequent appearances of LD peaks during weeks 4 and 8 can also be noticed. Linking Figure 19 and Figure 20, we estimated that the time lag between the peak of *B. fusca* male captured and the observed peak of LD is approximately 2 weeks.

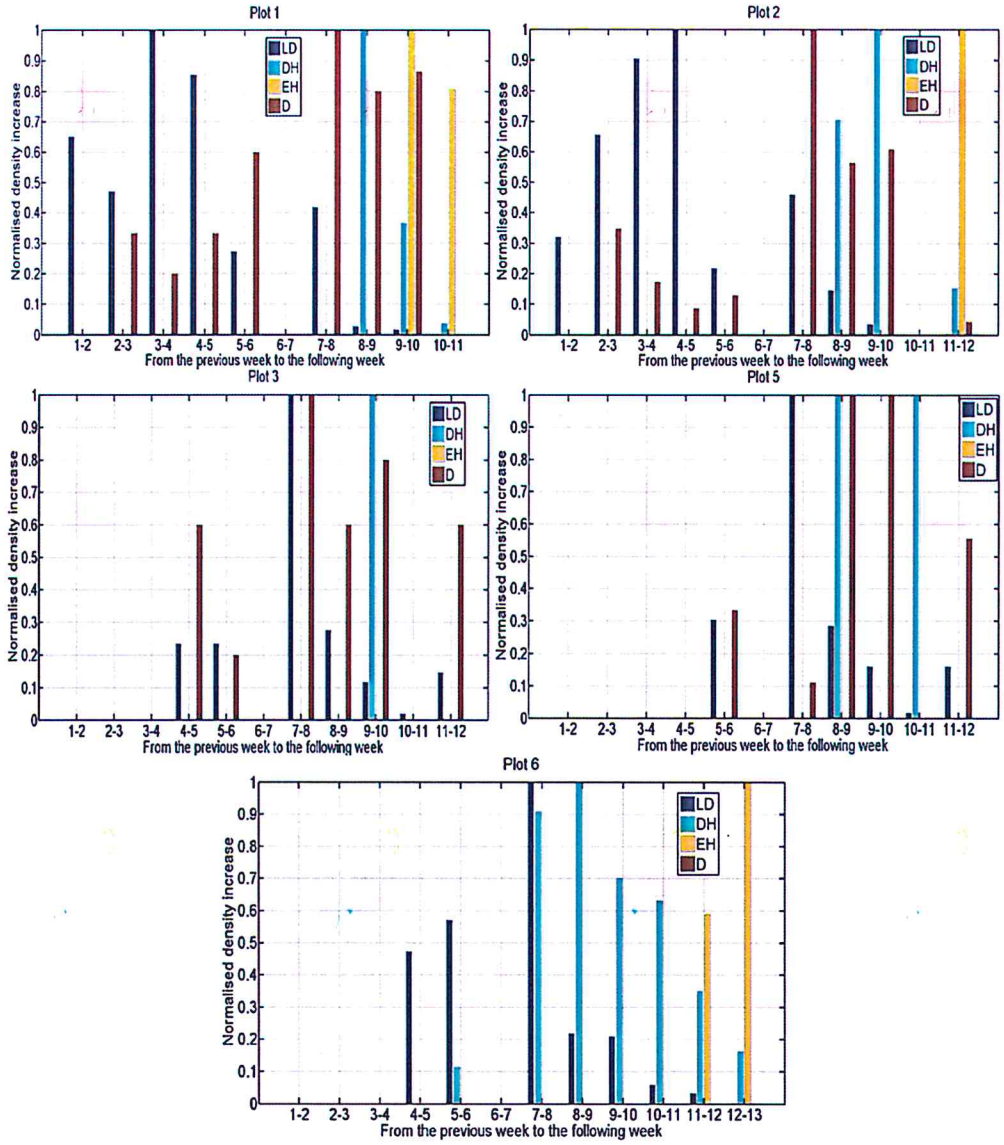

Figure 19: Differences in infested plants densities between two consecutive weeks. The computation has been done for the four infestation types, leaf damages (LD), death hearth (DH), exit hole (EH) and death (D).

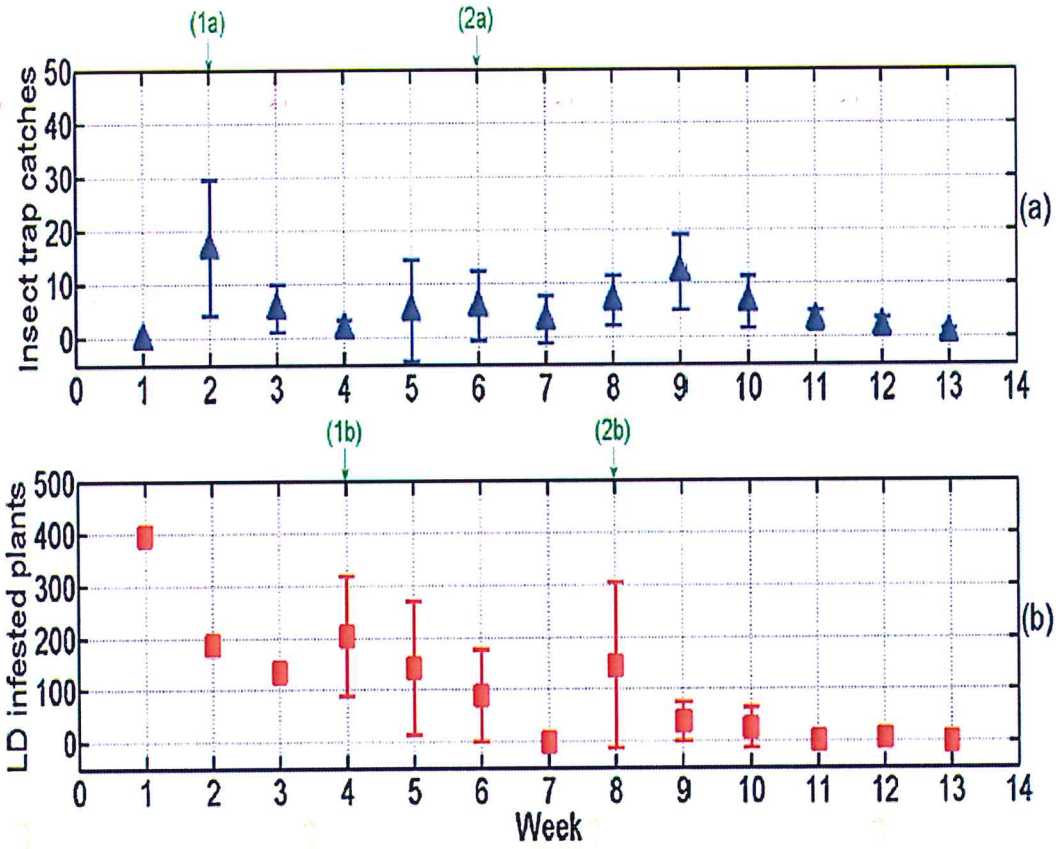

Figure 20: (a) Mean values of number of adult *B. fusca* caught weekly with pheromone traps at. (b) Mean values of plants with the leaf damage (LD) infestation recorded weekly. (1a) and (2a) represent the peaks observed before the apparition of the infestation peaks (1b) and (2b) respectively. The bars represent the standard deviation error of the mean

The conditional probability for a randomly selected plant to die following different situations is given in Table 5. In plots 1 and 2, the probability for a plant to die given that it has LD is the highest. For plots 3, 4, 5 and 6 those probabilities are null. Table 6 shows the mean transition time between different types of damage. The time spans are similar for plots 1 and 2 and, longer for plot 5. In plot 4, the transitions are faster compared to the other plots. Plots 3, 4 and 6 have a shorter transition time between damages. The transition LD→DH seems to be the fastest. Overall, if all the plots are considered as a unique field, the results

would demonstrate that the transition time between different types of damage is not uniform, which means the phenomenon is stochastic.

Probabilities						
Events	Plot 1	Plot 2	Plot 3	Plot 4	Plot 5	Plot 6
P(D|LD)	0.0116	0.0337	0	0	0	0
P(D|EH∪ DH)	0.0082	0.0303	0	0	0	0
P(D|EH∪ DH∪ LD)	0.0102	0.0330	0	0	0	0

Table 5: Conditional probability for a plant to die following different cases. P(D|i) is a probability that a plant died, given that it has an infestation *i*. LD =leaf damage, EH= exit hole, DH=dead heart and D =dead. The symbol (-) means null probability and the symbol (∪) stands of "or".

Mean time ± SEM				
Transition	Plot 1	Plot 2	Plot 3	Plot 6
LD → DH	6.34 ± 0.12	6.42 ± 0.17	6.75 ± 1.60	6.49 ± 0.11
DH → D	7.14 ± 0.30	7.45 ± 0.31	7.03 ± 0.53	-
LD → D	7.17 ± 0.28	7.07 ± 0.31	7.03 ± 0.53	-
LD → EH	7.23 ± 0.08	8.28 ± 0.16	-	7.77 ± 0.20

Table 6: Mean time in weeks for transition between infestation types. It is given in the format: mean time ±standard error of the mean (SEM). The symbol (-) means that such transition was not observed. For the plot 4 and 5 see the appendix.

The weekly evolution of spatial and temporal autocorrelation (Moran's *I*) for the LD is depicted in Figure 21. For plots 2, 3, 5, and 6 the infestation is strongly spatially correlated for a very low radius of proximity between infested plants, but over time, the spatial link between damaged plants became more and more considerable. The spatial correlation distance for damaged plants inside these four plots did not exceed 10 meters. A considerable spatial autocorrelation was observed between damaged plants within a radius of proximity exceeding 10 meters in plot 1 and 4. These results help us to understand the level of similarity and

dependence between the point locations of damaged plants. Figure 22 shows the weekly tracking of spatial iso-barycentre (IB) for LD plants. The initial IB position is random; the others are located around the former IB. After the first cycle of infestation, we observed a general trend towards an IB further from the previous recorded during the first cycle. Indeed, a spatio-temporal pattern of infestation is clearly visible: a spiral-like pattern of LD at the beginning, which goes farther from the origin point with time.

Spatial clustering analysis was carried only on plots 3, 5 and 6 where the damage was at the initial stage of plants growth. Figure 23,

Figure 24 and Figure 25 displays the initial spatial classification of LD plants in plots 3, 5 and 6 respectively. The spatial clusters generated by patches of infested plants are dissimilar in terms of the number of damaged plants at the start of observation; however the gap reduced as it approaches the last weeks. In plot 3, we initially observed a small number of damaged and scattered plants; whereas plot 5 and 6 engorged big number of damaged plants. The cluster shape made by damaged plants is typically ellipsoidal. With time, two phases were observed; during the first phase, the number of clusters remained almost the same but the shape of the initial clusters and their respective size (number of plants) changed gradually. During the second phase, new clusters arose possibly from the fragmentation of the initial clusters rather than the creation of isolated new entities.

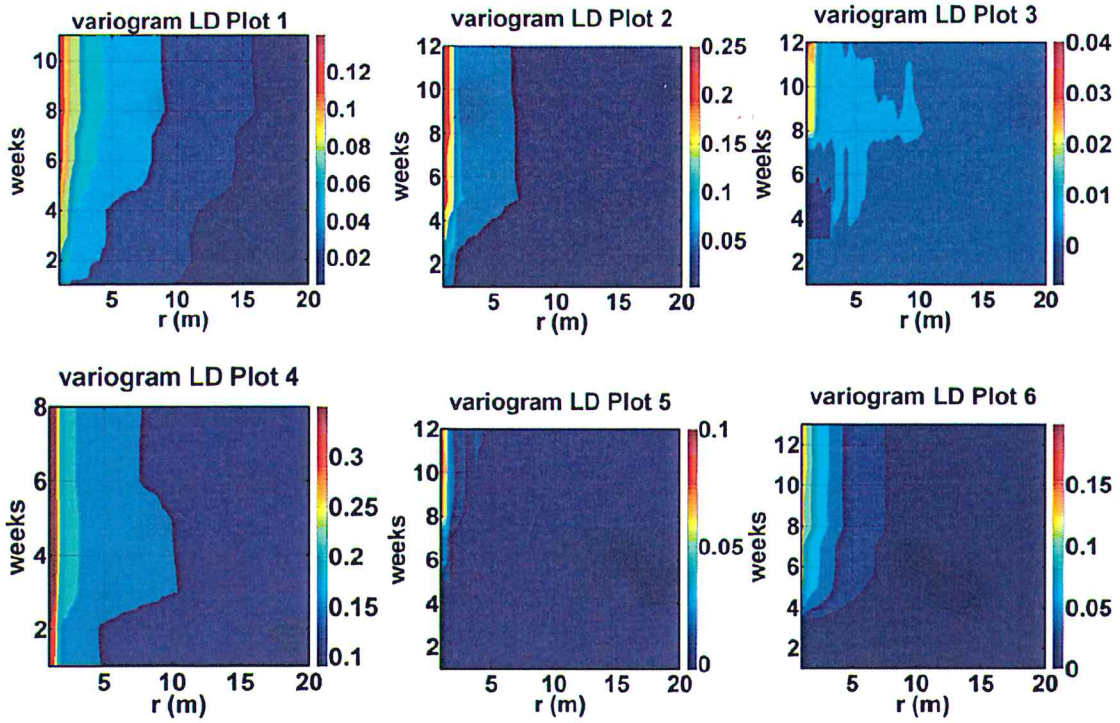

Figure 21: Spatial and temporal autocorrelation for leaf damage (LD) on plants. The computation has been done for a radius of proximity (r) from 1 meter to 20 meters. The colour bar on the right side of each figure represents the spatial autocorrelation level

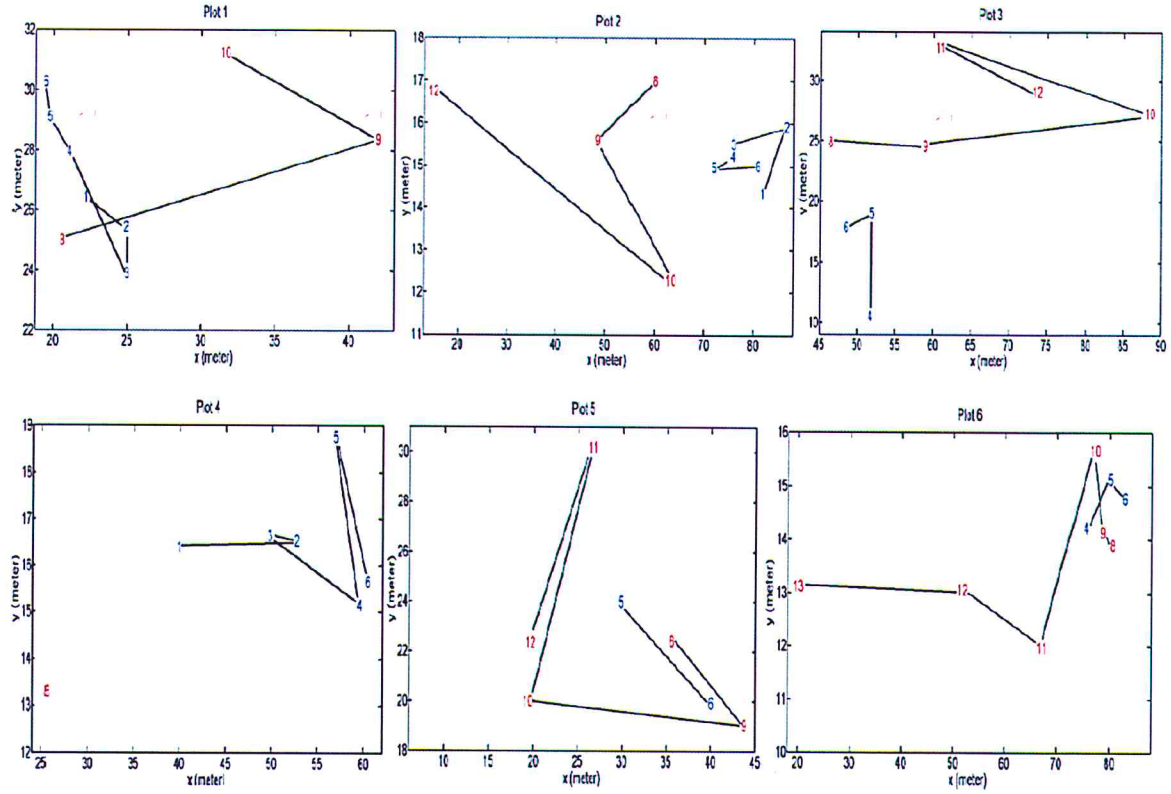

Figure 22: Temporal evolution of the isobarycentre (IB) for leaf damaged infested plants. The integer values represent the corresponding week. The position of the number is the spatial position of the IB. The IB from the first and second cycle are colored in blue and red respectively.

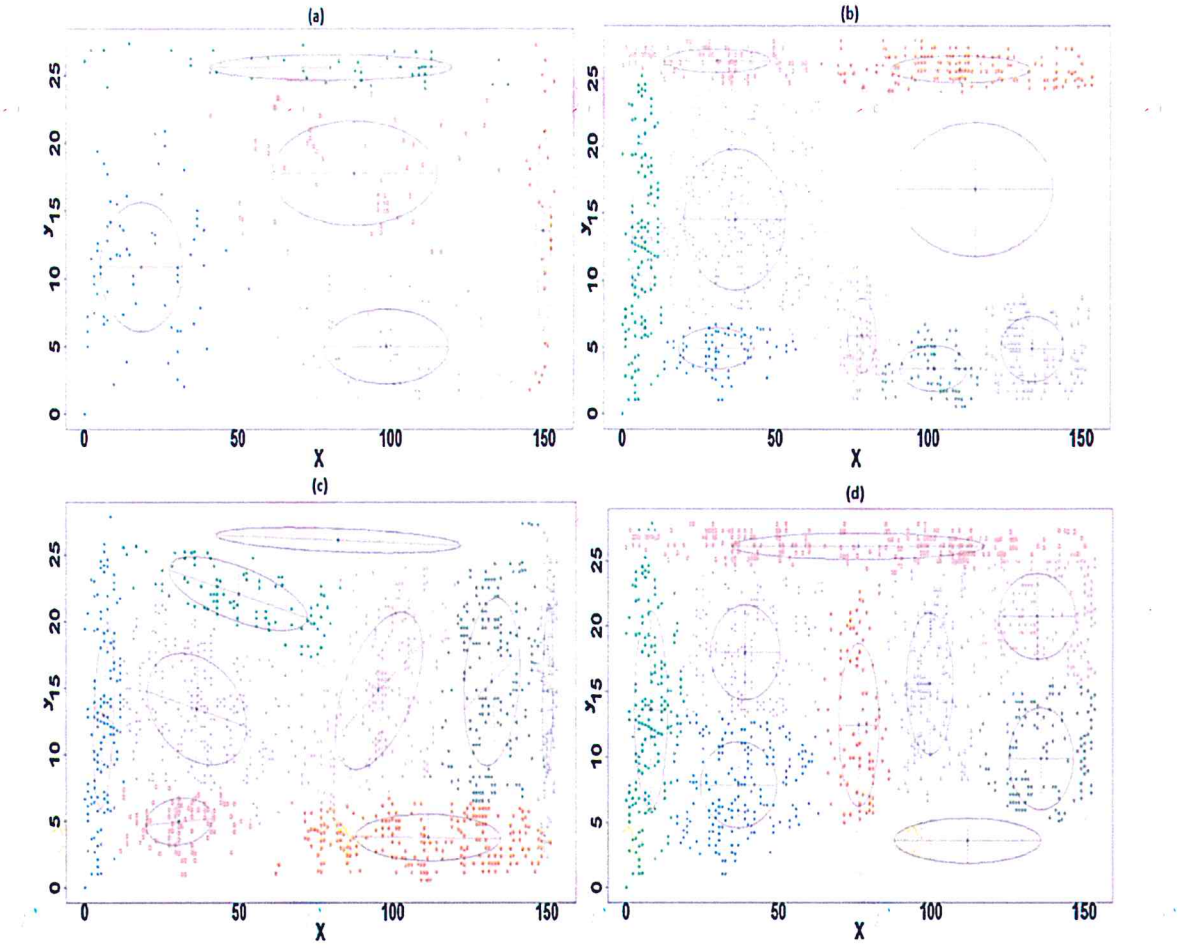

Figure 23: Spatial clustering of plants with LD infestation for plot 3 at week 4 (a), week 5 (b), week 8 (c) and week 12 (d). Each colour represents a cluster. The ellipsoids/circles represent the bottom of two dimensional probability density functions (PDF). The shapes are chosen accordingly to the Bayesian information criteria. The centers represent the centroid of the cluster distributions. The dot outside the circular represents plants positions with weak probabilities compared to the center of the PDF.

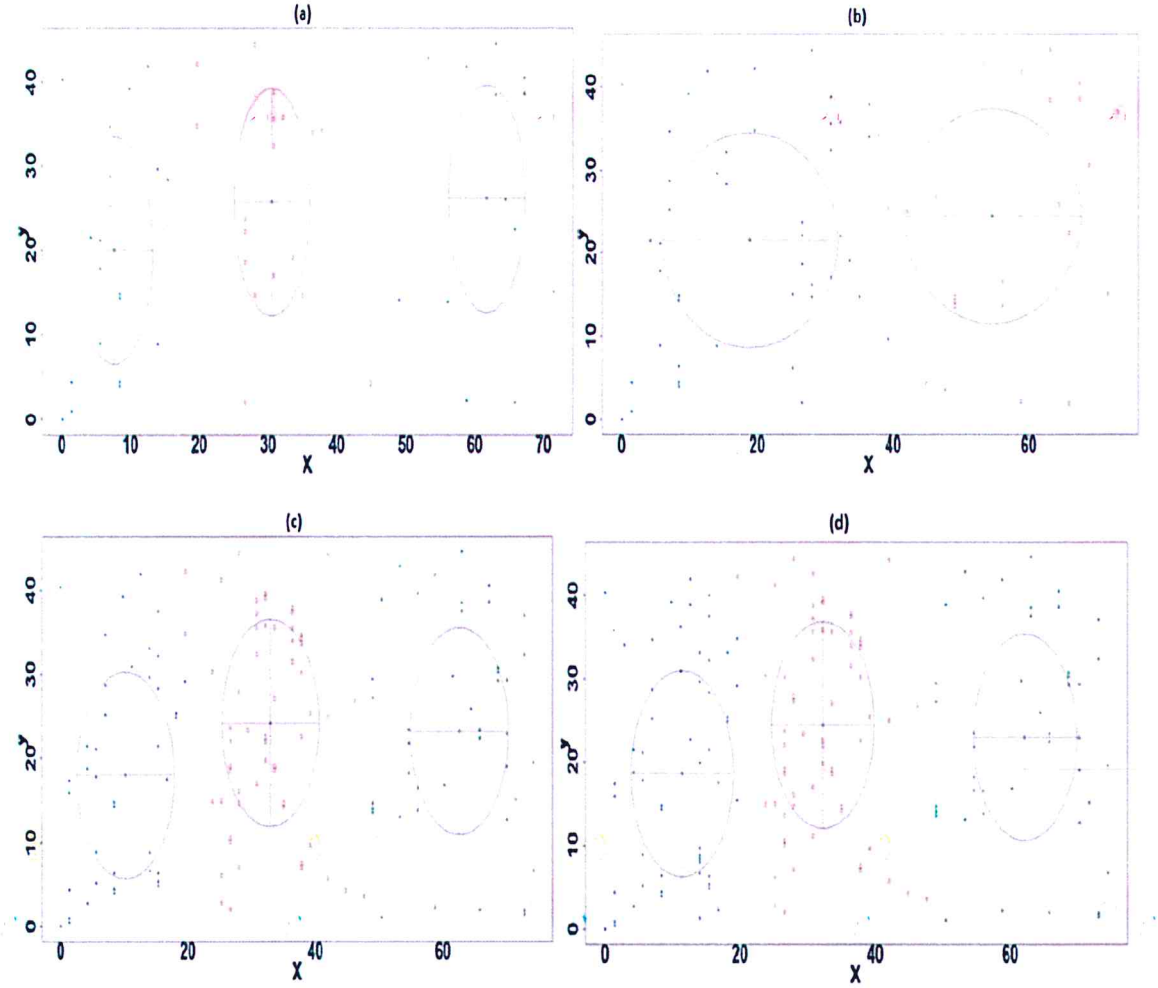

Figure 24: Spatial clustering of plants with LD infestation for plot 5 at week 5 (a), week 7 (b), week 9 (c) and week 12 (d). Each colour represents a cluster. The ellipsoids/circles represent the bottom of two dimensional probability density functions (PDF). The shapes are chosen accordingly to the Bayesian information criteria. The centers represent the centroid of the cluster distributions. The dot outside the circular represents plants positions with weak probabilities compared to the center of the PDF.

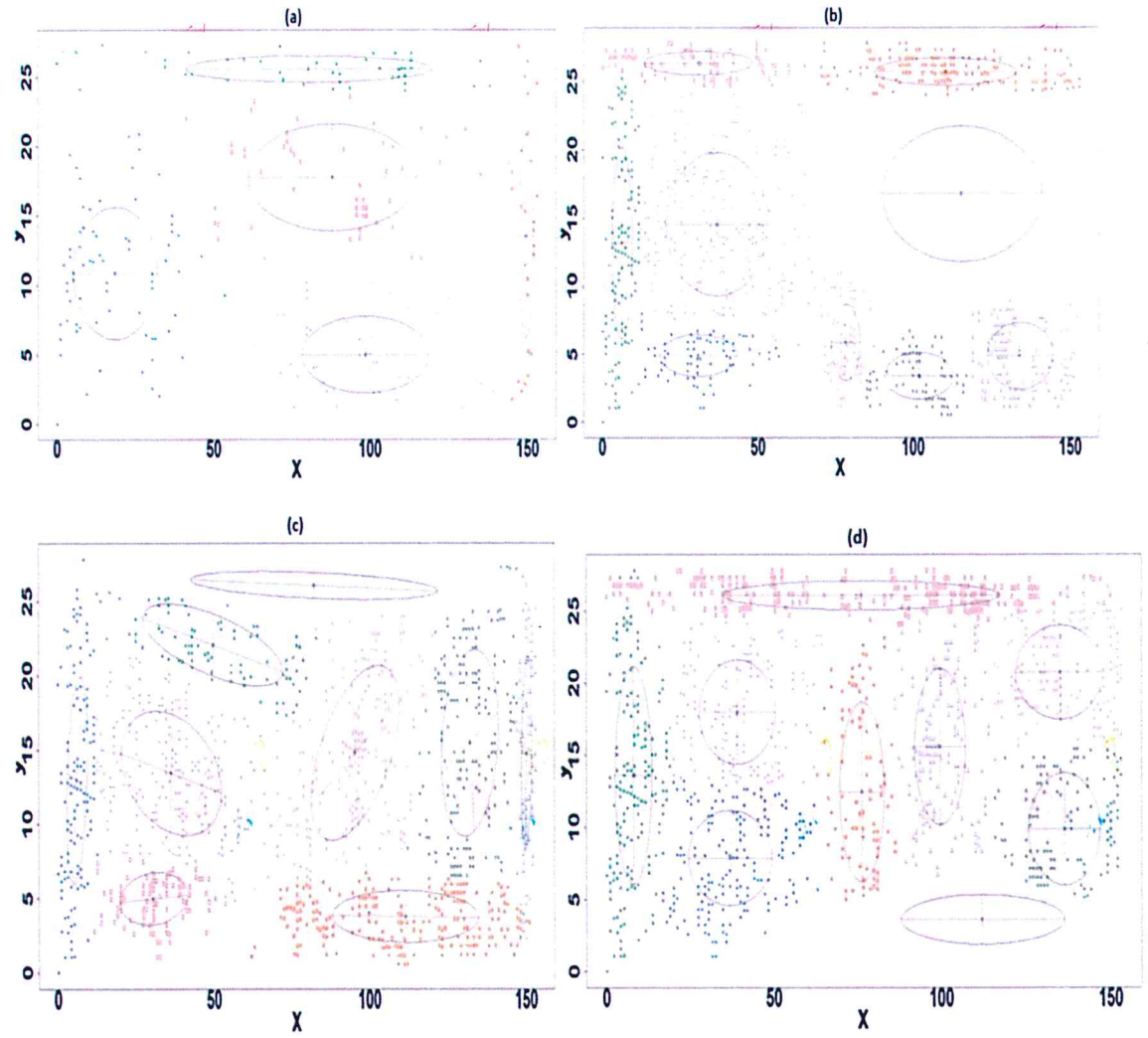

Figure 25: Spatial clustering of plants with LD infestation for plot 6 at week 4 (a), 9 (b), 11 (c) and 13 (d). Each color represents a spatial cluster. The ellipsoids/circles represent the bottom of two-dimensional probability density functions (PDF). The shapes are chosen according to the Bayesian information criteria. The centers represent the centroid of the cluster distributions. The dot outside the circular represents plants positions with weak probabilities compared to the center of the PDF.

According to Table 7, the LD dynamics in plot 1, 2 and 4 followed a cellular automata law. It is demonstrated that, if four plants are infested following the Moore neighbourhood of contagion pattern, the plant at the central position is most likely to be infested during the subsequent week. However, in plot 3, 5 and 6 the algorithm reduced the initial neighbourhood to the central cell, indicating the failure to estimate the neighbourhood in these cases. Such results are justified by the non-linear and perhaps chaotic behaviour of the spread of the infestations of pests within plants at field level. A summary of all the spatial results are provided in Table 8.

Plots	Initial number of neighbors	Number after reduction made during step (ii)	Number after reduction made during step (iii)	Maximal Bayesian information criteria after step (iv)
Plot 1	25	25	4	4
Plot 2	25	25	4	4
Plot 3	25	25	1	1
Plot 4	25	25	4	4
Plot 5	25	25	1	1
Plot 6	25	25	1	1

Table 7:Results obtained after estimations of the neighbourhood configuration of the cellular automata (CA). Step (ii), (iii) and (iv) are briefly describe in the text, in the methodology 3.7. The number represents the number of plants in the neighbourhood (including the central cell).

Method	Purpose of the method				Main result
	Evaluates with time the spatial link between infested plants located at different positions	Tracks the positions of the center of patches formed by infested plants with time	Follows the evolution of the initial shape, the density and the number of clusters of infested plants formed with time	Estimates the rules by which plants get infected through neighbors	
Morans' I	✓	×	×	×	The spatial correlation between infested plants is considerable at a radius of 10 m
Center tracking	×	✓	×	×	The spatial shift of the patterns created by an infested plant moves with time in a form of a spiral from an origin point to other parts of the plot
Model based cluster analysis	×	×	✓	×	The initial shape and number of spatial clusters remain stable during a certain period of time and, later disaggregate to create new clusters
Cellular automata	×	×	×	✓	A safe plants surrounded by four infected plants is most likely to become damaged in the next subsequent week

Table 8: A summary of the purpose of applying each spatial analysis symbols × and ✓ stand for no and yes respectively

Second data collection

Data collected at harvest show that plants infested by *B. fusca* outnumbered the proportion containing the crambid *Chilo partellus* (Swinhoe) and the noctuid *Sesamiacalamistis* Hampson. The relative percentages of the tunnelled maize plants were 92.57%, 0.57% and 6.87% for *B. fusca,C. partellus* and *S. calamistis* respectively (Table 9).The majority of larvae were found in stem tunnels and less in cob tunnels (Table 9); the ratio (%) of the total number of larvae inside stem tunnels-cob tunnel is 90.63-9.37 for *B. fusca,* 52.94-47.06 for *S. calamistis.* The unique *C. partellus* larvae have been found in stem tunnel. The average number of larvae per plant and per cob did not exceed 2 (Table 9).

	Busseola fusca inside tunnels				*Chilo partellus* inside tunnels				*Sesamia calamistis* inside tunnels			
	Bf/S	Bf Total in Stem	Bf/C	Bf Total in Cob	Cp/S	CP Total in Stem	Cp/C	Cp Total in Cob	Sc/S	Sc Total in Stem	Sc/C	Sc Total in Cob
Plot 1	1.25	45	1	7	1	1	0	0	1	5	1.66	5
Plot 2	1.15	37	1	1	0	0	0	0	1.5	3	1	3
Plot 3	1.38	63	1.33	8	0	0	0	0	1	1	0	0
Plot 4	1.07	29	1	2	0	0	0	0	0	0	0	0
	Total of plants tunneled		Total of cob tunneled		Total of plants tunneled		Total of cob tunneled		Total of plants tunneled		Total of cob tunneled	
Plot 1	40		7		1		0		5		3	
Plot 2	32		1		0		0		2		3	
Plot 3	47		6		0		0		1		0	
Plot 4	27		2		0		0		0		0	

Table 9: Number of larvae found in the plants during sampling on the field. Bf/S, Cp/S, and Sc/C are the average number of *B. fusca* (Bf), *C. partellus* (Cp) and *S. calamistis* (Sc) per maize stem (S). Bf/C, Cp/C, and Sc/C are the average number of *B. fusca, C. partellus* and *S.calamistis* per maize cob (C).

The comparison between average physical traits of infested and un-infested maize plant is depicted in Figure 26. Only the cob masses between non-infested and infested plant were significantly different across all plots. The variance homogeneity among infested plants cob masses across all plots was less significant (p-val<0.05) compared to all other factors.

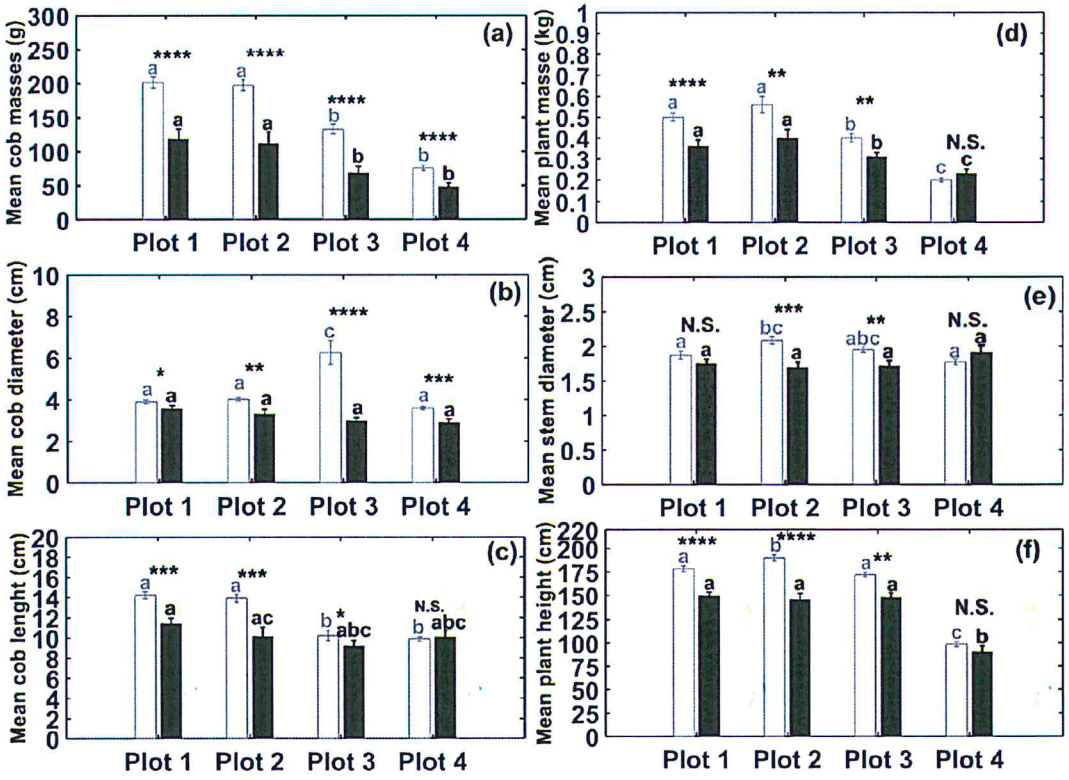

Figure 26: The black and white bar represent infested and non-infested sets of plants. The star is the significance level between means. The symbols N.S. (Not Significant) for P-value>0.05, *for P-value <0.05, **for P-value <0.01, ***for P-value<0.001, ****for P-value<0.0001. Bars with the same colored letter are not significantly different (P-value> 0.05).

The relative yield losses in term of average cob masses reductions are estimated for each plot as 40.79%, 43.14%, 48.19% and 35.96% for plot 1, 2, 3 and 4 respectively. Given the plant density across plots ranging from 58111plants/ha to 58940plants/ha with an average of one cob per plant, infestations from *B. fusca* inflicted losses ranging from 56.85kg/ha to

133.48 kg/ha. Total yield losses due to stem tunnelling and cob tunnelling were 42.86% and 62.52% respectively.

Busseola fusca was able to bore 60.23% and 15.18% in average in term of length of maize cob and plant stem respectively. An investigation of damages severity in cobs according to the type of infestation such as leaf damages (LD), dead heart (DH), exit hole (EH) has been conducted. It is observed that all infested plants have on average a lower cob mass compared to the non-infested (Figure 27(a)). The cob tunnelling induced lowest cob masses directly followed in term of incidence by LD+DH (Figure 27(b)). It can be noticed that a high proportion (greater than 70%) of infested plants has the stem tunnelled. A lower number of infected plants has cob tunnelling; it was also noticed that a reduced proportion (less than 20%) of plants were damaged with stem tunnelling and cob tunnelling simultaneously. Additionally, 100%, 24.67%, 19.48% and 6.49% of infested plants with LD, LD+EH, LD+EH+DH, and LD+DH respectively had a cob at the time of harvest.

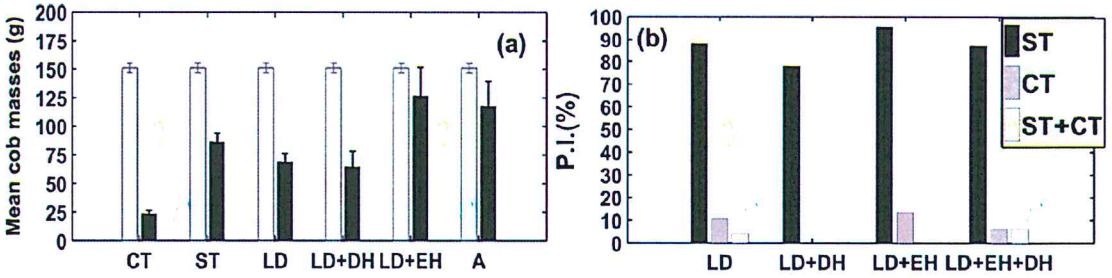

Figure 27: (a) Effect of the first infestation on the mean cob biomass reduction. The letter A stands for LD+DH+EH. (b) The proportion of plants infested (P.I.), plant with stem tunnelling (ST) and cob tunnelling (CT) according to the type of infestation such as leaf damage (LD), dead heart (DH), exit hole (EH).

Yield losses patterns due to different damages with time are depicted in Figure 28. When the damages are taken separately, a particular trend of variation of yield according to the week of the first infestation is not observed. No yield losses for plants with LD at week 11 was noticed; for weeks 4, 7 and 10no new damages were recorded (Figure 28(a)). The time of infestation does not matter for leaf damage incidence. The EH graph (Figure 28(b)) does not show any particular trend. For the DH (Figure 28(c)), the time factor seems important; when

this damage occurred at the initial stages of maize development, the incidence on yield loss is high. However when DH occurred later in the plant life cycle (after the 7th week of planting), yield losses are lower. In general, the maize variety selected showed that after 5 weeks almost half of the plants in each plot have managed to generate cobs. When the analysis is conducted by pooling data without distinguishing the type of infestations, the losses tend to decrease with the time period of infestation (Figure 28(d)). The linear regression between the yield losses (y) and the time (t) of infestation in week (y=at+b) has the slope a=-4.28$\pm$0.02 and the intercept b=60.48$\pm$0.17 (P-val>0.05, R^2=0.31); the Pearson correlation coefficient is -0.56. This suggests that the linear function is not a good function for that data set. However, the linear regression between the average cob tunnel (y)and the time of infestation (t) in week (y=at+b) has the slope a=0.50$\pm$0.13 and the intercept b=3.14$\pm$0.11 (P-val<0.05, R^2=0.78); the Pearson correlation coefficient is 0.88; then the mean cob tunneling increases with time in a linear tendency.

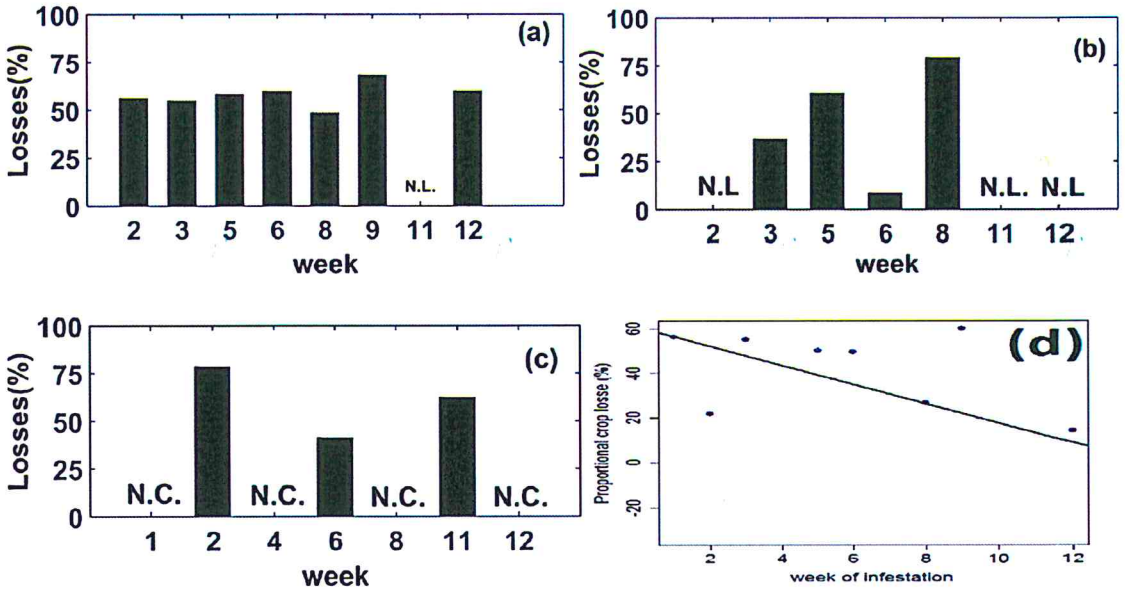

Figure 28: In subfigures (a), (b), (c) the temporal patterns of yield losses for plant with leaf damage, exit hole and dead heart respectively are depicted. The abbreviations N.L and N.C stands for no losses and no cob respectively. (d) linear regression between the week of infestation and the yield losses

Analysis of the link between the cob masses and severity of damages on the stem and cob is presented in Figure 29. After several trials to select a bell-shaped nonlinear function using the AIC, it was observed that the link between cob mass (y) and the cob tunnel length (x) follows a trend represented by a cubic function (Figure 29(a)). The analytical expression is: $y=a+bx+cx^3$ and the coefficients are: a=-54.46±19.70, (P-val>0.05), b=26.13±4.99 (P-val<0.05) and c=-0.16±0.03 (P-val<0.05); $R^2 = 0.92$. We were not able to find any function linking the cob mass and tunnel length (Figure 29(b)). This result implies that while the average value of cob tunnel length increases linearly with time of infestation, the cob masses of infested plants follow a pattern depicted by a cubic functional curve.

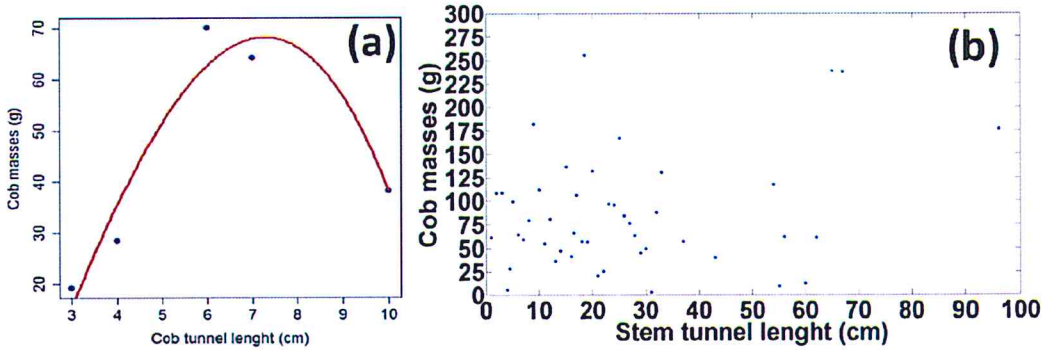

Figure 29: (a) Relationship between length of cob tunnel and cob mass. The blue dots are the data and the red curve is the estimated function. (b) cob mass as a function of cob tunnel.

III-4-2 Discussions

Developed sampling schemes for assessing lepidopteran stem borer pest infestations in maize farms are often focusing on checking/collecting at random a few plants infested/uninfested by the larvae without taking into consideration the precise point location of the plants within the field [208–211]. In our study, all the plants had a precise geo-referenced position in each field. We did not used destructive sampling, as the dissection of plants can interfere with the spread of the larvae and the oviposition distribution of the females in the plots. In addition, farmers perceive destructive sampling as unacceptable, and it is time consuming and expensive [425]. The presence/absence infestation data collected from visual inspection of external and comprehensive signs of insect pest damages in the plants may be more appropriate. Particular attention was given to leaf damage because young larvae are

often responsible for this type of damage and it occurs mainly on young maize plants; therefore making it easy to be used as a proxy for relating the spread of the infestation. In addition, leaf damage has also been reported as an important factor in contributing to yield losses in maize farms [155,231].

Considering that *B. fusca* egg development is completed during 8-10 days at 25-20°C [320], the first flight period started at least 10 days before the first set of leaf damage, and ended in all plots at least 10 days before the end of the 5th week. This suggests an absence of *B. fusca* female oviposition during days 10-15 days around week 5-6 as no damage was recorded in week 7 in all plots. The second peak of damages is observed on all plots between weeks 7 and 8. No exit holes were noticed in all plots during the second peak; which suggest that majority of eggs laid within this period of time was caused by females from other localities. The observation of a fixed time lag between the occurrence of peaks of LD and adult male abundance in pheromone traps is in accordance with previous studies [382–390]. The abundance of males in pheromone-baited traps is significantly correlated to observed damages in studies [382–390]. Additionally, the spacing of two weeks is the *B. fusca* egg development time, after which it emerges to larva stage and starts damage. It has been reported that *B. fusca* prefer to lay eggs in young maize plants [155,184,187]; however, the continuous infestation pattern observed in this study suggest that oviposition on older plants is possible.

Although the main goal of this study was to examine the spatial and temporal spread of maize stem borer *B. fusca* under field conditions, we though necessary to comprehend the sequence of plants infestations by estimating the conditional probabilities of each damage type causing death of the plant. A higher mortality of maize plants with LD was observed. However, the stem tunnelling which is logically expected to occur after LD and before DH, D, EH was not considered here. Moreover, the data collection protocol of the present study was unsuitable for assessing stem tunnelling, which effect is a major cause of grain yield reduction in maize [178]. It might be convenient to sample and dissect a few plants to assess and account for the incidence of tunnelling.

The mean transition time from a type of damage to another damage type was different from one plot to another. This suggests either a variability of the phenological stage of the

plants due to the difference in sowing time in each plot and/or the heterogeneous characteristics of the soil and nutrients managements, which were different from one plot to another. Variability might be also due to the phenological stage of the stem borer larvae and the difference in nutritional quality of the plants. Temperatures difference may as well play a part in the discrepancy.

The mean transition time from one damage type to another was different from one plot to another. This suggests either variability of the phenological stage of the plants due to difference in sowing time at each plot and/or the heterogeneous characteristics of the soil and nutrients managements, which was different from one plot to another. Variability might be also due to the phenological stage of the stem borer larvae due to the difference in nutritional quality of the plants or differences in average temperature from one plot to another.

An increase of the spatial correlation with time implies an overall trend toward a single gradient. The results of independence of damaged plants noticed via negative spatial autocorrelations in some plots are likely an artefact and not a biological phenomenon. The variogram is expected to depict no spatial autocorrelation for some distances [135,136,189,190]. During data collection, independent samples must be taken at random at different locations so that each sample has an equal chance to be selected [426]. However, infested plants separated by a small radius of proximity (less than 10 meters) were considerably correlated. Therefore, such evidence of a spatial link between infested plants leads to the conclusion that sequential plant samples may not be a proper representative of a statistically independent sample procedure, thus violating the assumptions of random sampling in the field [426]. In improving traditional sampling schemes devoted to lepidopteran stem borer infestation through a selection of samples far enough from each other to ensure total independence, this finding should be taken into account.

The movements of the focal area (centroid) associated with infestations might reflect shifts in the spatial and temporal patterns of adult and larval dynamics during the damaging process. Centroid infestation tracking was used to monitor the movement of *Eoreuma loftini* by pheromones baited traps throughout Texas rice belt [132], to check the spatial evolution of *Nasonavia ribisnigri* after release of few adults at the center of lettuce field [133], and quantifying spatio-temporal infestation patterns of *Ips typographus*in the Bavarian Forest

National Park via dead wood patches surveillance [134]. These studies provided an approximate speed of leading edge of Rice borer infestation movement [132], the ability of Aphid to spread far away from a source plant of release over time in a green house [133] and spatio-temporal dispersion patterns of bark beetle damages on trees at a wide area scale over years [134]. A similarmethod was applied here, but with regular monitoring of all plants within the fields and their precise damage characters. Such consistency in the experiments helps to detect that the dynamical spatial and temporal pattern of *B. fusca* infestations had a geometrical trend of occurrence under a form of a spiral around initial patches of damaged plants. The identification of such infestation pattern can be very difficult or impossible to describe with the previous approaches [132–134].

It has been reported that oviposition of females insect species such as *Delia radicum* on cabbage plants [427], *Eurosta solidaginis* on late golden rod plants [428], *Lygocoris pabulinus* on potato plants [429] and *Anthocoris nemorum* on apple/pear/peartrees [430] can be observed where conspecifics have already oviposited; the contrary has been reported for *Trichoplusia ni* on cotton plants [431], *Narnia femorata* on cactus plants [432], *Heliothis virescens* on tobacco plants [433] and *Pieris rapae* on Crucifer plant [434]. In the present study, results of spatial clustering suggest that *B. fusca* females tend to oviposition patches of maize plant already infested; and thus, exhibit the fisrt behavorial characteristic. The homogenization of distribution inside each cluster might be due to overcrowding during plant host selection [435,436]. Furthermore, a strong instability (drastic changes in clusters shapes and a number of plants inside each spatial cluster) during the evolution of initial damage distributions might be due to a combination of adult moth oviposition and larvae interplant movements [184,187,437].

Spatial pattern dynamics generated by insect pest can be used to improve sampling strategy, site-specific pest management, and sowing distribution. However, when agricultural practices are undertaken, the precise spatial and temporal dynamic of the damages are usually not well known [131]. Moreover, most of the existing statistical techniques used in similar agro-ecological frameworks than ours are not strongly accurate in order to detect a precise plant-to-plant contagion patterns [129–147,189,190,192,194–198,201]. The methodologies used in these studies focused on two main aspects: analyzing the count-variance of samples

without taking into account the spatial locations (indices of dispersion, aggregation and clumping indices, Taylor power law, quadrat-variance methods, probability distribution models) or focus on count-variance on few samples and the locations of samples (semi variography, spatial autocorrelation analysis, local spatial statistics) [26,129,358,438–443]. In order to gain a considerable amount of information from spatial data, use of several methodologies is recommended [441]. However, it is noticed that conducted studies in a similar framework than ours usually employ one method [129–147,189,190,192,194–198,201]. Thus, our study aimed to be more precise using several approaches which have not been used in the literature such as centroid tracking and spatial clustering in order to track easily the shift of spatial patches and their relative stability respectively. In addition, the cellular automata method was used in our study to go beyond these classical analyses in order to investigate on the likely geometrical configuration of infested plants to contaminate healthy maize plants.

As an attempt to advance the knowledge on movement ecology, the quantification and qualification of the delocalization pattern of the damages spread of *B. fusca* with time were studied. We examined whether the infestation is initiated from an origin point from which it spreads to other locations to create a big cluster of plants damages, or whether multiple damages of plants erupted simultaneously in different locations to create clusters, which merged with time. Through the record of point location for individual infested plants at each week and their respective centroid, it is noticed that the shift of the focal point moves as a spiral centered around the first set of damaged plants. The formation of new spiral during the second cycle of damages could be explained by the ability of *B. fusca* to distinguish patches of larvae/eggs and oviposit in different zones. Practically, while probing for more host plant and flying toward adjacent stems, the pest female is showing preference to the areas with less density of infection, thus spreading their offsprings more widely by creating a new spiral at a distant radius. This result corroborates the hypothesis stating that a lepidopteran is able to adopt a regular pattern during host selection [435].

We observed that the selection of the first plants to be infested by the *B. fusca* female is likely to be random; subsequently the neighbours to the infected plants are most likely to be infected. In addition, it is noticed that the initial infestations occurred simultaneously in

numerous plants. The enhancement of the spatial expansion of damage clusters can be explained by the pest larvae short-range movement ability to migrate from a maize plant to another [187]. This displacement is considered as a survival mechanism; because of competition, the larvae of *B. fusca* are likely to die in a highly infested maize stem [319]. Although *B. fusca* females have the ability to fly over several kilometers [207,444], it was observed that the number of plants infested within a cluster increase progressively and, the shape of the cluster was relatively maintained with time; this can be explained by the ability of lepidopteran to visit patches of plants already infested by their conspecifics [435]. The competition among *B. fusca* female for the same set of host plants during oviposition may be further considered as a key factor that influences the appearance of the patterns observed in this study.

In regard to the yield losses and damages due to *B. fusca* in maize farm, all recorded studies are based on different methodological approaches, yielding a high variability of results [159–170]. This problem of standardization of experimental methods makes a comparison of results difficult or subjective; thus, causing a serious problem in the choice of the information concerning the damaging ability of *B. fusca* that may be given to farmers and decision makers. In this study, a simple, realistic and accurate approach has been implemented to study this topic.

In our study all the plants in the field were considered in contrast to what is presented in literature [159–170]. Focusing on few samples can create a considerable bias which reduces the accuracy of the results because the selected plants could not be a good representation of the whole farm. Majority of methods used in the literature for studying yields losses due to lepidopteran stem borers are visual damage rating, in which grain or cob masses are assessed [159–170]. Weekly visual rating and measuring of cob masses at harvest were applied here.

Although several studies about the link between *B. fusca* damaging factors and yields losses were conducted during decades [159–170], it is noticed that a rigorous selection of the plant physical features suitable to study incidence of the pest has not been done. Comparing features of infested and uninfested plants has been suggested as a systematic method for assessing yield losses in cereals [52]; however, studies considered directly cob mass (infested

versus non-infested) as an indicator for assessing the pest impact without much justification [160,163,165,375]. In this study, a statistical comparison of the plants physical features has been conducted in order to select cob masses as the key factor.

The study of pest damage incidence provides crucial data to decision makers in order to allocate meaningful resources for research and management [173,175,445,446]. Therefore, making decisions for controlling lepidopteran stem borers rely on an accurate estimate of damage incidences and yield losses. However, the values of the overall yield losses in maize due to *B. fusca* reported in the literature varies greatly from one country to another and different agro-ecological zones [155]. It is 10% to100% in South-Africa [155], 0.4% to 36% in Lesotho [165], 0.4% to 41% in Cameroon [160,161,176,447] and 17% in Zimbabwe [212]. In Kenya and Tanzania,12% of yield reduction for every 10% of plants attacked were reported [170] and, later on, yield losses of 14% was reported in [212]. All the methods for estimating the yields losses were done either by comparing grain masses or cob masses from few plants infested in the field [160] or by comparing grain masses from few samples of the field that were protected and unprotected by insecticide [161,165,170,176,212,447]. The present research opted to sample all the damaged plants in naturally infested farms. Average yield losses estimates in this study are between 35.96% and 48.19%.

In order to identify the type of damages implying higher yield losses due to *B. fusca*, several studies have been conducted [159,160,163,165,168,375]. Because of various experimental approaches adopted in these different studies, it was difficult to specify the type of damages (LD, DH, EH, ST or internodes attack) having the most significant effect in the reduction of maize yield. About tunnelling, *B. fusca* was reported to tunnel from 15% to 30% of the length of the stem [180], a range almost similar to our results. In this study, although the stem tunnelling considerably reduced the cob masses, the obtained results suggest that cob tunnelling of *B. fusca* has more effect on the yield.

Busseola fusca is reported to attack young plants preferably [155,184,187]; this is a primary reason leading integrated pest management (IPM) practitioners to apply control measures at the early stage of development of maize crop [155]. However, the results obtained in this study suggested that all the plants with leaf damages (primary infestation damage from *B. fusca*) had a cob at the end in contrast to those having secondary and ternary

damages like dead heart and exit hole respectively. Therefore, control measures should be applied continuously during maize life cycle.

Numerous information on the temporal patterns of stem borers infestations are reported in the literature [155,165,231,448,449]. It is demonstrated that *C. partellus* infestation on younger plants has a higher incidence on the yield losses than infestation on older plants; additionally, it is reported that the intensity of leaf damage is significant in younger plant and, stem tunnelling is significantly correlated to yield losses in older plants [231]. In this study, we did not observe any particular trend in yield losses according to the leaf damage and exit hole made by *B. fusca*. For the dead heart, the time of infestation is important; when it happens within a two-week interval from planting, yield losses is high. Furthermore, the decrease of the yield losses with the time of infestation observed in this study is similar to what has been reported in the literature [450].

Numerous studies attempted to link the stem tunnelling damages and the cob masses [160,163,165,375]. A linear link was presented with little significance in [163]. We failed also to establish a link between the two variables in this study. It implies that others factors should be considered while liking yield losses and stem tunnelling or, no link could exist between these two variables. We went beyond existing studies by estimating the type of link between the cob tunnelling and the cob masses. In general, yield due to a pest on a crop is reported to be a linear or a non-linear function decreasing with pest damage intensity [158,171–173]. This trend was observed in maize in the case of *B. fusca* [160,161,163,170,174] and, *C. partellus* [231,445,451]. In this study, a different tendency was observed while analyzing cob mass function of the length of the tunnel in a cob wich is a cubic function.

Control of negative impacts of lepidopteran stem borers is a serious challenge [452]. These pests can be reduced using: chemical insecticides [453], botanical agents, habitat managements, synthetic pheromone, genetically resistant maize varieties, cultural control and biological control [155]. Based on the previously mentioned methods, IPM strategies for lepidopteran stem borers were developed [51,155,282,283,285,286]. Despite the fact that precise spatio-temporal dispersal of the insect pest damages is of primary importance, this information was not taken into account in IPM strategies toward *B. fusca*. The spatial

arrangement of trap plants should be reflective of the patterns of natural field colonization/infestation by the pests [454]. The insect pest *B. fusca* is reported to attack young plants preferably [155,184,187]; this is a primary reason leading IPM practitioner to apply control measures at the early stage of development of maize crop [155]. However, the continuous pattern of infestation observed in this study throughout the whole growing stages of maize plants suggests that the application of chemical insecticides should be done in older plants also. The present study provides a prior overview of *B. fusca* damage spread, which can be used by IPM practitioners during spatial and temporal disposal of the control measures. Therefore, allow cost strategy can be developed by optimizing the applications of control measures embedded in existing IPM methods for *B. fusca*.

The understanding of the timing of damages induced by the offspring of *B. fusca* moth subsequent to its first arrival in the field and, a precise characterization of spatial patterns resulting from the spread of the damages in the field with time are two major challenges in pest management. These keys information can be used to improve the field application of existing control methods such as pheromones traps [155], parasitoids [455,456], entomopathogenic fungi [457] and insecticides [155]. The extended flight periods of *B. fusca* observed in this study suggest that oviposition occurs continuously with time; therefore, pheromone traps should be installed throughout the whole plant growth period. A biological control approach such as egg parasitoids release has been suggested [455,456]; however its efficient application can be improved by the knowledge of the flight dynamics of *B. fusca* male observed in the current study. Once adult moths have been noticed in pheromones baited trap, egg parasitoids should be released the next week to limit eggs hatching. The disposal of pheromone-baited trap combined with the dissemination of entomopathogenic fungi using *B. fusca* male as the vector can be done by a protocol described in [457]. The current study suggests that such device containing the fungi must be kept in the field during the whole plant growth period in order to increase the probability to kill neonates from staggered oviposition during several weeks. If the farmer does not have an access to the previously mentioned control methods, the use of the results obtained by spatial analyses in this study can help to make a site-specific management more efficient by offering the advantage of limiting the amount of insecticide used within a maize farm, as well as the time and labor involved with its

application. Since this method allowed us to estimate a plant-to-plant contagion rule with time, it is possible to predict potential hot spots or aggregated infestation sites and to apply targeted and preventive sprays of insecticides located within a few meters around the areas where the first leaf damages are observed.

III-5 Modelling damages spread of stem borer

III-5-1 Results

Although the sizes of the plots are different, the scale of percolation is relatively constant in all the plots (Table 10). The observed dynamic of cluster densities at different observation scales for each plot is depicted in Figure 4. During data processing, when at least one plant in the k times k matrix was found infested, the resulting cell was considered as infested. If the scale of observation of the infestation process is above a certain threshold value, the infested clusters are connected with each others. In contrast, below that threshold scale value, the infested plants are restricted to small and non-connected patches scattered on the farm. The sub-figure with the gray curve represents the critical resolution whereby the reduction of the number of infested patches started decreasing. A similar pattern for plot 2, 3 and 4 was observed (Figure 30). Apart from plot 1 where the resolution threshold for percolation is 1/5, other 3 plots have a resolution threshold of 1/4. The critical concentrations of infested cells for plots 1-4 are 0.0707, 0.0406, 0.0140 and 0.0224 respectively. The time of occurrence of the maximal number of clusters in each plot at the scale of percolation was observed the fifth week in plot 1 and 2, the second week in plot 3 and the eighth week in plot 4. It can be noted that the cluster density decreases when the scale is too large (sub-Figure 30).

Before conducting the spatial and temporal spread of the pest damages, all plots were rescaled at the percolation dimensions (Figure 30). The sensitivity analysis that models precisions variability according to rules of CA infestation at each plot is presented in Figure 32 (a). The ability of the linear model to explain the variability of $\bar{p}$ around its mean as well as the significance level was acceptable (r^2=0.72, P-value=9.29×10^{-54} for plot 1; r^2=0.65, P-value=3.67×10^{-44} for plot 2; r^2=0.74, P-value=6.38×10^{-56} for plot 3 and r^2=0.63 and P-

value=8.51×10^{-42} for plot 4). Results illustrate that the transition rules are crucial components in modelling in order to replicate accurately the observed experiment in the field. Although the Moore-2 contains more cells and is more extended spatially, the mean correlation coefficient seems to be more sensitive to Moore-1 neighbourhood. This suggests that nearest infested plants in the modelling framework have more impact than the distant infected plants. The sensitivity of the running time of the simulations in a computer for deferent scales is depicted in Figure 32 (b). The time spent by a personal computer to simulate the damages spread decrease significantly. When comparing the model simulation at a scale of 1/1 and the time taking to simulate using percolation scale; over 50% in reduction of time was noticed. The initial conditions for simulations were the same for each plot as displayed in the data obtained from all fields. The positions of the first infested cells during the first observation are recorded in Figure 31. After several trials, the couples of parameters (δ_1, δ_2) were fixed to be equal to (3,11), (2,9), (3,11) and (2,5) for plot 1, 2, 3 and 4 respectively. Others choice did not provided good results. The model predictions of the spatial and temporal evolution of infested cells for plots 1 are presented in Figure 33 (for plot 2-4 see the appendix); the predictions are more accurate for plots 2 and 3 than for plots 1 and 4. Simulations of infested cells in plot 1 and 2 predicted fewer cells compared to the data. In addition, the simulated pattern of plots 4 is different to the data. Such discrepancy may be due to the initial conditions of the model simulations or to the non-linear pattern of the insect species oviposition pattern. An additional explanation for this difference is that, a number of infested cells in the neighbourhood as parameterized in the model might be lower or higher than what exists in reality.

A comparison between CA simulations of a weekly sequence of plant infestations and the observed data is presented in Figure 34 . The correlation level was greater than 60% in each plot for the subsequent weeks once we have initialized the simulation with the position of infested cells at the first week of infestation occurrence. It was noticed that the level of similarity decreased over time. This level of agreement shows that IPM practitioners can use the results for improving management of *B. fusca*. The temporal trend for the density difference between the spatial distribution of data and the simulations increased with time, meaning that the data and the simulations the fact that CA replicates very well the data during

the first weeks. Differences between model results and observations are relatively minimal given the significant spatial correlation and comparisons between multifractals at each week. In addition, it can be noticed that the multifractals approach can be a good mean to evaluate the accuracy of CA model output. This finding reveals that the model assumptions were effective at ensuring that the simulated infestation dynamic is close to those observed in the field.

Plots	Plot 1	Plot 2	Plot 3	Plot 4
Size (in meter)	51.03×53.93	150.66×31.57	120.69×30.50	153.3×27.82
Spacing between columns (in meter) – spacing between rows (in meter)	0.81 - 1.05	1.86 - 0.65	1.49 - 2.10	1.05 - 0.53
Percolation scale	1/5	1/4	1/4	1/4
Unit cell size at the percolation scale (in meter)	4.05×5.25	7.44×2.6	5.96×8.4	4.2×2.12

Table 10:Results obtained after searching for the percolation scale. Each decimal dimension is given in meters.

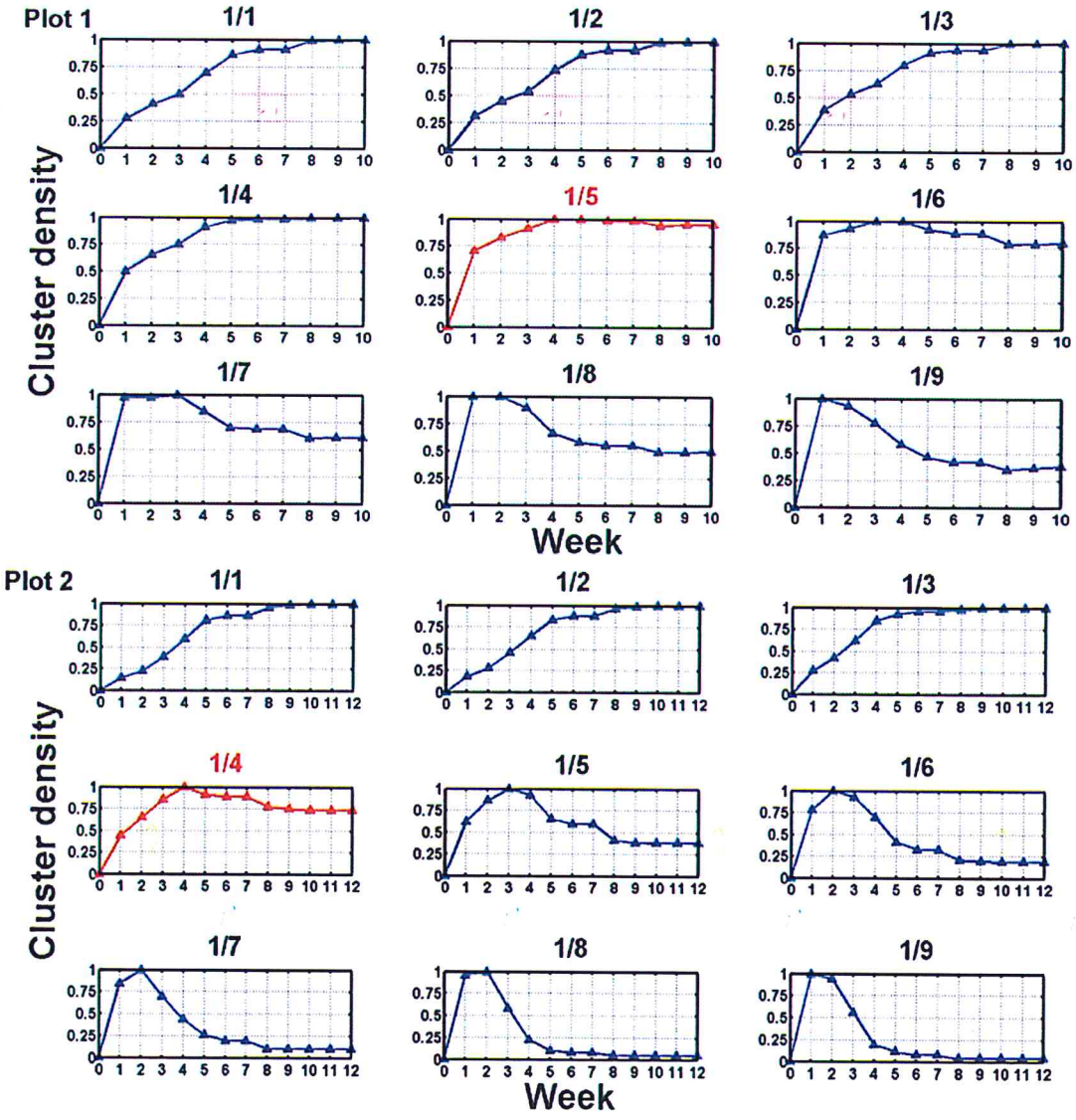
Plot 1
1/1
1/2
1/3
1/4
1/5
1/6
1/7
1/8
1/9
Cluster density
Week
Plot 2
1/1
1/2
1/3
1/4
1/5
1/6
1/7
1/8
1/9
Cluster density
Week

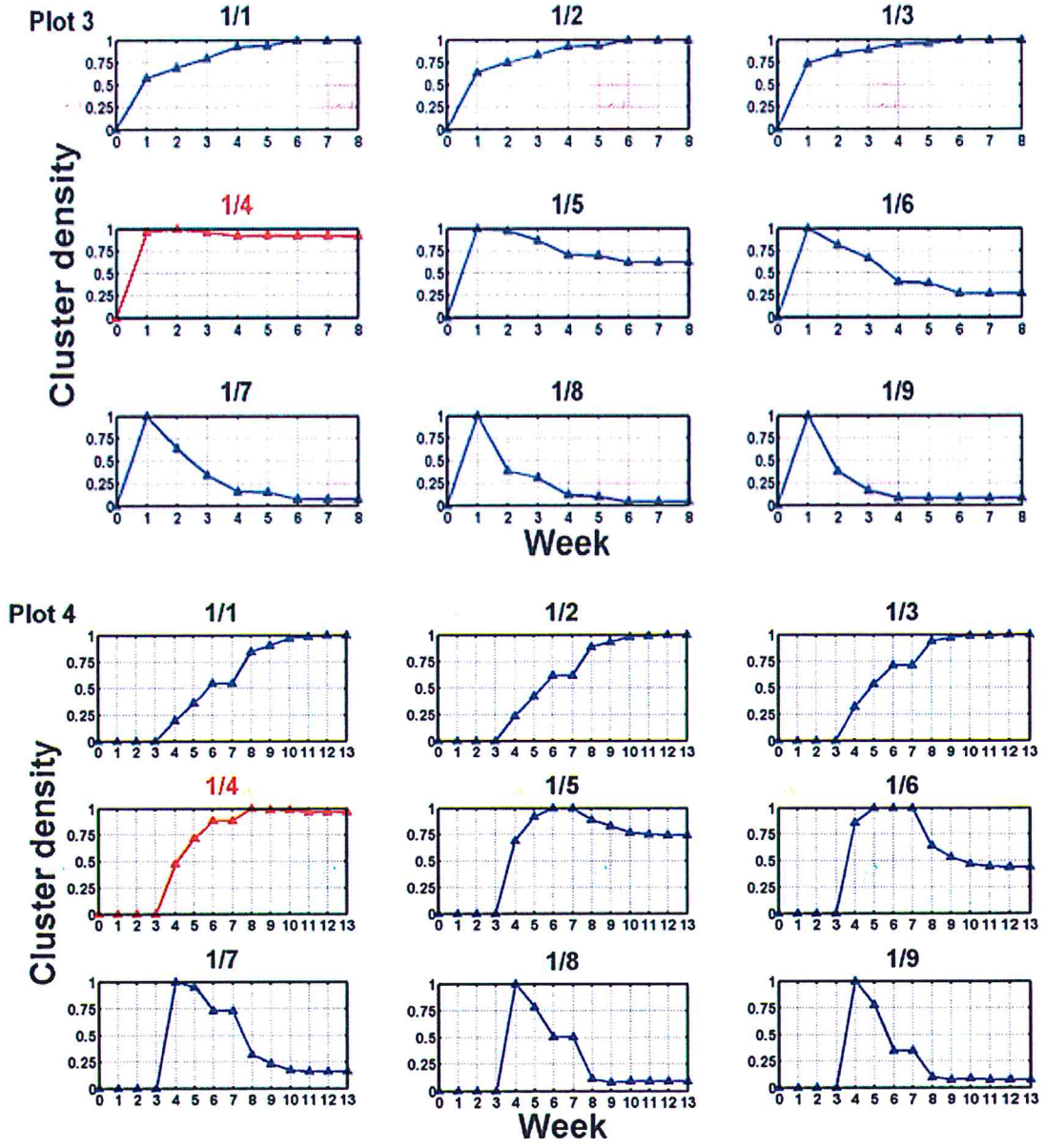

Figure 30: Estimation of the percolation scale in plot 1,2,3 and 4. The cluster density represents the number of infested cells week after week. This number was normalized between 0 and 1. The fraction above each sub-figure represents the scale of observation. The denominator of each fraction represents the square root of a number of maize plants inside each unit square. In clear, *1/p* means that the maize plot was observed by taking a unit of $p \times p$

plants. If at least one plant in the $p \times p$ matrix was infested then the resulting cell was considered as infested. The sub-figure with the gray curve represents the critical resolution whereby the reduction of the number of infested patches start decreasing after a certain number of weeks.

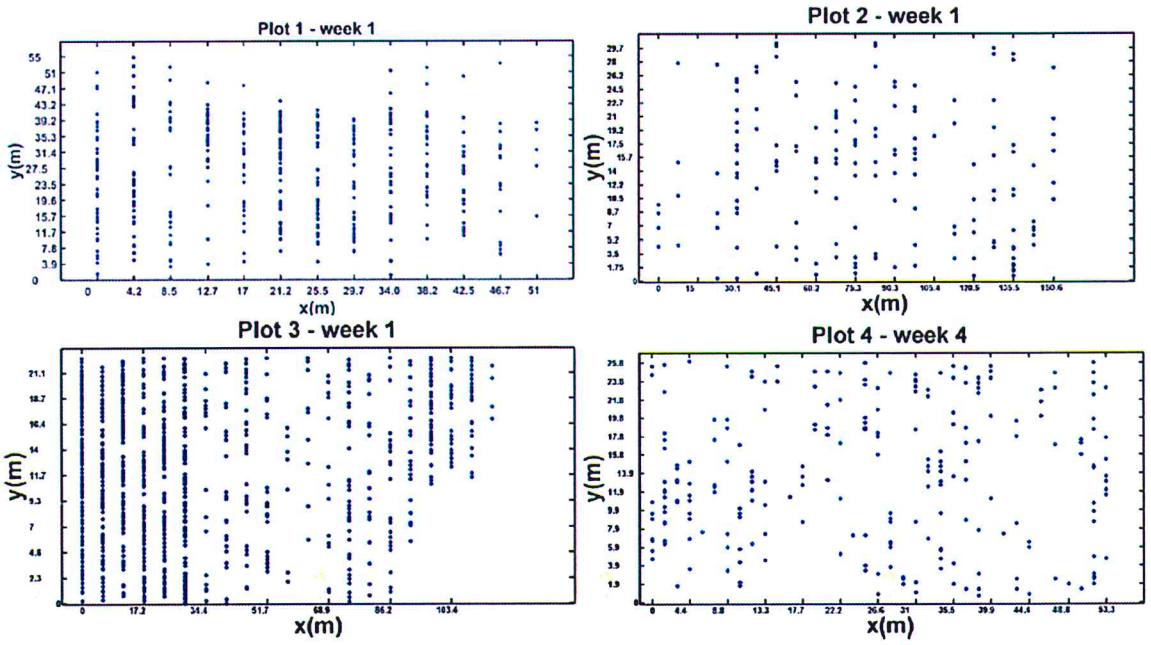

Figure 31:Position of the infested cells during the first week whereby infested plants were noticed during the data collection on the field. The blue dots represents the infested cells and the white cells are the non-infested cells.

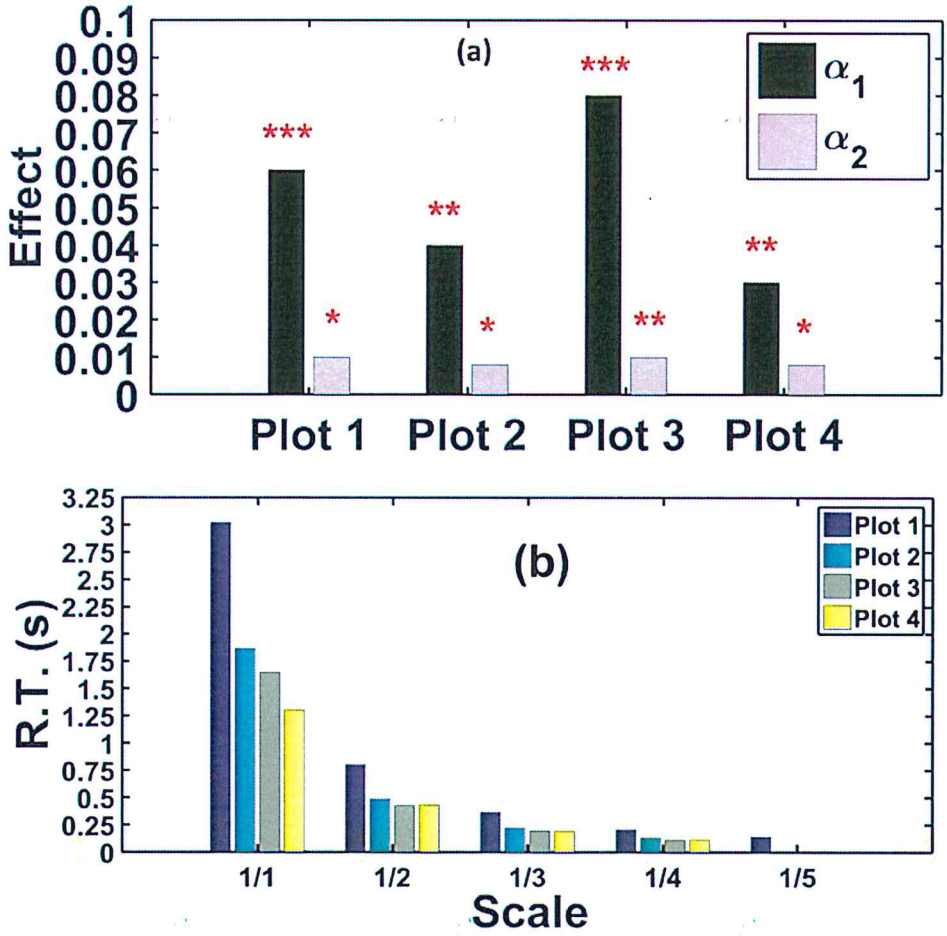

Figure 32: (a) Estimated parameters $\alpha_1$and α_2 after multi-linear regression with the integer parameters $0 \leq \delta_1 \leq 7$ and $0 \leq \delta_2 \leq 23$. The mean correlation coefficient $\bar{\rho}$ between the predicted and observed data was estimated for all the possible combinations between δ_1 and δ_2 before the regression. The stars on the top of each bars stand for the level of significance: * p-value $< 10^{-15}$, ** p-value $< 10^{-30}$ and *** p-value $< 10^{-40}$. In Figure 6(b), we computed the running time (R.T.) of the program simulating the damage spread at different spatial scale. The unit of this time is in seconds.

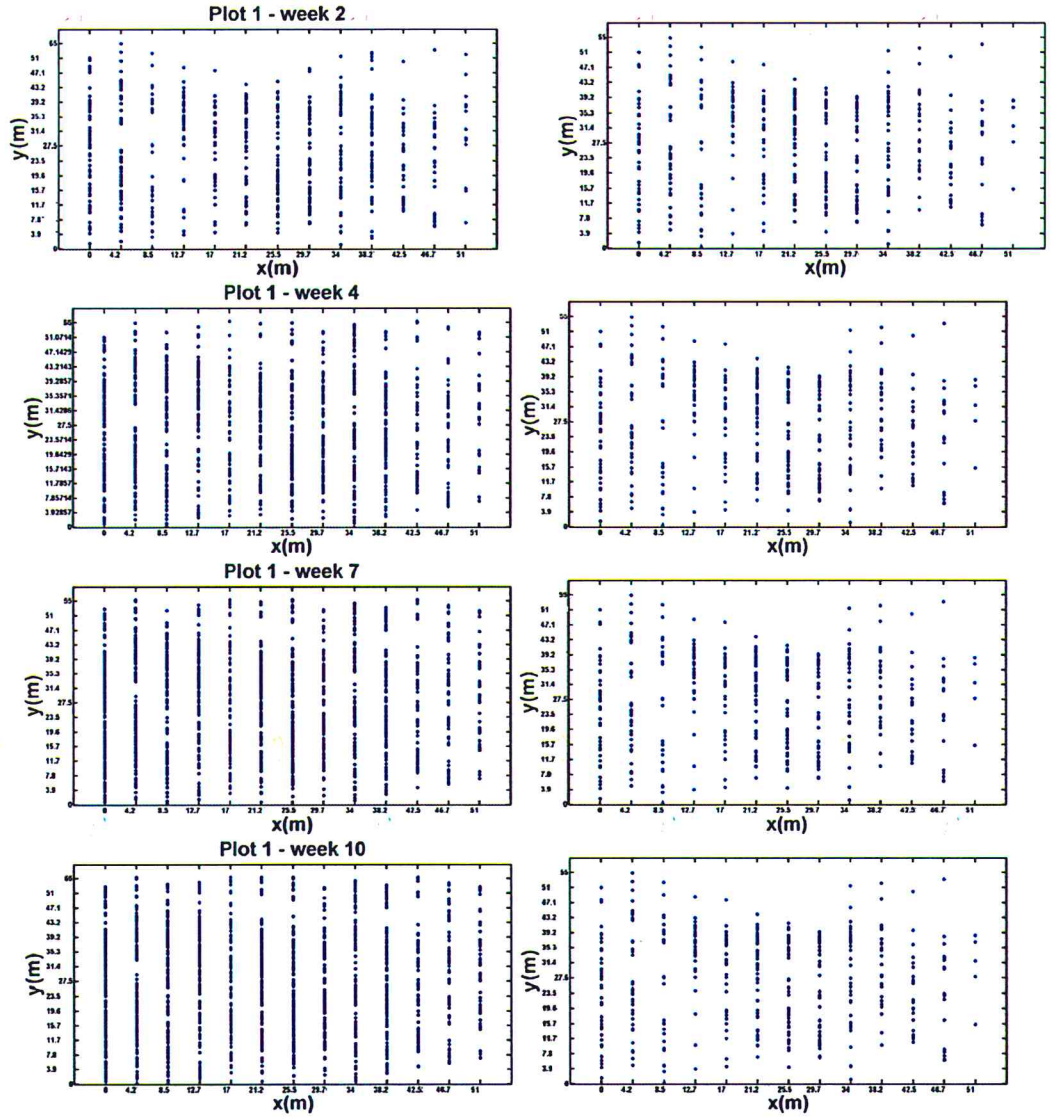

Figure 33: Representation of the spatial and temporal evolution of infested cells in plot 1. On the left are the collected data and at the right the simulated infestations. The blue dots represents the infested cells and the white cells are the non-infested cells.

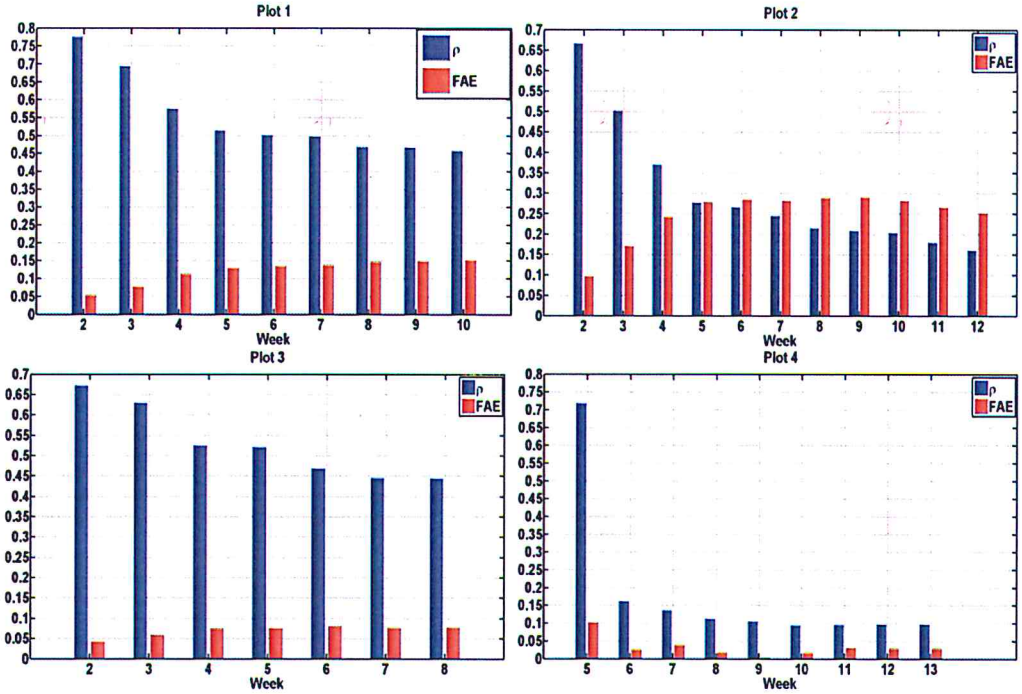

Figure 34: Comparison between observed and simulated infestations at each iteration. The black bar represents the correlation coefficient (ρ) between the observed and the simulated results. The gray bar represents the fractal average error (FAE) between the spatial distribution of infested cells in the observed and predicted results. The coefficient of determination r^2 was greater than 0.95 for each plot during the estimate of the multifractal dimension.

III-5-2 Discussions

Percolation, one of the method applied in this study has been extensively used in different contexts such as spatial epidemiology [241–244], petroleum geosciences [458], geometrical effects in physical properties [459] and on the connectivity among fragmented landscapes [460,461]. In animal behaviour research, effects of the observation scale on the movement were also quantified with the percolation [462]. However, the theoretical conjectures of these numerous studies were mainly based on numerical simulations without connection with experimental data for performance evaluation and validation [241–244,458–462]. The present study shows the link between the percolation and the spatial resolution during *B. fusca* infestation and spread in maize farm via a spatial magnification threshold. The

results obtained with the percolation theory are in agreement with those of [462] and [460]. Their findings demonstrated that the scale of observation and the distances between elements could play a significant role in the percolation threshold; we also arrived at similar conclusions. Furthermore, the approach used allowed simultaneous estimation of the distance threshold and occurrence time period of the percolation threshold.

In multiples studies using CA, the cell representing an infestation is most often a surface or a set of plants [246–248,270]. The choice of the unit cell size is usually subjective and mostly guided by the aim of optimizing the computation efforts for reducing the simulation time. In an agro-ecological context such as the present study, an approach was proposed to choose the optimal cell size based on the theory of percolation. Contrary to numerous studies [241–243,458–460], the resolution scale in our context was used as a parameter that directly affects the start-up of the percolation phenomena during the spread of infestation of *B. fusca* damages. Such choice of a resolution was made to allow a good balance between the cell size and the percolation of plant damage spots caused by *B. fusca*. Although a trial and error method was proposed to select an appropriated spatial scale thought multiples simulations for different cells sizes [293], a simpler process using the percolation theory has been suggested here; our results suggest that percolation theory can be used as a method to select cell size of CA in order to solve this recurrent challenge reported in literature [240,287–292].

The direct implication of using percolation with CA goes beyond ordinary CA simulation framework find in literature [246–248,270]. The ability to scale-up and scale-down is crucial to overcome the difficulties dues to the limited amount of data [463]. Moreover, it offers to IPM experts a new opportunity of improving sampling methodology based on the choice of the optimal quadrate size of infested plants. Instead of sampling systematically within the entire field, it may be more relevant to work at a certain unit size of surface capable of capturing the infestation spread. Therefore, our findings suggest the application of the theory of percolation to supplement the sampling design for collecting spatial and temporal information of insect pest damages spread; and to complement to the existing methods for spatial and temporal statistical analysis of data in the literature [129,359,438,439]. Cellular automata with its fundamental features of homogeneous

transitions rules, synchrony in the changes of state of cells and static neighbourhood configuration are not appropriate in yielding good replication of a spatial and temporal ecological process [268]. Modifications of these fundamental features are required in order to generate good results [232,233,235,237,239,263–268]. In addition, there are situations where important factors influencing the spreading of the pest are known, but the exact link between the damage spread and these factors are unknown or imprecise [245–249,269,270]; for instance, the impact of wind intensity [245], the suitability level of spatial grid point [246,249], the level of plant susceptibility [247], the concentration level of the chemical substances [248], climatic conditions [464], pesticides [465] and the level of population density of the natural enemies [269,270]. Because of the pitfalls in the use and direct application of homogeneous CA, we opted for *B. fusca* male abundance inference by mean of fuzzy logic concept. A direct correlation of adults abundance obtained via pheromone-baited traps to infestation rate has been done in several several studies on others crops and different insect pests [382–390]. Therefore, since life duration of *B. fusca* adult is very short (2-4 days) and the mean sex ratio between males and females is 1:1.1 [187,405,466,467], the abundance of adult males can be considered as a good indicator of the density of females whose larvae offspring will cause damages on maize plants. In reality, the efficiency of a CA model is highly influenced by the neighbourhood configuration [288,290]. During the implementation of ecological CA with fuzzy logic inference, the neighbourhood configuration is often unchanged for the simulations [245–248,269,270]. Static neighbourhood configurations have been used in numerous applications [381,468–474]. However, in the current exploration, we opted for a dynamical neighbourhood, similar to what was applied to optimize the speed of computation [298] and in land use modelling [296,297]. The approach consisted on provoking dynamical changes of the radius of the CA neighbourhood based on expert knowledge coupled with the optimal selection of the cell size via the percolation theory.

This study gives an insight into the effect of different transition rules, which is not an explored field in sensitivity analysis for CA models for insect pest infestation in agro-ecological models [232,233,235,245,249,263–266,268,269]. Meaningful IPM decisions in the management of *B. fusca* damages can be obtained through adequate understanding and exploitation the impact of the variation of the CA neighbourhood highlighted in this research.

In clear, specific neighbourhood triggering infestation coupled with pest control measures can be represented in the model framework to develop a strategic and tactical decisions support system for IPM practitioners.

The evaluation of the performance of ecological CA simulation is sometimes conducted by the use of mean absolute error and root mean square error [245,299]. In this case, such approach did not provide an indicator of the spatial repartition of infested plants inside the farm. Fractal dimension was applied with CA model outputs to represent and understand the complexity and fragmentation of land use [288,475]. However, the multifractal dimension was viewed suitable for describing the spatial repartition of spatial point data instead of providing only a global geometrical description of the area as the fractal dimension [276,279,280]. Multi-fractal dimension was selected as a means to characterize the spatial repartition of living organism in a surface [274–277,279,280] and the spatial characterization of disturbance pattern from biological invasion [278], but it can also characterize the spatial distribution of insect pest infestation [250]. Although there are several multifractal dimensions, the present study focused on the information dimension (D_i) because it is the most informative in the dimension spectrum [274]. The D_i was used for comparing the model simulation outputs and the collected data.

We further suggest multi-fractal as a tool for uncertainty analysis of CA models dealing with insect pest damage spread. The multifractal concept brings two simultaneous benefits: it guides on the estimate of the level of spatial distribution and assists on the comparison of spatial clustering level between observed data points and model outputs.

With a combination of several approaches (percolation, CA, fuzzy logic and multi-fractal) the developed model for stem borers infestation spread dynamics gave a satisfactory result for mimicking the observed infestations but some slight imperfections in the accuracy still persist. Such pitfalls could be due to the stochastic nature of living organism behaviour within their environment. The flight and egg laying tactic of insect are probabilistic phenomena [181,476–479]. That is why a stochastic behaviour is often explicitly taken into account during modelling flight, post/prelanding comportment and female oviposition [480–482]. The larvae movements of stem borers, which impact on damage spread was neglected in

the current study could possibly be another factor responsible for the model predictions skills [184,187,437,483]. In addition , the non-consideration of natural enemy effects on the population density of the insect pest could be a supplementary reason for the model imprecision [375,484–487]. Despite these limitations, the developed model is able to forecast with an acceptable level of accuracy the spread of the plant infestation in the field. The accuracy increases if the model inputs the observed plants infected at any specific week and try to predict potentially infested plants in the next consecutive week. Thus, it is possible to foresee the next set of plants infested and apply adequate preventives control measures.

III-6 Coupling the pest dynamics and crop simulation model

III-6-1 Results

In order to compare the effect of the pest damages on the plant, a simulation have been done with and without the effect of presence of *B. fusca* (see Figure 35). The initial conditions are 10 Adults, no eggs, no larvae and no pupae.. The plants were able to compensate the removed biomass by the larvae during the first weeks of growing season. The leaf area index showed the same pattern. At the middle of the growing season, the plants attempts to compensate the relative yield losses in biomass but the difference in biomass from damaged and undamaged plant became more considerable with time. The leaf area index and the total consumption of the larvae population decreases drastically with time 80 days after planting. The initial number of adult decreased quickly with time and remerged from pupae

approximately 60 days after planting (

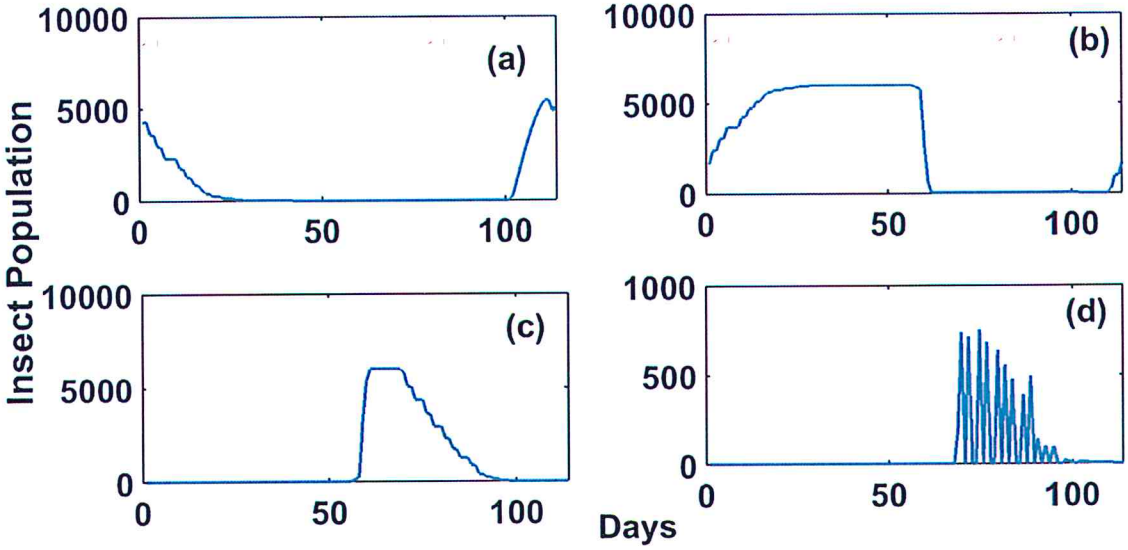

Figure 36). In general, adults died very quickly compared to immature life stage and, larvae lived for a longer period of time which is in accordance to what is observed in experiments [320]. In addition, the eggs hatched in 09 to 10 days after oviposition similar to what is reported in the literature.

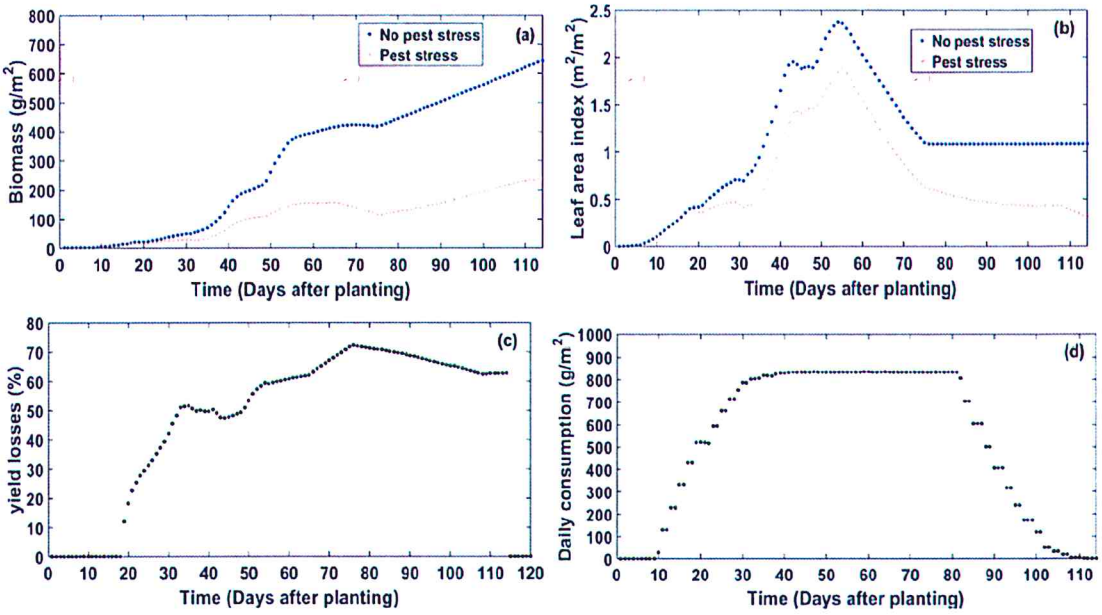

Figure 35: Simulations of the potential effect of *B. fusca* on maize plants

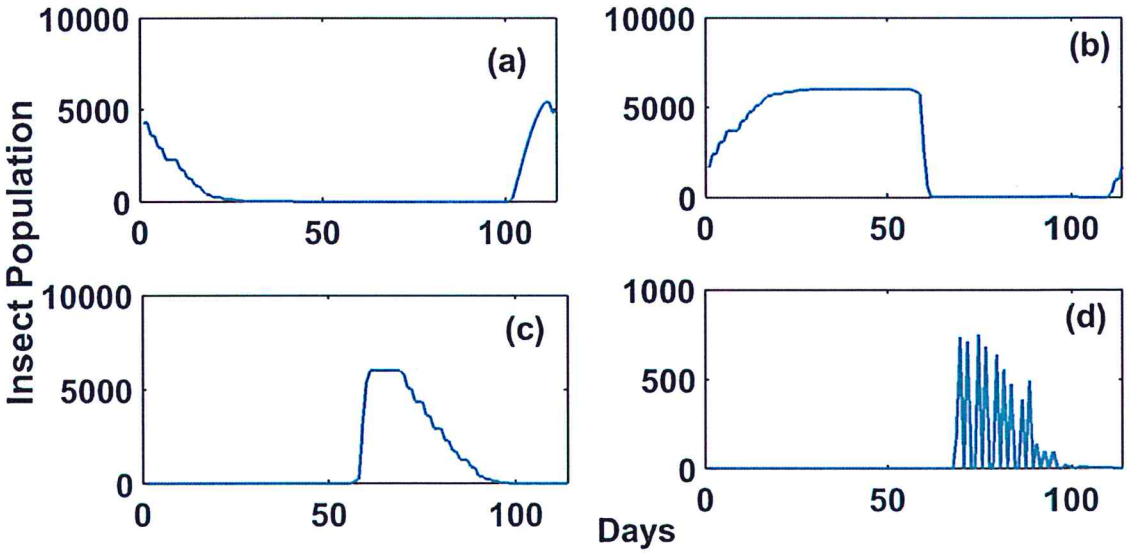

Figure 36:Population dynamics of the insect at each life stage (a) eggs, (b) larvae, (c) pupae and (d) adults

III-6-2 Discussions

Simulation of the population dynamic of insect pest such as, the apple orchard pest *Cydia pomonella* (L.) [314], the fruit pest *Carposina sasakii* [315], *Bactrocera (Dacus) tyoni* [316] and tea pest, *Caloptilia theivora* [317] have been done mostly using dynamical equation with coefficients derived from experimental data. Numerous experiments regarding the biology of *B. fusca* have been conducted in order to assess the effect of humidity, temperature, nutrients contained in maize plant but were not exploited with the aim of modeling the population dynamic and the maize-insect interactions [318–320,409].

Although the biology and the ecology of *B. fusca* have been extensively studied but no one has developed a dynamical model to simulate the number of insect with time [51,155,187]. By using the experimental result from reference [320], the pest component of this model was developed in a similar way than other conducted studies [314–317]. However, in these studies, the plant dynamic itself was not considered which is not the case here. Although a varying the temperature can considerably influence the survival and ageing of insects [488,489], the mortality rate of adults was fixed in these models [314–317]. Similarly to the approaches used for the daily development rate, the longevity rate estimating the daily accumulation of heat or cold effect on female adults over time was used here as suggested in [490].

The classic method to assess yield losses due to cereal stem borers consists in comparing the feature of damaged and undamaged plants [52]. Furthermore, the estimate of the losses was most often made at the end of the growing season or, by uprooting few damaged plants collected in the field with time [160,163,165,375]. In this study, we suggested a dynamical system approach to simulate the daily consumption of maize by *B. fusca* whit a simultaneous estimate of the dry matter accumulation inside the plant and the *B. fusca* life cycle dynamic.

The existing model in the literature integrating the interaction with the plant and the pest was "one-way"; meaning that the pest have an impact on the plant but the plant does not

have an effect on the insect [308–310,491]. Furthermore, the main driving variable influencing the whole pest-crop system was the external temperature. In this study, a crop simulator model which includes more factors was used to overcome such limitation.

In the CSM named CERES-rice, the effect of multiple pest effects on rice has been included by functional responses [59]. In the software InfoCrop, the effect of rice insect pest has been simulated with a constant assimilation rate of larvae and no feedback from the plant [55,492–495]. In APSIM-wheat, the leaf area was the link between the pest and the CSM; however, feedback mechanisms from the crop and the pest were neglected [58]. The existing generic pest module in DSSAT/CSM linked the effect of the pest by a linear response to a fixed number of the pest in the field with no dynamical prediction of the pest population and life cycle driven by environmental factors [57]. In this study, we simulated the plant dynamic in parallel with the insect pest dynamic including a "two-way" interaction between maize and *B. fusca*.

Although the negative influence of wind speed and Nitrogen deficiency have been modelled using fuzzy logic [325–328], it is observed that none of the existing pest-crop models is able to consider uncertainty during the plant-pest interaction. In this study, fuzzy logic has been used to modulate the assimilation rate of dry matter from maize plant and the relative growth rate of *B. fusca* larva.

General conclusion and perspectives

In summary, this study attempted to improve the Daydov's model by accounting for the influence of mobile inhomogeneity and the introduction of a hyperbolic nonlinear potential. This work led to conclude that the mobility could be achieved by a traveling energy

mode among in the protein lattice. The approach used here has the potential to be generalized to any type of DNLS physical system .

The nonlinear coupling in the DNLSE contributes to the localization of the energy. Furthermore, in the DNLSE derived from Davydov's equations after adiabatic approximation, the nonlinear term depends on the potential energy function of hydrogen bonds. Indeed, there is a high probability that the rapid decoherence of waves under thermal bath obtained in previous studies on Davydov's model might be due to either the initial conditions or the usage of an inappropriate hydrogen bond potential.

The current study showed that the electrical wave propagation in microtubule (MT) could be modelled by a discrete nonlinear transmission line including a cubic negative nonlinear resistance. Nonlinear resistance was used to represents the ionic flow through nanopores of MT. The nonlinear supratramission threshold can be estimated by the NLRM. In a dissipative system, nonlinear supratransmission threshold can be lower than the infratransmission threshold; when these two thresholds are closer, the supratransmission threshold could be considered as infratransmission threshold. At the biological viewpoint, a specific intensity of ionic flow through nano pores of MTs can allow the high frequency of electrical signal processing by neurons. Also, the infratransmission phenomenon in MTs of neurons can be leeway for the explanation of why repetitive transcranial stimulation with the high frequency magnetic field can attenuate the motors signs of the Parkinson's disease. The wave amplification of MT-induced by calcium wave could be explained with a model including nonlinear resistance.

The current study attempted to understand the spatial and temporal patterns generated by the damages of *B. fusca* within a smallholder maize farm. This investigation provides an estimate of the time interval between the incidence of the peaks of abundance of *B. fusca* adult male and the leaf damage in the field. It was found that leaf damage caused by the immature live stage of *B. fusca* seems to be a key factor causing the death of maize plants. This research further helps in illustrating the evidence of considerable spatial autocorrelation with time of damaged plants within a small radius and, the initial area of infestation and spread from foci under a form of cluster/spiral pattern. Finally, the rules by which a plant gets infested by neighbors were identified. These findings lead us to conclude that the known biological and

ecological processes of infestation by the African maize stem borer *B. fusca* reported in the literature occurs under the form of explicit spatial and temporal patterns. To be more specific: (i) there is a time synchrony during the appearance of damage peaks and males moth abundance, (ii) particular attention should be paid for the leaf damage and, (iii) spatial distribution of the infestation with time occurs in a pattern which can be tracked. In this context our findings can assist in identifying and, in prioritizing an adjacent set of plants for either reactive, direct control efforts, or anticipative strategy optimizing the existing biological controls in order to reduce *B. fusca* damages. We hope this study will pave the way for a deeper understanding of movement ecology of *B. fusca* and stimulate further investigations.

The important role of cob damages by *B. fusca* infestation is emphasized. The results confirm that both early and late infestation can be important causes of maize yield losses during the plant life cycle. There is real need for standardization of experimental approaches to investigate damages and yield losses of *B. fusca* in order to ensure replication of studies and facilitation of comparisons between results from different authors. The important yield losses recorded in this study in small-scale farms in Central Kenya indicate that *B. fusca* remains a major pest of maize in spite of many methods deployed to control it since decades. Our results suggest that the current control methods like male disruption, cultural control, habitat management should be improved and intensified and probably innovative new control methods such as, dissemination of entomopathogenic fungi and more specific natural enemies should be deployed.

The results of this study revealed that *B. fusca* induced leaf damage pattern spread at farm scale can be simulated using a fuzzy-CA approach linking local dispersal of *B. fusca* adult populations' density. The spatially explicit cell-based approach for modelling the damages incorporates *B. fusca* adult abundance by combining the population density and dynamics of cell neighbourhood configuration for infestation seems suitable here. It is believed that the proposed hybrid modelling approach adequately captures the dynamics of *B. fusca* damage spread.

The use of spatial dynamic modelling for understanding the spread of the lepidopteran *B. fusca* was useful for creating a framework for assembling known information about how the insect pest damage can spread. Modelling the damages spread of *B. fusca* in maize farm is

important insofar as it enhances the development of appropriate control measures for minimizing the negative impact of the pest on maize crop. Practitioners interested in IPM for optimizing the timing of control measures need accurate predictions of the dynamic of pest damage spread with the aim of reducing losses. The fuzzy-CA inference approach permits to better understand the implication of adult population on spatial and temporal spread of maize crop damaged by the insect pest. IMP practitioners could design, efficient timing strategy knowing the most likely pattern of farm contagion week after week. The developed model to simulate damages spread of *B. fusca*in selected maize farms in Kenya can also be applied/adapted to others types of insect pests and agricultural crops in others areas. In the futures studies, it could be of a particular interest to predict the quantitative impact of pest such *B. fusca* on the yield of maize crops.

Finally, we have developed a simple dynamical system for the population dynamics of *B. fusca* and coupled it to a crop model. Although the model did not included other attacks likes cob boring, effect of parasitoids, the obtained results are encouraging in trhe sense that the generic approach can be applied or adapted for another crop and pest (weed, diseases, or insect).

Bibliography

[1] H. Mathieu, *Physique Des Semie Conducteurs et Des Composants Electroniques* (1990).

[2] J.-C. Peuzin, *Magnetisme II, Materiaux et Applications* (EDP Sciences, 2000).

[3] S. Ungar, *Fibres Optiques, Theorie et Applications* (Dunod, Paris, 1989).

[4] A. C. Scott, *Neuroscience* (Springer New York, New York, NY, 2002).

[5] J. Keener and J. Sneyd, editors , *Mathematical Physiology* (Springer New York, New York, NY, 2009).

[6] S. Zdravković and M. V. Satarić, Phys. Lett. A **373**, 4453 (2009).

[7] A. M. Kenneth, B. L. Jonathan, and R. S. Susan, *Biology*, 9th ed. (McGraw-Hill, New York, 2011).

[8] A. Bruce, B. Dennis, H. Karen, J. Alexander, L. Julian, R. Martin, R. Keith, and W. Peter, *Essential Cell Biology*, 3rd ed. (Garland Science, Taylor & Francis Group, 2010).

[9] N. G. Berloff, Phys. Lett. A **337**, 391 (2005).

[10] A. S. Davydov, J. Theor. Biol. **38**, 559 (1973).

[11] A. Scott, Phys. Rep. **217**, 1 (1992).

[12] J. P. Cottingham and J. W. Schweitzer, Phys. Rev. Lett. **62**, 1792 (1989).

[13] J. A. Tuszynski, A. Priel, A. Brown, H. F. Cantiello, and J. M. Dixon, *Electronic and Ionic Conductivities of Microtubules and Actin Filaments, Their Consequences for Cell Signalling and Applications to Bioelectronics* (Francis & Taylor, London, 2007).

[14] K. R. Brunden, V. M.-Y. Lee, A. B. Smith, J. Q. Trojanowski, and C. Ballatore, Neurobiol. Dis. (2016).

[15] D. E. Friesen, T. J. A. a Craddock, A. P. Kalra, and J. A. Tuszynski, Biosystems **127**, 14 (2015).

[16] A. Priel, J. A. Tuszynski, and N. J. Woolf, J. Biol. Phys. **36**, 3 (2010).

[17] A. Priel and J. a. Tuszyński, EPL (Europhysics Lett. **83**, 68004 (2008).

[18] D. I. Ilić, S. M. V, and R. N., Chinese Phys. Lett. **26**, 73101 (2009).

[19] M. V. Satarić, D. I. Ilić, N. Ralević, and J. A. Tuszynski, Eur. Biophys. J. **38**, 637 (2009).

[20] M. V. Sataric, D. L. Sekulic, B. M. Sataric, and S. Zdravkovic, Prog. Biophys. Mol. Biol. **119**, 162 (2015).

[21] M. V. Satarić, D. Sekulić, and M. Živanov, J. Comput. Theor. Nanosci. **7**, 2281 (2010).

[22] D. L. Sekulić, B. M. Satarić, J. A. Tuszynski, and M. V. Satarić, Eur. Phys. J. E **34**, 49 (2011).

[23] A. Priel, A. J. Ramos, J. A. Tuszynski, and H. F. Cantiello, J. Biol. Phys. **34**, 475 (2008).

[24] P. J. Gullan and P. S. Cranston, *THE INSECTS:AN OUTLINE OF ENTOMOLOGY*, 5th ed. (Wiley-Blackwell, 2014).

[25] D. Mazzi and S. Dorn, Ann. Appl. Biol. **160**, 97 (2012).

[26] F. Vinatier, P. Tixier, P.-F. Duyck, and F. Lescourret, Methods Ecol. Evol. **2**, 11 (2011).

[27] H. Willaime, O. Cardoso, and P. Tabeling, Phys. Rev. E **48**, 288 (1993).

[28] S. Das Sarma, M. P. Lilly, E. H. Hwang, L. N. Pfeiffer, K. W. West, and J. L. Reno, Phys. Rev. Lett. **94**, 136401 (2005).

[29] Y.-J. Yun, I.-C. Baek, and M.-Y. Choi, Phys. Rev. Lett. **97**, 215701 (2006).

[30] G. Allison, E. A. Galaktionov, A. K. Savchenko, S. S. Safonov, M. M. Fogler, M. Y. Simmons, and D. A. Ritchie, Phys. Rev. Lett. **96**, 216407 (2006).

[31] V. I. Kozub, A. A. Zyuzin, Y. M. Galperin, and V. Vinokur, Phys. Rev. Lett. **96**, 107004 (2006).

[32] Y. V. Kartashov, V. A. Vysloukh, and L. Torner, Opt. Express **15**, 12409 (2007).

[33] A. Agranovich and Y. Louzoun, Phys. Rev. E **85**, 31911 (2012).

[34] D. Takahashi and J. Satsuma, J. Phys. Soc. Japan **59**, 3514 (1990).

[35] J. Matsukidaira, J. Satsuma, D. Takahashi, T. Tokihiro, and M. Torii, Phys. Lett. A **225**, 287 (1997).

[36] J. K. Park, K. Steiglitz, and W. P. Thurston, Phys. D Nonlinear Phenom. **19**, 423 (1986).

[37] T. Tokihiro, D. Takahashi, J. Matsukidaira, and J. Satsuma, Phys. Rev. Lett. **76**, 3247 (1996).

[38] A. Adamatzky, *Reaction-Diffusion Automata: Phenomenology, Localisations, Computation*, 1st ed. (Springer Berlin Heidelberg, Berlin, Heidelberg, 2013).

[39] J. R. Weimar and J.-P. Boon, Phys. Rev. E **49**, 1749 (1994).

[40] R. M. Zorzenon dos Santos and S. Coutinho, Phys. Rev. Lett. **87**, 168102 (2001).

[41] M. J. Leamy, Int. J. Solids Struct. **45**, 4835 (2008).

[42] V. V. Nishawala, M. Ostoja-Starzewski, M. J. Leamy, and P. N. Demmie, Wave Motion **60**, 73 (2016).

[43] B. Chopard and M. Droz, *Cellular Automata Modeling of Physical Systems* (The press syndicate of the University of Cambridge, United Kingdom at the University Press, Cambridge, 1998).

[44] B. Chopard, A. Dupuis, A. Masselot, and P. Luthi, Adv. Complex Syst. **5**, 103 (2002).

[45] R. P. Cowburn, Science (80-.). **287**, 1466 (2000).

[46] C. Oscar, Int. J. Bifurcat. Chaos **8**, 1743 (1998).

[47] A. Poursamad and A. H. Davaie-Markazi, Appl. Soft Comput. **9**, 970 (2009).

[48] A. D'Onofrio, Appl. Math. Lett. **21**, 662 (2008).

[49] V. S. Anishchenko, T. E. Vadivasova, and G. I. Strelkova, *Fractals in Nonlinear Dynamics* (2014).

[50] A. Kathleen, S. Tim, and J. A. Yorke, *Chaos-An Introduction to Dynamical Systems*, 1st ed. (Springer-Verlag, New York, 1996).

[51] A. Polaszek, editor , *African Cereal Stem Borers Economic Importance, Taxonomy, Natural Enemies and Control* (CTA/CABI Wallinford, U.K., 1998).

[52] P. T. Walker, Int. J. Trop. Insect Sci. **4**, 99 (1983).

[53] G. Y. Tsuji, G. Hoogenboom, and P. K. Thornton, editors , *Understanding Options for Agricultural Production* (Springer Netherlands, Dordrecht, 1998).

[54] M. J. Kropff, J. Bouma, and J. W. Jones, Agric. Syst. **70**, 369 (2001).

[55] P. K. Aggarwal, B. Banerjee, M. G. Daryaei, A. Bhatia, A. Bala, S. Rani, S. Chander, H. Pathak, and N. Kalra, Agric. Syst. **89**, 47 (2006).

[56] K. . Boote, J. W. Jones, J. W. Mishoe, and R. D. Berger, Phytopathology **73**, 1581 (1983).

[57] J. . Jones, G. Hoogenboom, C. . Porter, K. . Boote, W. . Batchelor, L. . Hunt, P. . Wilkens, U. Singh, A. . Gijsman, and J. . Ritchie, Eur. J. Agron. **18**, 235 (2003).

[58] J. P. M. Whish, N. I. Herrmann, N. A. White, A. D. Moore, and D. J. Kriticos, Environ. Model. Softw. **72**, 418 (2015).

[59] H. O. Pinnschmidt, W. D. Batchelor, and P. S. Teng, Agric. Syst. **48**, 193 (1995).

[60] C. A. Jones and J. R. Kiniry, *CERES-Maize: A Simulation Model of Maize Growth and Development.* (Texas A&M University Press, College Station, Texas, 1986).

[61] G. Careri, U. Buontempo, F. Galluzzi, A. C. Scott, E. Gratton, and E. Shyamsunder, Phys. Rev. B **30**, 4689 (1984).

[62] A. C. Scott and M. Tabor, Philos. Trans. R. Soc. A Math. Phys. Eng. Sci. **315**, 423 (1985).

[63] J. Edler and P. Hamm, J. Chem. Phys. **117**, 2415 (2002).

[64] A. S. S. Davydov, J. Theor. Biol. **66**, 379 (1977).

[65] A. C. Scott, Phys. Rev. A **26**, 578 (1982).

[66] A. S. Davydov and A. V. Zolotariuk, Phys. Status Solidi **115**, 115 (1983).

[67] A. S. Davydov and A. V. Zolotariuk, Phys. Scr. **30**, 426 (1984).

[68] A. S. Davydov, *Solitons in Molecular Systems* (Springer, 1985).

[69] P. Pérez and N. Theodorakopoulos, Phys. Lett. A **124**, 267 (1987).

[70] J. D. T. Tchinang, A. B. Togueu Motcheyo, and C. Tchawoua, Phys. Rev. E **90**, 43203 (2014).

[71] A. Barth, C. Zscherp, B. Andreas, and Z. Christian, Q. Rev. Biophys. **33**, 369 (2003).

[72] J. Edler, P. Hamm, and A. C. Scott, Phys. Rev. Lett. **88**, 67403 (2002).

[73] J. Edler, R. Pfister, V. Pouthier, C. Falvo, and P. Hamm, Phys. Rev. Lett. **93**, 106405/1 (2004).

[74] L. Ristovski, D. Todorović, G. Davidović, and B. Stojković, Zeitschrift Für Phys. B Condens. Matter **78**, 265 (1990).

[75] D. Todorović, M. Pantić, M. Škrinjar, D. Kapor, and S. Stojanović, Int. J. Mod. Phys. B **23**, 5835 (2009).

[76] Y. B. Gaididei, K. Ø. Rasmussen, and P. L. Christiansen, Phys. Rev. E **52**, 2951 (1995).

[77] P. S. Lomdahl and W. C. Kerr, Phys. Rev. Lett. **55**, 1235 (1985).

[78] A. F. Lawrence, J. C. McDaniel, D. B. Chang, B. M. Pierce, and R. R. Birge, Phys. Rev. A **33**, 1188 (1986).

[79] X. Wang, D. W. Brown, and K. Lindenberg, Phys. Rev. Lett. **62**, 1796 (1989).

[80] G. A. van Velzen and J. A. Tjon, Phys. Lett. A **116**, 167 (1986).

[81] W. Forner, J. Phys. Condens. Matter **4**, 4333 (1991).

[82] Y. Xiao, Phys. Lett. A **243**, 174 (1998).

[83] H. Motschmann, W. Forner, and J. Ladik, J. Phys. Condens. Matter **1**, 5083 (1989).

[84] P. Xiao-feng, Prog. Biophys. Mol. Biol. **108**, 1 (2012).

[85] J. Cuevas, P. A. S. Silva, F. R. Romero, and L. Cruzeiro, Phys. Rev. E **76**, 11907 (2007).

[86] A. Sulaiman, F. P. Zen, H. Alatas, and L. T. Handoko, Phys. Rev. E **81**, 61907 (2010).

[87] G. P. Tsironis, A. R. Bishop, A. V. Savin, and A. V. Zolotaryuk, Phys. Rev. E **60**, 6610 (1999).

[88] P. Dustin, *Microtubules*, 2nd ed. (Springer Berlin Heidelberg, Berlin, Heidelberg, 1984).

[89] M. Schliwa and G. Woehlke, Nature **422**, 759 (2003).

[90] L. Jacken, IUBMB Life **59**, 127 (2007).

[91] J. Pokorný, J. Hašek, and F. Jelínek, J. Biol. Phys. **31**, 501 (2005).

[92] T. J. A. Craddock, J. A. Tuszynski, A. Priel, and H. Freedman, J. Integr. Neurosci. **9**, 103 (2010).

[93] P. M. Vassilev, R. T. Dronzine, M. P. Vassileva, and G. A. Georgiev, Biosci. Rep. **2**, 1025 (1982).

[94] E. D. Kirson, Cancer Res. **64**, 3288 (2004).

[95] R. K. Hobbie and B. J. Roth, *Intermediate Physics for Medicine and Biology* (Springer New York, New York, NY, 2007).

[96] I. Minoura and E. Muto, Biophys. J. **90**, 3739 (2006).

[97] C. Ballatore, K. R. Brunden, D. M. Huryn, J. Q. Trojanowski, V. M.-Y. Lee, and A. B. Smith, J. Med. Chem. **55**, 8979 (2012).

[98] K. Lou, Y. Yao, A. T. Hoye, M. J. James, A.-S. Cornec, E. Hyde, B. Gay, V. M.-Y. Lee, J. Q. Trojanowski, A. B. Smith, K. R. Brunden, and C. Ballatore, J. Med. Chem. **57**, 6116 (2014).

[99] B. Zhang, J. Carroll, J. Q. Trojanowski, Y. Yao, M. Iba, J. S. Potuzak, A.-M. L. Hogan, S. X. Xie, C. Ballatore, A. B. Smith, V. M.-Y. Lee, and K. R. Brunden, J. Neurosci. **32**, 3601 (2012).

[100] A. R. Esteves, I. Gozes, and S. M. Cardoso, Biochim. Biophys. Acta - Mol. Basis Dis. **1842**, 7 (2014).

[101] I. Magen and I. Gozes, Neuropeptides **47**, 489 (2013).

[102] B. B. Elahi, B. B. Elahi, and R. Chen, Mov. Disord. **24**, 357 (2009).

[103] M. Reale, M. A. Kamal, A. Patruno, E. Costantini, C. D'Angelo, M. Pesce, and N. H. Greig, PLoS One **9**, e104973 (2014).

[104] R. Lekhraj, D. E. Cynamon, S. E. DeLuca, E. S. Taub, A. A. Pilla, and D. Casper, J. Neurosci. Res. **92**, 761 (2014).

[105] A. Priel, A. J. Ramos, J. A. Tuszynski, and H. F. Cantiello, Biophys. J. **90**, 4639 (2006).

[106] H. Freedman, V. Rezania, A. Priel, E. Carpenter, S. Y. Noskov, and J. A. Tuszynski, Phys. Rev. E **81**, 51912 (2010).

[107] F. Geniet and J. Leon, Phys. Rev. Lett. **89**, 134102 (2002).

[108] D. Chevriaux, R. Khomeriki, and J. Leon, Phys. Rev. B **73**, 214516 (2006).

[109] J. E. Macías-Díaz and A. Puri, Phys. Lett. A **372**, 5004 (2008).

[110] J. E. Macías-Díaz and A. Puri, Phys. D Nonlinear Phenom. **228**, 112 (2007).

[111] L. Brillouin, *Periodic Structure: Electronic Filters and Crystall Lattices*, Mc Graw-Hi (1946).

[112] J. Lydon, G. Theocharis, and C. Daraio, Phys. Rev. E **91**, 23208 (2015).

[113] R. Khomeriki, Phys. Rev. Lett. **92**, 63905 (2004).

[114] H. Susanto and N. Karjanto, J. Nonlinear Opt. Phys. Mater. **17**, 159 (2008).

[115] R. Khomeriki, S. Lepri, and S. Ruffo, Phys. Rev. E **70**, 66626 (2004).

[116] M. A. B. Togueu, C. Tchawoua, M. Siewe Siewe, J. D. Tchinang Tchameu, M. A. B. Togueu, C. Tchawoua, M. Siewe Siewe, and T. J. D. Tchinang, Commun. Nonlinear Sci. Numer. Simul. **18**, 946

(2013).

[117] K. Tse Ve Koon, J. Leon, P. Marquié, and P. Tchofo-Dinda, Phys. Rev. E **75**, 66604 (2007).

[118] S. B. Yamgoue, S. Morfu, and P. Marquie, Phys. Rev. E **75**, (2007).

[119] A. B. Togueu, Motcheyo, C. Tchawoua, J. D. Tchinang Tchameu, M. A. B. Togueu, C. Tchawoua, and T. J. D. Tchinang, Phys. Rev. E **88**, 40901 (2013).

[120] K. T. V. Koon, P. Marquié, and P. T. Dinda, Phys. Rev. E **90**, 52901 (2014).

[121] G. Kopidakis and S. Aubry, Phys. Rev. Lett. **84**, 3236 (2000).

[122] P. Maniadis, G. Kopidakis, and S. Aubry, Phys. D Nonlinear Phenom. **216**, 121 (2006).

[123] M. Johansson, G. Kopidakis, S. Lepri, and S. Aubry, EPL (Europhysics Lett. **86**, 10009 (2009).

[124] L. Winder, C. J. Alexander, C. Woolley, J. N. Perry, and J. M. Holland, Arthropod. Plant. Interact. **7**, 21 (2013).

[125] A. W. Ferguson, Z. Klukowski, B. Walczak, S. J. Clark, M. A. Mugglestone, J. N. Perry, and I. H. Williams, Agric. Ecosyst. Environ. **95**, 509 (2003).

[126] G. Hughes, Crop Prot. **15**, 407 (1996).

[127] D. O. Caldiz, F. . Gaspari, A. Moreno Kiernan, and P. . Struik, Agric. Ecosyst. Environ. **88**, 3 (2002).

[128] G. C. M. van Leeuwen, A. Stein, I. Holb, and M. J. Jeger, Eur. J. Plant Pathol. **106**, 519 (2000).

[129] I. Ishaaya and A. R. Horowitz, *Insect Pest Management Field and Protected Crops*, 1st ed. (Springer-Verlag Berlin Heidelberg, 2004).

[130] J. N. Perry, Asp. Appl. Biol. 1 (1994).

[131] C. Wang, D. Li, Y. Hu, X. Wu, and Y. Qi, in *Proc. SPIE*, edited by Y. Liu and X. Tang (2009), p. 74923A–74923A–7.

[132] F. P. F. Reay-Jones, L. T. Wilson, M. O. Way, T. E. Reagan, and C. E. Carlton, J. Econ. Entomol. **100**, 54 (2007).

[133] B. M. Diaz, L. Barrios, and A. Fereres, Bull. Entomol. Res. **102**, 406 (2012).

[134] A. Lausch, M. Heurich, and L. Fahse, Ecol. Indic. **31**, 73 (2013).

[135] N. Cocu, R. Harrington, M. Hulle, and M. D. A. Rounsevell, Agric. For. Entomol. **7**, 31 (2005).

[136] M. T. Smith, P. C. Tobin, J. Bancroft, G. Li, and R. Gao, Environ. Entomol. **33**, 435 (2004).

[137] C. F. G. F. G. Thomas, L. Parkinson, G. J. K. J. K. Griffiths, a. F. Garcia, and E. J. P. J. P. Marshall, J. Appl. Ecol. **38**, 100 (2001).

[138] H. Kim, S.-T. Kim, M.-P. Jung, and J.-H. Lee, Ecol. Res. **22**, 204 (2007).

[139] J. M. Holland, C. F. G. THOMAS, T. BIRKETT, S. Southway, and H. OATEN, J. Appl. Ecol. **42**, 1140 (2005).

[140] K. M. Zimmerman, J. A. Lockwood, V. Alexandre, K. M. Zimmerman, J. A. Lockwood, and A. V Latchininsky, Environ. Entomol. **33**, 257 (2004).

[141] T. Keasar, K. Adi, B. Ori, S. Shimon, A. Kalish, O. Becher, and S. Steinberg, J. Econ. Entomol. **98**, 222 (2005).

[142] A. F. P. F. Reay-jones, **39**, 944 (2010).

[143] R. T. Wright, T. A. Deries, L. J. Young, K. J. Jarvi, and R. C. Saymour, Environ. Entomol. **31**, 160 (2002).

[144] D. a Emmen, S. J. Fleischer, and A. Hower, Environ. Entomol. **33**, 890 (2004).

[145] B. H. Aukema, A. L. Carroll, J. Zhu, K. F. Raffa, T. a Sickley, and S. W. Taylor, Ecography (Cop.). **29**, 427 (2006).

[146] F. J. Moral García, Biosyst. Eng. **93**, 253 (2006).

[147] M. Kautz, K. Dworschak, A. Gruppe, R. Schopf, and S. Reinhard, For. Ecol. Manage. **262**, 598 (2011).

[148] H. De Groote, G. Owuor, C. Doss, J. Ouma, L. Muhammad, M. K. Danda, K. De Groote, H.; Owuor, G.; Doss, C.; Ouma, J.; Muhammad, L.; Danda, H. De Groote, G. Owuor, C. Doss, J. Ouma, L. Muhammad, M. K. Danda, and K. De Groote, H.; Owuor, G.; Doss, C.; Ouma, J.; Muhammad, L.; Danda, eJADE Electron. J. Agric. Dev. Econ. **2**, 32 (2005).

[149] A. K. Kipkoech, F. Schulthess, W. K. Yabann, H. K. Maritim, and D. Mithöfer, Ann. La Société Entomol. Fr. **42**, 519 (2006).

[150] R. Stevens, J. Sci. Food Agric. **88**, 745 (2008).

[151] W. A. Overholt, Maes, KVN, and G. FR, *Field Guide to the Stem Borer Larvae of Maize, Sorghum and Sugarcane in Eastern and Southern Africa* (ICIPE Science Press, 2001).

[152] H. De Groote, Int. J. Trop. Insect Sci. **22**, 89 (2002).

[153] G. O. Ong'amo, B. P. Le Rü, S. Dupas, P. Moyal, P.-A. Calatayud, and J.-F. Silvain, Ann. La Société Entomol. Fr. **42**, 171 (2006).

[154] P. Ranum, J. P. Peña-Rosas, and M. N. Garcia-Casal, Ann. N. Y. Acad. Sci. **1312**, 105 (2014).

[155] R. Kfir, W. A. Overholt, Z. R. Khan, and A. Polaszek, Annu. Rev. Entomol. **47**, 701 (2002).

[156] H. De Groote, W. Overholt, J. O. Ouma, and S. Mugo, in *Int. Agric. Econ. Conf. Durban* (Durban, 2003).

[157] P. T. Walker, EPPO Bull. **11**, 101 (1981).

[158] D. A. Herbert, *Biotic Stress and Yield Loss* (CRC Press, 2000).

[159] J. B. J. van Rensburg, J. H. Giliomee, and M. C. Walters, Bull. Entomol. Res. **78**, 101 (1988).

[160] K. F. Cardwell, F. Schulthess, R. Ndemah, and Z. Ngoko, Agric. Ecosyst. Environ. **65**, 33 (1997).

[161] A. Chabi-Olaye, C. Nolte, F. Schulthess, and C. Borgemeister, Bull. Entomol. Res. **95**, (2005).

[162] R. . Ndemah and F. . Schulthess, Insect Sci. Its Appl. **22**, 183 (2002).

[163] R. Ndemah, F. Schulthess, S. Korie, C. Borgemeister, and K. F. F. Cardwell, J. Econ. Entomol. **94**, 1434 (2001).

[164] J. van den Berg, J. B. J. van Rensburg, and J. H. Giliomee, South African J. Plant Soil **8**, 85 (1991).

[165] a. a. Ebenebe, J. van den Berg, and T. C. van der Linde, South African J. Plant Soil **16**, 180 (1999).

[166] J. H. Macfarlane, Trop. Pest Manag. **36**, 131 (1990).

[167] K. M. Harris, Bull. Entomol. Res. 169 (1962).

[168] W. R. Ingram, Bull. Entomol. Res. **49**, 367 (1958).

[169] E. J. Usua, J. Econ. Entomol. **61**, 375 (1968).

[170] P. T. Walker, Ann. Appl. Biol. **48**, 780 (1960).

[171] L. V. Madden, J. F. W. Nutter, and F. W. Nutter, Can. J. Plant Pathol. **17**, 124 (1995).

[172] R. Bardner, K. E. Flecher, and K. E. Fletcher, Bull. Entomol. Res. **64**, 141 (1974).

[173] P. T. Walker, Agric. Ecosyst. Environ. **9**, 119 (1983).

[174] R. Ndemah, F. Schulthess, S. Korie, C. Borgemeister, H.-M. Poehling, and K. Cardwell, Environ. Entomol. **32**, 51 (2003).

[175] J. C. Zadoks, Annu. Rev. Phytopathol. **23**, 455 (1985).

[176] A. Chabi-Olaye, F. Schulthess, and C. Borgemeister, J. Econ. Entomol. **101**, 90 (2008).

[177] A. Chabi-Olaye, C. Nolte, F. Schulthess, and C. Borgemeister, Ann. La Société Entomol. Fr. **42**, 471 (2006).

[178] S. O. Ajala and K. N. Saxena, Appl. Entomol. Zool. **29**, 469 (1994).

[179] J. K. O. Ampofo, Int. J. Trop. Insect Sci. **9**, 87 (1988).

[180] D. Cugala, F. Schulthess, C. P. O. Ogol, and C. O. Omwega, Ann. La Société Entomol. Fr. **42**, 503 (2006).

[181] P. A. Calatayud, H. Guénégo, P. Ahuya, A. Wanjoya, B. Le Rü, J.-F. Silvain, and B. Frérot, Entomol. Exp. Appl. **129**, 348 (2008).

[182] P. A. Calatayud, G. Juma, P. G. N. Njagi, N. Faure, S. Calatayud, S. Dupas, B. Le Rü, G. Magoma, J.-F. Silvain, and B. Frérot, J. Appl. Entomol. **132**, 255 (2008).

[183] P. A. Calatayud, H. Guénégo, B. Le Rü, B. LeRü, J.-F. Silvain, and B. Frérot, Ann. La Société Entomol. Fr. **43**, 63 (2007).

[184] K. M. M. Harris and K. E. E. Nwanze, *Busseola Fusca (Fuller), the African Maize Stalk Borer: A Handbook of Information* (1992).

[185] N. A. Bosque-Pérez and J. . Mareck, in *African Cereal Stem Borers Econ. Importance, Taxon. Nat. Enemies Control*, edited by A. Polaszek (CAB International, Wallingford Oxford, U.K., 1998), pp. 11–24.

[186] J. Brenière, Ann. Zool. Ecol. Anim. **3**, 287 (1971).

[187] P. A. Calatayud, B. Le Ru, J. van den Berg, F. Schulthess, B. P. Le Ru, J. Van Den Berg, and F. Schulthess, Insects **5**, 539 (2014).

[188] F. P. . Reay-Jones, M. D. D. Toews, J. K. K. Greene, and R. B. B. Reeves, Environ. Entomol. **33**, 956 (2010).

[189] R. P. Blackshaw and H. Hicks, J. Pest Sci. (2004). **86**, 53 (2013).

[190] C. Bone, M. A. Wulder, J. C. White, C. Robertson, and T. A. Nelson, Appl. Geogr. **40**, 161 (2013).

[191] B. Li, L. V. Madden, and X. Xu, Methods Ecol. Evol. **3**, 368 (2012).

[192] A. Reineke, J. Hirsch, and G. Kubach, J. Pest Sci. (2004). **84**, 297 (2011).

[193] A. Cocco, G. Serra, A. Lentini, S. Deliperi, and G. Delrio, Pest Manag. Sci. **71**, 1311 (2015).

[194] B. Dáder, S. Legarrea, A. Moreno, M. Plaza, M. Carmo-Sousa, F. Amor, E. Viñuela, and A. Fereres, Pest Manag. Sci. **71**, 1397 (2015).

[195] M. Schumann, A. Patel, M. Vemmer, and S. Vidal, Pest Manag. Sci. **70**, 642 (2014).

[196] C. D. Rogers, R. M. L. Guimarães, K. A. Evans, and S. A. Rogers, J. Pest Sci. (2004). **88**, 75 (2015).

[197] F. L. Fernandes, M. C. Picanço, M. E. S. Fernandes, R. A. C. Dângelo, F. F. Souza, and R. N. C. Guedes, J. Pest Sci. (2004). **88**, 289 (2015).

[198] J. Zhang, Y. Huang, L. Yuan, G. Yang, L. Chen, and C. Zhao, Pest Manag. Sci. **72**, 335 (2016).

[199] M. A. Massoud, A. A. Sallam, J. R. Faleiro, and S. Al-Abdan, Int. J. Trop. Insect Sci. **32**, 108 (2012).

[200] M. Begon, J. L. Harper, and C. R. Townsend, *Ecology: Individuals, Populations and Communities*, 3rd ed. (Wiley-Blackwell, 1996).

[201] A. Cocco, S. Deliperi, and G. Delrio, J. Appl. Entomol. **137**, 16 (2013).

[202] S. Mwalusepo, H. E. Z. Tonnang, E. S. Massawe, G. O. Okuku, N. Khadioli, T. Johansson, P.-A. Calatayud, and B. P. Le Ru, PLoS One **10**, e0130427 (2015).

[203] K. Hauptfleisch, T. Yonow, D. J. Kriticos, N. Ota, and S. Africa, Harvest. Pest Geogr. St. Paul, MN InSTePP-HarvestChoice 1 (2014).

[204] B. P. Le Ru, G. O. Ong'amo, P. Moyal, E. Muchugu, L. Ngala, B. Musyoka, Z. Abdullah, T. Matama-Kauma, V. Y. Lada, B. Pallangyo, C. O. Omwega, F. Schulthess, P.-A. Calatayud, and J.-F. Silvain, Ann. La Société Entomol. Fr. **42**, 353 (2006).

[205] Z. Guofa, W. A. Overholt, and M. Mochiah, Insect Sci. Its Appl. **21**, 395 (2001).

[206] M. Sezonlin, S. Dupas, B. Le Rü, P. LE GALL, P. Moyal, P.-A. P. Calatayud, I. GIFFARD, N. FAURE, and J.-F. J.-F. Silvain, Mol. Ecol. **15**, 407 (2006).

[207] S. Dupas, B. le Ru, A. Branca, N. Faure, G. Gigot, P. Campagne, M. Sezonlin, R. Ndemah, G. Ong'amo, P.-A. Calatayud, and J.-F. Silvain, Mol. Ecol. **23**, 2313 (2014).

[208] R. Ndemah, F. Schulthess, N. Poehling, C. Borgemeister, M. Poehling, and C. Borgemeister, J. Appl. Entomol. Fur Angew. Entomol. **125**, 507 (2001).

[209] W. A. Overholt, A. J. Ngi-Song, S. W. Kimani, J. Mbapila, P. Lammers, and E. Kioko, Bull. Entomol. Res. **84**, 367 (1994).

[210] J. B. J. Van Rensburg and K. L. Pringle, J. Entomol. Soc. South. Afr. **52**, 223 (1989).

[211] B. Amoako-Atta, E. O. Omolo, and E. K. Kidega, Insect Sci. Its Appl. **4**, 47 (1983).

[212] P. T. Walker, Int. J. Trop. Insect Sci. **8**, 665 (1987).

[213] E. O. Oben, N. N. Ntonifor, S. Kekeunou, and M. N. Abbeytakor, J. Ethnobiol. Ethnomed. **11**, 77 (2015).

[214] A. A. Ebenebe, J. Van Den Berg, and T. C. Van Der Linde, Int. J. Pest Manag. **47**, 41 (2001).

[215] M. J. Bonhof, A. Van Huis, F. G. Kiros, and N. Dibogo, Int. J. Trop. Insect Sci. **21**, 33 (2001).

[216] K. Shea, H. P. Possingham, W. W. Murdoch, and R. Roush, Ecol. Appl. **12**, 927 (2002).

[217] M. Mackauer, L. E. Ehler, and J. Roland, editors , *Critical Issues in Biological Control.* (UK: Intercept, 1990).

[218] M. J. Kropff, P. S. Teng, and R. Rabbinge, Agric. Syst. **49**, 413 (1995).

[219] J. E. Banks and B. Ekbom, Agric. For. Entomol. **1**, 165 (1999).

[220] H. N. Comins, J. Theor. Biol. **65**, 399 (1977).

[221] H. Cerda and D. J. Wright, Agric. Ecosyst. Environ. **102**, 163 (2004).

[222] C. Vacher, D. Bourguet, F. Rousset, C. Chevillon, and M. E. Hochberg, J. Evol. Biol. **16**, 378 (2003).

[223] S. H. Levine and R. E. Wetzler, Ecol. Modell. **89**, 183 (1996).

[224] L. Fahse and M. Heurich, Ecol. Modell. **222**, 1833 (2011).

[225] R. Seidl, M.-J. J. Schelhaas, M. Lindner, and M. J. Lexer, Reg. Environ. Chang. **9**, 101 (2009).

[226] C. Lopes, T. Spataro, and R. Arditi, Ecol. Complex. **7**, 1 (2010).

[227] C. Lopes, T. Spataro, C. Doursat, L. Lapchin, and R. Arditi, J. Theor. Biol. **248**, 164 (2007).

[228] K. Shea, H. P. Possingham, A. Ecology, W. Campus, and S. Barbara, J. Appl. Ecol. **37**, 77 (2000).

[229] F. Rebaudo and O. Dangles, PLoS Comput. Biol. **7**, e1002222 (2011).

[230] F. Rebaudo and O. Dangles, Environ. Model. Softw. **45**, 141 (2013).

[231] K. V. S. Reddy, K. O. . O. S. Sum, R. K. V. Seshu, and K. O. . O. S. Sum, Int. J. Trop. Insect Sci. **12**, 269 (1991).

[232] I. E. de P. Ferreira, R. D. A. Moral, C. P. Ferreira, and W. A. C. Godoy, Ecol. Inform. **14**, 53 (2013).

[233] A. Gronewold and M. Sonnenschein, Ecol. Modell. **108**, 37 (1998).

[234] V. Crespo-Pérez, F. Rebaudo, J.-F. Silvain, and O. Dangles, Landsc. Ecol. **26**, 1447 (2011).

[235] L. Perez and S. Dragicevic, Ecol. Modell. **231**, 53 (2012).

[236] J. Yang, Z.-R. Wang, D.-L. Yang, Q. Yang, J. Yan, and M.-F. He, Biotechnol. Adv. **27**, 1132 (2009).

[237] S. D. Lee, S. Park, Y.-S. Park, Y.-J. Chung, B.-Y. Lee, and T.-S. Chon, Ecol. Modell. **203**, 157 (2007).

[238] T. Pukkala, T. Möykkynen, and C. Robinet, For. Pathol. **44**, 341 (2014).

[239] R. Seidl, P. M. Fernandes, T. F. Fonseca, F. Gillet, A. M. Jönsson, K. Merganičová, S. Netherer, A. Arpaci, J.-D. Bontemps, H. Bugmann, J. R. González-Olabarria, P. Lasch, C. Meredieu, F. Moreira, M.-J. Schelhaas, and F. Mohren, Ecol. Modell. **222**, 903 (2011).

[240] N. Samat, Comput. Environ. Urban Syst. **30**, 905 (2006).

[241] D. J. Bailey, W. Otten, and C. A. Gillian, New Phytol. **146**, 535 (2000).

[242] S. Davis, P. Trapman, H. Leirs, M. Begon, and J. A. P. Heesterbeek, Nature **454**, 634 (2008).

[243] W. Otten, D. J. Bailey, and C. a. Gilligan, New Phytol. **163**, 125 (2004).

[244] J. J. Ludlam, G. J. Gibson, W. Otten, and C. A. Gilligan, J. R. Soc. Interface **9**, 949 (2012).

[245] M. da S. Peixoto, L. C. L. C. L. C. de Barros, R. C. Bassanezi, M. da S. Peixoto, L. C. L. C. L. C. de Barros, and R. C. Bassanezi, Ecol. Modell. **214**, 45 (2008).

[246] S. Marsili-Libelli, E. Giusti, and F. Gherardi, in *Int. Environ. Model. Softw. Soc. Int. Congr. Environ. Model. Software, Manag. Ressources Limited. Planet, Sixth Bienn. Meet. Leipzig, Ger.*, edited by R. Seppelt, A. A. Voinov, S. Lange, and D. Bankamp (2012), p. 8pp.

[247] C. Bone, S. Dragicevic, A. Roberts, B. Christopher, D. Suzana, R. Arthur, C. Bone, S. Dragicevic, A. Roberts, B. Christopher, D. Suzana, and R. Arthur, Ecol. Modell. **192**, 1 (2006).

[248] Q. Chen and A. E. Mynett, Ecol. Modell. **199**, 73 (2006).

[249] N. Zhang, Y.-C. Jing, C.-Y. Liu, Y. Li, and J. Shen, Ecol. Modell. **329**, 5 (2016).

[250] J. G. P. Gamarra and F. He, J. Anim. Ecol. **77**, 796 (2008).

[251] A. A. Saberi, Phys. Rep. **578**, 1 (2015).

[252] R. Ewing and A. Hunt, *Percolation Theory for Flow in Porous Media* (Springer Berlin Heidelberg, Berlin, Heidelberg, 2009).

[253] A. G. Hunt, *Percolation Theory for Flow in Porous Media* (Springer Berlin Heidelberg, Berlin, Heidelberg, 2005).

[254] A. L. Efros, *Physics and Geometry of Disorder: Percolation Theory* (Mir Publishers, Moscow, 1986).

[255] S. R. Broadbert and J. M. Hammersley, Math. Proc. Cambridge Philos. Soc. **53**, 629 (1957).

[256] Ilachinski, *Cellular Automata: A Discrete Universe* (River Edge, NJ, USA, 2001).

[257] S. Wolfram, *Cellular Automata and Complexity* (Addison-Wesley Publishing Company, 1994).

[258] S. Wolfram, Rev. Mod. Phys. **55**, 601 (1983).

[259] S. Wolfram, Phys. D Nonlinear Phenom. **10**, 1 (1984).

[260] J. Von Neumann, Phys. Today **10**, 58 (1957).

[261] S. Ulam, in *Proceeding Int. Congr. Math. 1950 Vol. 2 (American Math. Soc. Provid. RI)* (1950), pp. 264–275.

[262] J. Wang, M. J. J. Kropff, B. Lammert, S. Christensen, and P. K. K. Hansen, Ecol. Modell. **166**, 277 (2003).

[263] S. a. Cannas, S. a. Páez, and D. E. Marco, Comput. Phys. Commun. **121–122**, 131 (1999).

[264] E. P. M. Grist, Ecol. Modell. **121**, 63 (1999).

[265] O. Inghe, J. Theor. Biol. **138**, 257 (1989).

[266] M. Kondoh, J. Theor. Biol. **225**, 453 (2003).

[267] T. Toffoli, Phys. D Nonlinear Phenom. **10**, 117 (1984).

[268] P. Hogeweg, Appl. Math. Comput. **27**, 81 (1988).

[269] C. Leal-Ramírez, O. Castillo, P. Melin, and H. Echavarria-Heras, Appl. Math. Model. **39**, 1794 (2015).

[270] M. S. Piexoto, L. Carvalho de Barros, and R. C. Bassanezi, Appl. Math. **5**, 1213 (2014).

[271] L. a. Zadeh, Inf. Control **8**, 338 (1965).

[272] W. Pedrycz and F. Gomide, *An Introduction to Fuzzy Sets: Analysis and Design* (Massachusetts Institutes of Technology, 1998).

[273] R. Lopes and N. Betrouni, Med. Image Anal. **13**, 634 (2009).

[274] L. A. Saravia, A. Giorgi, and F. Momo, Oikos **121**, 1810 (2012).

[275] L. A. Saravia, A. Giorgi, and F. Momo, PLoS One **7**, e34096 (2012).

[276] B.-L. Li, Ecol. Modell. **132**, 33 (2000).

[277] L. Seuront, J. Plankton Res. **21**, 877 (1999).

[278] G. Zurlini, I. Petrosillo, K. B. Jones, B.-L. Li, K. H. Riitters, P. Medagli, S. Marchiori, and N. Zaccarelli, J. Environ. Manage. **128**, 192 (2013).

[279] L. Seuront, *Fractals and Multifractals in Ecology and Aquatic Science* (Taylor and Francis Group, LLC., 2010).

[280] J. M. Halley, S. Hartley, a. S. Kallimanis, W. E. Kunin, J. J. Lennon, and S. P. Sgardelis, Ecol. Lett. **7**, 254 (2004).

[281] S. Gounou and F. Schulthess, African Entomol. **12**, 171 (2004).

[282] J. Van den Berg, A. A. Ebenebe, S. Africa, F. State, and S. Africa, Int. J. Trop. Insect Sci. **21**, 389 (2001).

[283] T. Abate, A. van Huis, and J. K. O. Ampofo, Annu. Rev. Entomol. **45**, 631 (2000).

[284] S. Gonou, F. Schulthess, T. Shanower, W. H. O. Hammond, H. Braima, A. R. Cudjoe, R. Adklaoe, K. K. Antwi, and I. Olaleye, *Stem and Ear Borers of Maize in Ghana* (Plant Health Management Research Monograph 4, International Institute of Tropical Agriculture, Ibadan, Nigeria, 1994).

[285] K. . . . S. Reddy, in *Int. Crop. Res. Inst. Semi-Arid Trop. 1985. Proc. Int. Sorghum Entomol. Work. 15-21 July 1984, Texas A M Univ. Coll. Station. TX, USA. Patancheru, A.P. 502324, India ICRISAT* (1985), p. 205.

[286] S. B. Sagnia, Insect Sci. Appl. **4**, 217 (1983).

[287] A. Altartouri, L. Nurminen, and A. Jolma, Environ. Model. Softw. **71**, 15 (2015).

[288] V. Kocabas and S. Dragicevic, in *Int. Arch. Photogramm. Remote Sens. Spat. Inf. Sci. Ed. by Altman M.O., XXth ISPRS Congr. Istanbul, Turkey, 12-23 July, Vol XXXV, Part B.* (2004).

[289] V. Kocabas and S. Dragicevic, Comput. Environ. Urban Syst. **30**, 921 (2006).

[290] X. Li, X. Liu, and L. Yu, Int. J. Geogr. Inf. Sci. **28**, 1317 (2014).

[291] A. Ménard and D. J. Marceau, Environ. Plan. B Plan. Des. **32**, 693 (2005).

[292] J. Wu and J. L. David, Ecol. Modell. **153**, 7 (2002).

[293] Q. Chen and A. E. Mynett, Simul. Model. Pract. Theory **11**, 609 (2003).

[294] D. C. Schneider, *Quantitative Ecology. Spatial and Temporal Scaling*, 1st ed. (Academic Press, San Diego, 1994).

[295] A. Sciarretta, P. Trematerra, S. Andrea, and T. Pasquale, Plant Prot. Sci. **50**, 99 (2014).

[296] M. Karimi, M. A. Sharifi, and M. S. Mesgari, Int. J. Appl. Earth Obs. Geoinf. **16**, 42 (2012).

[297] N. Moreno, F. Wang, and D. J. Marceau, Comput. Environ. Urban Syst. **33**, 44 (2009).

[298] S. Dantchev, in *Comput. J.* (2008), pp. 26–30.

[299] K. Al-Ahmadi, L. See, A. Heppenstall, and J. Hogg, Ecol. Complex. **6**, 80 (2009).

[300] I. Santé, A. M. García, D. Miranda, and R. Crecente, Landsc. Urban Plan. **96**, 108 (2010).

[301] J. A. Foley, N. Ramankutty, K. A. Brauman, E. S. Cassidy, J. S. Gerber, M. Johnston, N. D. Mueller, C. O'Connell, D. K. Ray, P. C. West, C. Balzer, E. M. Bennett, S. R. Carpenter, J. Hill, C. Monfreda, S. Polasky, J. Rockström, J. Sheehan, S. Siebert, D. Tilman, and D. P. M. Zaks, Nature **478**, 337 (2011).

[302] N. Colbach, Plant Sci. **179**, 1 (2010).

[303] K. Y. Lee, R. O. Barr, S. H. Gage, and A. N. Kharkar, J. Theor. Biol. **59**, 33 (1976).

[304] A. P. Guitierrez, J. B. Christensen, C. M. Merritt, W. B. Loew, C. G. Summers, and W. R. Cothran, Can. Entomol. **108**, 635 (1976).

[305] A. P. Gutierrez, G. D. J. Butler, Y. Wang, and D. Westphal, Can. Entomol. **109**, 1457 (1977).

[306] V. V. Rubtsov, Ecol. Modell. **18**, 269 (1983).

[307] R. I. Carruthers, G. H. Whitfield, R. L. Tummala, and D. L. Haynes, Ecol. Modell. **33**, 101 (1986).

[308] B. Graf, R. Lamb, K. L. Heong, and L. Fabellar, J. Appl. Ecol. **29**, 558 (1992).

[309] D. Gonzalez, J. A. Cabral, L. Torres, and M. Santos, Ecol. Modell. **296**, 46 (2015).

[310] A. B. Langille, E. M. Arteca, G. D. Ryan, L. M. Emiljanowicz, and J. A. Newman, Ecol. Modell. **336**, 70 (2016).

[311] A. Lebon, L. Mailleret, Y. Dumont, and F. Grognard, Ecol. Modell. **290**, 192 (2014).

[312] P. Amarasekare, J. Anim. Ecol. **84**, 665 (2015).

[313] L. Willocquet, S. Savary, L. Fernandez, F. . Elazegui, N. Castilla, D. Zhu, Q. Tang, S. Huang, X. Lin, H. . Singh, and R. . Srivastava, Ecol. Modell. **153**, 247 (2002).

[314] P. L. Shaffer and H. J. Gold, Ecol. Modell. **30**, 247 (1985).

[315] D.-S. Kim and J.-H. Lee, Ecol. Modell. **162**, 145 (2003).

[316] T. Yonow, M. . Zalucki, R. . Sutherst, B. . Dominiak, G. . Maywald, D. . Maelzer, and D. . Kriticos, Ecol. Modell. **173**, 9 (2004).

[317] A. Satake, T. Ohgushi, S. Urano, and K. Uchimura, Ecol. Res. **21**, 107 (2006).

[318] E. J. Usua, Entomol. Exp. Appl. **16**, 322 (1973).

[319] E. S. Ntiri, P.-A. Calatayud, J. Van Den Berg, F. Schulthess, and B. P. Le Ru, PLoS One **11**, e0148735 (2016).

[320] N. Khadioli, Z. E. H. Tonnang, G. Ong'amo, T. Achia, I. Kipchirchir, J. Kroschel, and B. Le Ru, Ann. Appl. Biol. **165**, 373 (2014).

[321] P. Harris, Agro-Ecosystems **1**, 219 (1974).

[322] A. J. Belsky, Am. Nat. **127**, 870 (1986).

[323] J. T. Trumble, D. M. Kolodny-Hirsch, and I. P. Ting, Annu. Rev. Entomol. **38**, 93 (1993).

[324] J. B. J. van Rensburg and J. van den Berg, South African J. Plant Soil **9**, 81 (1992).

[325] C. Q. Mi, Z. Liu, X. D. Zhang, X. N. Peng, and B. Huang, Int. J. Agric. Biol. Eng. **7**, 51 (2014).

[326] C. Mi, X. Zhang, S. Li, J. Yang, D. Zhu, and Y. Yang, Math. Comput. Model. **54**, 1053 (2011).

[327] N. Tremblay, M. Y. Bouroubi, B. Panneton, S. Guillaume, P. Vigneault, and C. Bélec, Precis. Agric. **11**, 621 (2010).

[328] N. Tremblay, M. Y. Bouroubi, B. Panneton, S. Guillaume, P. Vigneault, and C. Bélec, Efita 2009 397 (2007).

[329] D. Hennig, Phys. Rev. B **65**, 174302 (2002).

[330] D. Hennig, K. Ø. Rasmussen, H. Gabriel, and A. Bülow, Phys. Rev. E **54**, 5788 (1996).

[331] T. Bountis, H. . W. Capel, M. Kollmann, J. . C. Ross, J. . M. Bergamin, and J. . P. van der Weele, Phys. Lett. A **268**, 50 (2000).

[332] G. L. Alfimov, V. a. Brazhnyi, and V. V. Konotop, Phys. D Nonlinear Phenom. **194**, 127 (2004).

[333] G. R. Carretero, J. D. Talley, C. Chong, B. A. Malomed, R. Carretero-González, J. D. Talley, C. Chong, and B. A. Malomed, Phys. D Nonlinear Phenom. **216**, 77 (2006).

[334] M. A. Porter, R. Carretero-González, P. G. Kevrekidis, and B. A. Malomed, Chaos An Interdiscip. J. Nonlinear Sci. **15**, 15115 (2005).

[335] P. G. Kevrekidis, *The Discrete Nonlinear Schrödinger Equation* (Springer Berlin Heidelberg, Berlin,

Heidelberg. 2009).

[336] Z. You, E. J. Kostelich, and J. A. Yorke, Int. J. Bifurc. Chaos **1**, 605 (1991).

[337] W. H. Press, B. . Flannery, S. Teukolsky, and W. T. Vettering, *Numerical Recipes: The Art of The Scienti c Computing*, 2nd ed. (Cambidge University Press, 1986).

[338] P. Panagopoulos, T. Bountis, and C. Skokos, J. Vib. Acoust. **126**, 520 (2004).

[339] F. Palmero, R. Carretero-González, J. Cuevas, P. G. Kevrekidis, and W. Królikowski, Phys. Rev. E **77**, 36614 (2008).

[340] P. Lagevin, Comptes Rendus l'Académie Des Sci. **146**, 530 (1908).

[341] A. V. Savin and A. V. Zolotaryuk, Phys. D Nonlinear Phenom. **68**, 59 (1993).

[342] W. Forner, Int. J. Quantum Chem. **64**, 351 (1997).

[343] J. W. Schweitzer, Phys. Rev. A **45**, 8914 (1992).

[344] W. H. Press, S. A. Teukolsky, W. T. Vetterling, and B. P. Flannery, *Numerical Recipes in C: The Art of Scientific Computing*, 2nd ed. (1992).

[345] M. Toda, J. Phys. Soc. Japan **23**, 501 (1967).

[346] P. Marquié, J. M. Bilbault, and M. Remoissenet, Phys. Rev. E **51**, 6127 (1995).

[347] K. Wang, W.-J. Rappel, and H. Levine, Phys. Biol. **1**, 27 (2004).

[348] B. Wang, X. Zhao, J. Wang, H. Guo, W. Baigeng, Z. Xuean, W. Jian, and G. Hong, Appl. Phys. Lett. **74**, 2887 (1999).

[349] J. E. Macías-Díaz and J. E. Mac, Rev. Mex. Fis. **58**, 29 (2012).

[350] Y. Y. Y. Cao and K. W. W. Chung, Int. J. Numer. Anal. Model. Ser. B **3**, 429 (2012).

[351] N. R. Pereira and L. Stenflo, Phys. Fluids **20**, 1733 (1977).

[352] M. V Sataric, R. B. Zakula, S. Zekovic, J. Pokorny, J. Fiala, M. V. Satarić, R. B. Žakula, S. Zeković, J. Pokorny, and J. Fiala, Biosystems **39**, 127 (1996).

[353] M. V. Satarić, J. Pokorny, J. Fiala, R. B. Zakula, and S. Zeković, Bioelectrochemistry Bioenerg. **41**, 53 (1996).

[354] A. D. Cliff and J. . Ord, *Spatial Autocorrelation* (London : Pion, 1973).

[355] L. Anselin, R. J. G. M. Florax, and S. J. Rey, *Advances in Spatial Econometrics, Methodology, Tools and Application. Series: Advances in Spatial Science* (Springer, 2004).

[356] A. D. Cliff and J. K. Ord, *Spatial Processes : Models and Applications* (London : Pion, 1981).

[357] P. A. Jumars, D. Thistle, and M. L. Jones, Oecologia **28**, 109 (1977).

[358] P. A. P. Moran, Biometrika **37**, 17 (1950).

[359] A. F. Zuur, E. N. Ieno, and G. M. Smith, *Statistics for Biology and Health* (Springer, 2007).

[360] J. D. Banfield and A. E. Raftery, Biometrics **49**, 803 (1993).

[361] C. Fraley, A. E. Raftery, Raftery, and E. Adrian, J. Stat. Softw. **18**, 1 (2007).

[362] A. P. A. P. Dempster, N. M. N. M. Laird, and D. B. D. B. Rubin, J. R. Stat. Soc. Ser. B **39**, 1 (1977).

[363] H. Akaike, IEEE Trans. Automat. Contr. **19**, 716 (1974).

[364] G. Schawrz, Ann. Stat. **6**, 461 (1978).

[365] R Core Development Team, (2013).

[366] X. Sun, P. L. Rosin, and R. R. Martin, IEEE Trans. Syst. Man, Cybern. Part B **41**, 749 (2011).

[367] MATLAB, *Version 7.10.0 (R2010a)* (The MathWorks Inc., Natick, Massachusetts, 2010).

[368] A. N. Kolmogorov, G. dell'Istituto Ital. Degli Attuari **4**, 83 (1933).

[369] N. Smirnov, Ann. Math. Stat. **19**, 279 (1948).

[370] B. L. Welch, Biometrika **34**, 28 (1947).

[371] Student, Biometrika **6**, 1 (1908).

[372] F. Wilcoxon, Biometrics Bull. **1**, 80 (1945).

[373] W. J. Conover, M. E. Johnson, and M. M. Johnson, Technometrics **23**, 351 (1981).

[374] M. A. Fligner and T. J. Killeen, J. Am. Stat. Assoc. **71**, 210 (1976).

[375] R. Ndemah, F. Schulthess, S. Korie, C. Borgemeister, P. H.M., C. K, and M.-H. Poehling, Environ. Entomol. **32**, 51 (2003).

[376] K. Levenberg, Q. Appl. Math. **2**, 164 (1944).

[377] D. W. Marquardt, J. Soc. Ind. Appl. Math. **11**, 431 (1963).

[378] K. Pearson, in *Proc. R. Soc. London* (1895), pp. 240–242.

[379] L. G. Shapiro and R. M. Haralick, IEEE Trans. Pattern Anal. Mach. Intell. **3**, 504 (1981).

[380] J. Hoshen and R. Kopelman, Phys. Rev. B **14**, 3438 (1976).

[381] A. Deutsch and S. Dormann, *Cellular Automaton Modeling of Biological Pattern Formation* (Birkhäuser Boston, Boston, MA, 2005).

[382] A. Masetti, A. Butturini, A. Lanzoni, V. De Luigi, and G. Burgio, Agric. For. Entomol. **17**, 138 (2015).

[383] B. a. Mori, C. Yoder, J. Otani, and M. L. Evenden, Agric. For. Entomol. **16**, 207 (2014).

[384] G. Thöming, B. Pölitz, A. Kühne, H. Saucke, G. Th, K. Angela, H. Saucke, G. Thöming, B. Pölitz, A. Kühne, and H. Saucke, Agric. For. Entomol. **13**, 121 (2011).

[385] P. C. Tobin and S. L. Whitmire, Environ. Entomol. **34**, 1448 (2005).

[386] N. . K. Hillier, P. L. L. Dixon, and D. . J. Larson, Environ. Entomol. **32**, 405 (2004).

[387] J. G. J. G. Millar, K. M. K. M. Daane, J. S. S. Mcelfresh, J. a J. A. Moreira, R. Malakar-Kuenen, M. Guillén, and W. J. W. J. Bentley, J. Econ. Entomol. **95**, 706 (2002).

[388] L. B. Coop, R. J. Drapek, B. A. Croft, G. C. Fisher, and G. C. Fishe, J. Econ. Entomol. **85**, 240 (1992).

[389] Z. A. Qureshi and N. Ahmed, J. Appl. Entomol. **112**, 171 (1991).

[390] H. Riedl and B. A. Croft, Can. Entomol. **106**, 525 (1974).

[391] E. H. Mamdani and S. Assilian, Int. J. Man. Mach. Stud. **7**, 1 (1975).

[392] T. Takagi and M. Sugeno, IEEE Trans. Syst. Man. Cybern. **SMC-15**, 116 (1985).

[393] S. Geertman, M. Hagoort, and H. Ottens, Int. J. Geogr. Inf. Sci. **21**, 547 (2007).

[394] J. I. Barredo, M. Kasanko, N. McCormick, and C. Lavalle, Landsc. Urban Plan. **64**, 145 (2003).

[395] T. C. . de Nijs, R. de Niet, and L. Crommentuijn, J. Environ. Manage. **72**, 35 (2004).

[396] C. He, Sci. China Ser. D **48**, 1979 (2005).

[397] D. Stevens, S. Dragicevic, and K. Rothley, Environ. Model. Softw. **22**, 761 (2007).

[398] S.-H. S. Cha, Int. J. Math. Model. Methods Appl. Sci. **18**, 85 (2007).

[399] A. N. D. Posadas, D. Giménez, R. Quiroz, and R. Protz, Soil Sci. Soc. Am. J. **67**, 1361 (2003).

[400] N. R. Draper and H. Smith, *Applied Regression Analysis* (1998).

[401] F. Mesplé, M. Troussellier, C. Casellas, and P. Legendre, Ecol. Modell. **88**, 9 (1996).

[402] S. A. Glantz and B. K. Slinker, *Primer of Applied Regression and Analysis of Variance* (McGraw-Hill, 1990).

[403] R. G. D. Steel and J. H. Torrie, *Principles of Statistics with Special Reference to the Biological Science* (McGraw-Hill, 1960).

[404] P. Damos and M. Savopoulou-Soultani, Psyche A J. Entomol. **2012**, 1 (2012).

[405] G. C. Unnithan and S. O. Paye, J. Appl. Entomol. **109**, 295 (1990).

[406] E. S. Hudes and C. A. Shoemaker, Environ. Entomol. **17**, 97 (1988).

[407] R. Snyder, Agric. For. Meteorol. **35**, 353 (1985).

[408] S. Worner, Environ. Entomol. **21**, 689 (1992).

[409] E. S. Ntiri, P.-A. Calatayud, J. Van den Berg, and B. P. Le Ru, Entomol. Exp. Appl. 1 (2016).

[410] D. Denlinger, Annu. Rev. Entomol. **31**, 239 (1986).

[411] A. Fitter and R. Hay, *Environmental Physiology of Plants*, 3rd ed. (Academic Press, 2002).

[412] S. Flach and A. V. Gorbach, Phys. Rep. **467**, 1 (2008).

[413] S. Flach and K. Kladko, Phys. D Nonlinear Phenom. **127**, 61 (1999).

[414] H. Susanto, P. G. Kevrekidis, R. Carretero-González, B. A. Malomed, and D. J. Frantzeskakis, Phys. Rev. Lett. **99**, 214103 (2007).

[415] G. Kalosakas, S. Aubry, and G. P. Tsironis, Phys. Rev. B **58**, 3094 (1998).

[416] N. K. Voulgarakis and G. P. Tsironis, Phys. Rev. B **63**, 14302 (2000).

[417] Y. B. Gaididei, P. L. Christiansen, and S. . Mingaleev, Phys. Scr. **51**, 289 (1995).

[418] M. M. Latha and S. S. Veni, Phys. Scr. **83**, 35001 (2011).

[419] B. Tan and J. P. Boyd, Phys. Lett. A **240**, 282 (1998).

[420] V. A. Brazhnyi, C. P. Jisha, and A. S. Rodrigues, Phys. Rev. A **87**, 13609 (2013).

[421] A. Trombettoni, A. Smerzi, and A. R. Bishop, Phys. Rev. E **67**, 16607 (2003).

[422] F. Geniet and J. Leon, J. Phys. Condens. Matter **15**, 2933 (2003).

[423] B. Bodo, S. Morfu, P. Marquié, and M. Rossé, Electron. Lett. **46**, 123 (2010).

[424] R. Padinhateeri, A. B. Kolomeisky, and D. Lacoste, Biophys. J. **102**, 1274 (2012).

[425] J. P. Nyrop, M. R. Binns, and W. Van Der Werf, (1999).

[426] L. P. Pedigo, *Entomology and Pest Management*, 3rd ed. (Upper Sadle River, NJ, 1999).

[427] R. Baur, V. Kostal, B. Patrian, and E. Staedler, Entomol. Exp. Appl. **81**, 353 (1996).

[428] T. P. Craig, J. K. Itami, C. Shantz, W. G. Abrahamson, J. D. Horner, and J. V. Craig, Ecol. Entomol. **25**, 7 (2000).

[429] A. T. Groot, A. Heijboer, J. H. Visser, and M. Dicke, J. Appl. Entomol. **127**, 65 (2003).

[430] L. Sigsgaard, Entomol. Exp. Appl. **111**, 215 (2004).

[431] P. J. Landolt, Entomol. Exp. Appl. **67**, 79 (1993).

[432] C. W. Miller, R. J. Fletcher, and S. R. Gillespie, PLoS One **8**, 1 (2013).

[433] C. M. De Moraes, M. C. Mescher, and J. H. Tumlinson, Nature **410**, 577 (2001).

[434] Y. Sato, S. Yano, J. Takabayashi, and N. Ohsaki, Appl. Entomol. Zool. **34**, 333 (1999).

[435] J. N. Thompson and O. Pellmyr, Annu. Rev. Entomol. **36**, 65 (1991).

[436] L. M. Schoonhoven, J. J. A. Van Loon, and M. Dicke, *Insect-Plant Biology*, 3rd ed. (Oxford University Press Inc., New-York, 2005).

[437] J. B. J. Van Rensburg, M. C. Waltersa, and J. H. Giliomee, Bull. Entomol. Res. **77**, 205 (1987).

[438] T. Wiegand and K. K. A. Moloney, *Handbook of Spatial Point-Pattern Analysis in Ecology* (CRC Press, Taylor & Francis Group, 2014).

[439] H. Pritchard, Ann. Bot. **87**, 283 (2001).

[440] M. R. T. Dale, P. Dixon, M.-J. Fortin, P. Legendre, D. E. Myers, and M. S. Rosenberg, Ecography (Cop.). **25**, 558 (2002).

[441] J. N. Perry, A. M. Liebhold, M. S. Rosenberg, J. Dungan, M. Miriti, A. Jakomulska, and S. Citron-Pousty, Ecography (Cop.). **25**, 578 (2002).

[442] G. L. W. Perry, B. P. Miller, and N. J. Enright, Plant Ecol. **187**, 59 (2006).

[443] A. M. Liebhold and J. Gurevitch, Ecography (Cop.). **25**, 553 (2002).

[444] P. Campagne, P. E. Smouse, R. Pasquet, J.-F. Silvain, B. Le Ru, and J. Van den Berg, Evol. Appl. n/a (2015).

[445] K. S. Reddy and P. T. Walker, Insect Sci. Its Appl. **11**, 563 (1990).

[446] S. Savary, P. S. Teng, L. Willocquet, and F. W. Nutter, Annu. Rev. Phytopathol. **44**, 89 (2006).

[447] R. . Ndemah and F. . F. Schulthess, Insect Sci. Its Appl. **22**, 183 (2002).

[448] J. B. J. van Rensburg and J. van den Berg, South African J. Plant Soil **9**, 73 (1992).

[449] J. B. J. van Rensburg, South African J. Plant Soil **18**, 62 (2001).

[450] J. B. J. van Rensburg, M. C. Walters, and J. H. Giliomee, J. Entomol. Soc. South. Afr. **51**, 283 (1988).

[451] V. H. Mgoo, R. H. Makundi, B. Pallangyo, F. Schulthess, N. Jiang, and C. O. Omwega, Ann. La Société Entomol. Fr. **42**, 487 (2006).

[452] J. Pretty, Environ. Dev. Sustain. **1**, 253 (1999).

[453] P. T. Walker, Bull. Entomol. Res. **51**, 321 (1960).

[454] A. M. Shelton and F. R. Badenes-Perez, Annu. Rev. Entomol. **51**, 285 (2006).

[455] A. Y. Bruce, F. Schulthess, and J. Mueke, Environ. Entomol. **38**, 904 (2009).

[456] Y. A. Bruce, F. Schulthess, J. Mueke, and P.-A. Calatayud, BioControl **54**, 763 (2009).

[457] N. K. Maniania, E. Ouna, P. Ahuya, B. Frérot, A.-E. Félix, B. Le Ru, and P.-A. Calatayud, Biol. Control **58**, 374 (2011).

[458] P. R. King, J. S. Andrade, S. V. Buldyrev, N. Dokholyan, Y. Lee, S. Havlin, H. E. E. Stanley, J. S. A. Jr., S. V. Buldyrev, N. Dokholyan, Y. Lee, S. Havlin, and H. E. E. Stanley, Phys. A Stat. Mech. Its Appl. **266**, 107 (1999).

[459] E. J. Garboczi, K. A. Snyder, J. F. Douglas, and M. F. Thorpe, Phys. Rev. E **52**, 819 (1995).

[460] T. H. Keit, D. L. Urban, and B. T. Milne, Ecol. Soc. **1**, (1997).

[461] K. Gutzwiller, *Applying Landscape Ecology in Biological Conservation* (2002).

[462] R. H. Gardner, R. V O'Neill, M. G. Turner, and V. H. Dale, Landsc. Ecol. **3**, 217 (1989).

[463] M. Wheatley and C. Johnson, Ecol. Complex. **6**, 150 (2009).

[464] H. Scherm, Environ. Pollut. **108**, 373 (2000).

[465] D. O. Ferraro, C. M. Ghersa, and G. a Sznaider, Agric. Ecosyst. Environ. **96**, 1 (2003).

[466] M. Kruger, J. B. J. Van Rensburg, and J. Van den Berg, African Entomol. **20**, 35 (2012).

[467] M. Kruger, J. B. J. Van Rensburg, and J. Van den Berg, Crop Prot. **55**, 1 (2014).

[468] R. A. Meyers, editor , *Computational Complexity Theory, Techniques, and Applications* (Springer-Verlag New York, 2012).

[469] F. Jopp, H. Reuter, and B. Breckling, editors , *Modelling Complex Ecological Dynamics* (Springer Berlin Heidelberg, Berlin, Heidelberg, 2011).

[470] Y. Liu, *Modelling Urban Development with Geographical Information Systems and Cellular Automata* (Taylor & Francis Group, 2009).

[471] J. L. Schiff, *Cellular Automata: A Discrete View of the World* (Wiley-Interscience, New-York, 2008).

[472] L. B. Kier, P. G. Seybolg, and C. K. Chen, *Modeling Chemical Systems Using Cellular Automata* (Springer-Verlag, Berlin/Heidelberg, 2005).

[473] S. Maerivoet and B. De Moor, Phys. Rep. **419**, 1 (2005).

[474] T. Toffoli and N. Margolus, *Cellular Automata Machines: A New Environment for Modeling* (MIT Press series in scientific computation, 1988).

[475] R. White and G. Engelen, Environ. Plan. A **28**, 1175 (1993).

[476] M. Gilbert, G. Vouland, and J.-C. Grégoire, Ecol. Entomol. **26**, 133 (2001).

[477] S. Bin Horng, Anim. Behav. **53**, 1 (1997).

[478] S. A. West and P. J. Cunningham, J. Theor. Biol. **214**, 499 (2002).

[479] D. H. Zu, J. Anim. Ecol. **75**, 387 (2006).

[480] M. P. Zalucki, Res. Popul. Ecol. (Kyoto). **25**, 353 (1983).

[481] R. E. Jones, N. Gilbert, M. Guppy, and V. Nealis, J. Anim. Ecol. **49**, 629 (1980).

[482] R. E. Jones, J. Anim. Ecol. **46**, 195 (1977).

[483] A. Berger, Bull. Entomol. Res. **82**, 441 (1992).

[484] A. J. Ngi-Song, S. Kimani-Njogu, and W. A. Overholt, Biocontrol Sci. Technol. **11**, 381 (2001).

[485] a Chabi-Olaye, C. Nolte, F. Schulthess, and C. Borgemeister, Bull. Entomol. Res. **95**, 169 (2005).

[486] M. J. Bonhof, W. a. Overholt, A. Van Huis, and A. Polaszek, Int. J. Trop. Insect Sci. **17**, 19 (1997).

[487] R. Kfir, Bull. Entomol. Res. **85**, 369 (1995).

[488] M. A. Kelly, A. P. Zieba, W. A. Buttemer, and A. J. Hulbert, PLoS One **8**, e73781 (2013).

[489] G. Keil, E. Cummings, and J. P. de Magalhães, Biogerontology **16**, 383 (2015).

[490] J. Régnière, J. Powell, B. Bentz, and V. Nealis, J. Insect Physiol. **58**, 634 (2012).

[491] J. D. Logan, W. Wolesensky, and A. Joern, Ecol. Modell. **196**, 471 (2006).

[492] S. Krishnan and S. Chander, Clim. Change **131**, 259 (2015).

[493] M. Sujithra and S. Chander, Clim. Change **121**, 331 (2013).

[494] G. Reji, S. Chander, and P. K. Aggarwal, Crop Prot. **27**, 1194 (2008).

[495] D. S. Yadav and S. Chander, Crop Prot. **29**, 267 (2010).

[496] D. T. Pham and M. Castellani, Proc. Inst. Mech. Eng. Part C J. Mech. Eng. Sci. **216**, 747 (2002).

Appendix 1: Constants and functions used in the text

$$R_r = \frac{-2\omega_0\omega_c(rC_0 - LB_2)}{\omega_0^2(rC_0 - LB_2)^2 + 4\omega_c^2} \tag{56}$$

$$R_i = \frac{-\omega_0^2(rC_0 - LB_2)^2}{\omega_0^2(rC_0 - LB_2)^2 + 4\omega_c^2}, \tag{57}$$

$$D_r = \frac{-\omega_0(rC_0 - LB_2)}{\omega_0^2(rC_0 - LB_2)^2 + 4\omega_c^2}, \tag{58}$$

$$D_i = \frac{2\omega_c}{\omega_0^2(rC_0 - LB_2)^2 + 4\omega_c^2}, \tag{59}$$

$$\begin{aligned}
\beta_r &= \frac{-3B_1\omega_0(r(rC_0 - LB_2) + 2L\omega_c^2)}{\omega_0^2(rC_0 - LB_2)^2 + 4\omega_c^2}, \\
\beta_i &= \frac{-3B_1\omega_c(L\omega_0^2(rC_0 - LB_2) - 2r)}{\omega_0^2(rC_0 - LB_2)^2 + 4\omega_c^2}. \\
z^2 &= \frac{3D_iR_r + 3D_r\nu}{2D_r\beta_i - 2D_i\beta_r}, \\
p^2 &= \frac{3(D_iR_r + \nu D_r)(D_r\beta_r + D_i\beta_i)}{2(D_r\beta_i - D_i\beta_r)} + \frac{2(D_rR_r - D_i\nu)(D_r\beta_i - D_i\beta_r)}{2(D_r\beta_i - D_i\beta_r)}, \\
q^2 &= \frac{3(D_iR_r + \nu D_r)(D_r\beta_r + D_i\beta_i)}{2(D_r\beta_i - D_i\beta_r)} + \frac{4(D_rR_r - D_i\nu)(D_r\beta_i - D_i\beta_r)}{2(D_r\beta_i - D_i\beta_r)}.
\end{aligned} \tag{60}$$

$$\begin{aligned}
\mathrm{Y} &= \frac{2(rC_0 - LB_2)}{LB_1\omega_c}, \\
\Phi &= \left(\frac{\omega_0(rC_0 - LB_2)}{2\omega_c}\right)^2
\end{aligned} \tag{61}$$

$$R_{E\to L}(T)=117.3314\left(\frac{1}{1+3474.168\exp\left(-0.1303(T-4.5429)\right)}-\exp\left(\frac{-56.7699-(T-4.5429)}{6.2207}\right)\right)$$

$$R_{L\to P}(T)=0.0012\left(\exp\left(0.1163T\right)-\exp\left(0.1163\times 31.2287-\frac{31.2287-T}{1.6537}\right)\right)$$

$$R_{P\to A}(T)=0.0060\left(\exp\left(0.1641T\right)-\exp\left(0.1641\times 33.0391-\frac{33.0391-T}{5.2269}\right)\right)$$

(62)

$$SR(T)=\frac{79.0854}{1+\exp\left(8.1594-0.073T\right)} \tag{63}$$

Appendix 2: Supplementary tables and figures

Mean time ± SEM		
Transition	Plot 4	Plot 5
LD→EH	4.86±0.05	7.00±0.00
DH→D	-	8.93±0.39
LD→DH	4.95±0.10	9.00±0.70
LD→D	-	8.93±0.39

Table S1 Mean time in weeks for transition between infestation types. It is given in the format: mean time ± standard error of the mean (SEM). The symbol (-) means that such transition was not observed.

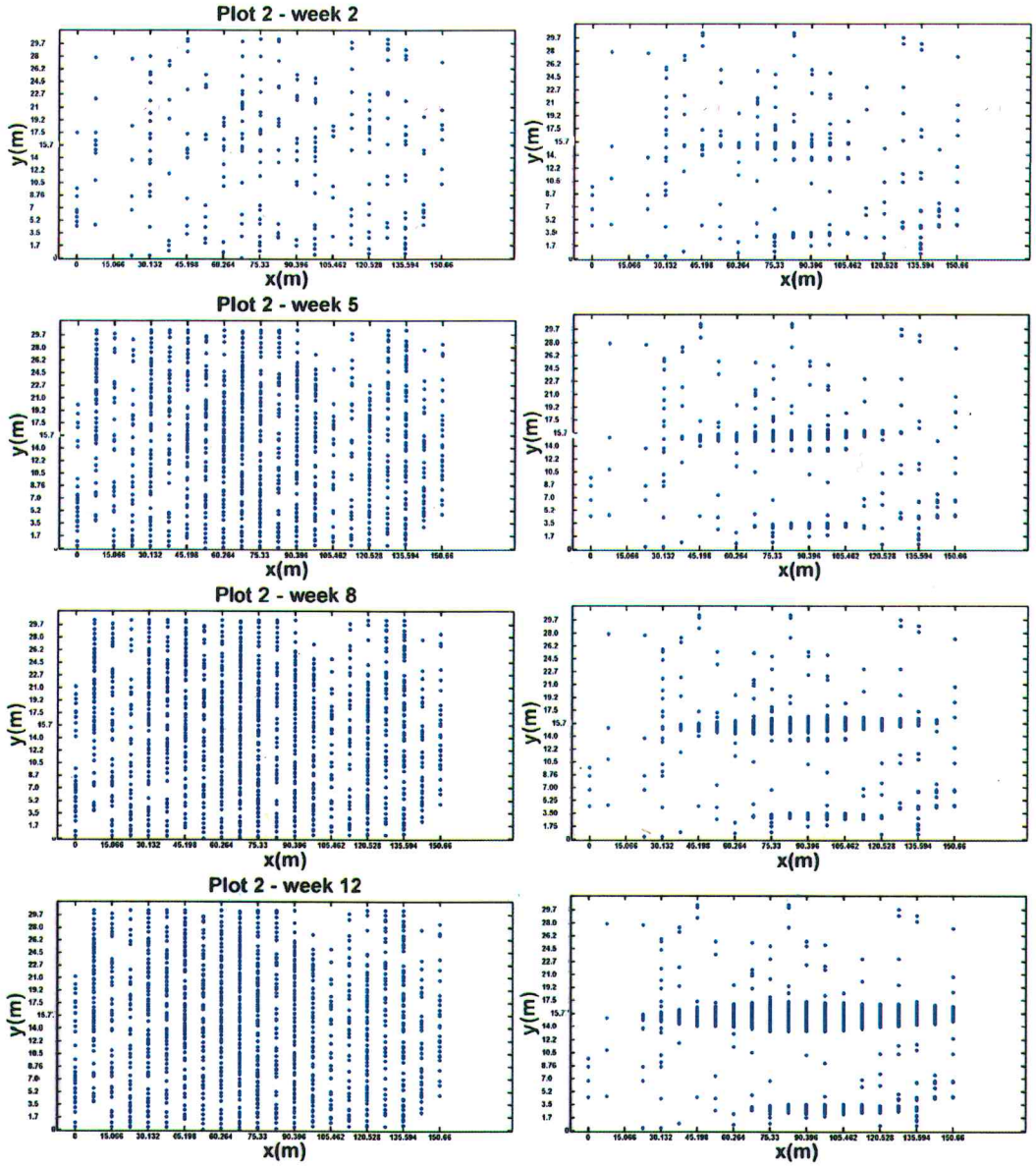

Figure A1: Representation of the spatial and temporal evolution of infested cells in plot 2. On the left are the collected data and at the right the simulated infestations. The blue dots represents the infested cells and the white cells are the non-infested cells

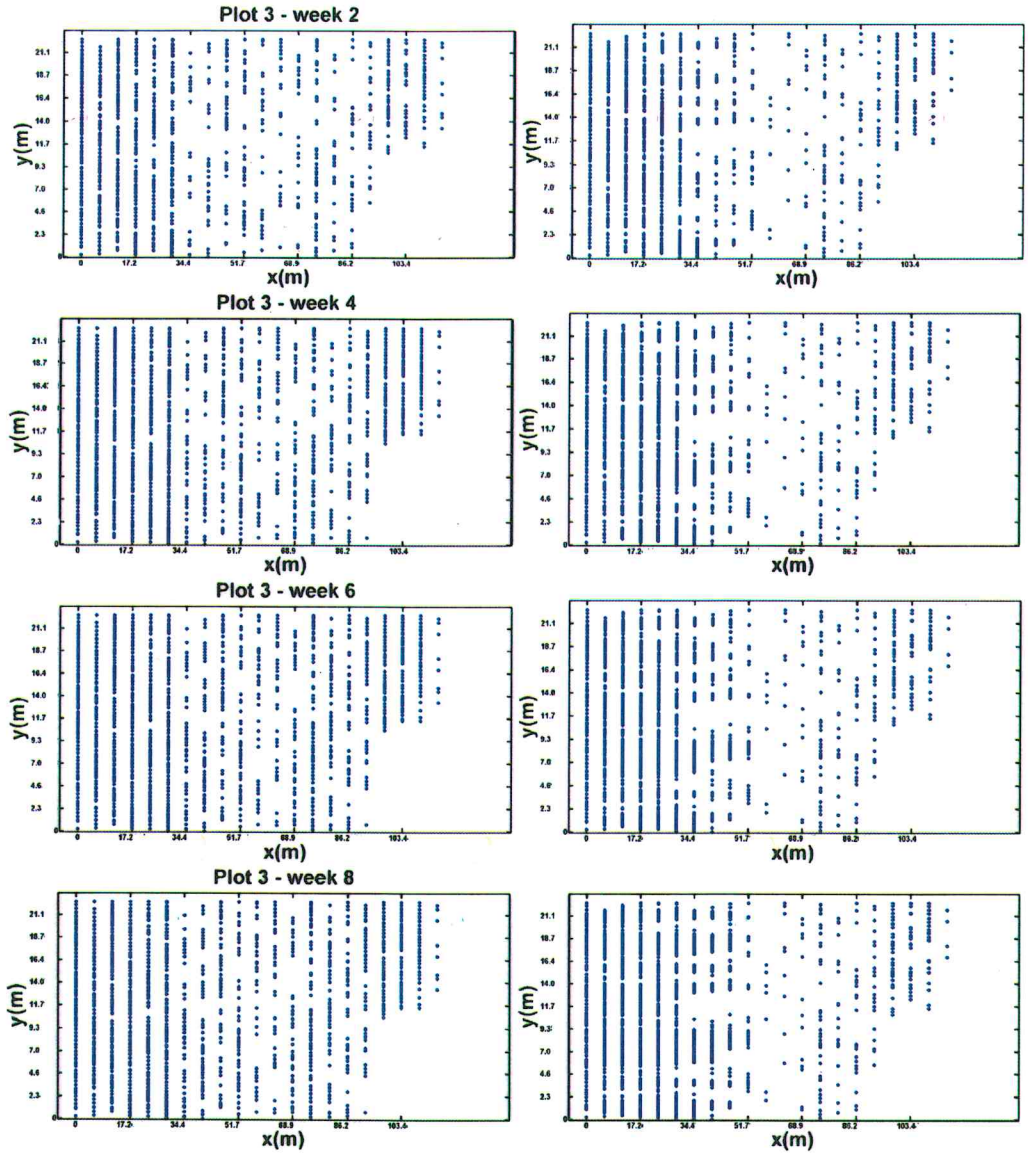

Figure A2: Representation of the spatial and temporal evolution of infested cells in plot 3. On the left are the collected data and at the right the simulated infestations. The blue dots represents the infested cells and the white cells are the non-infested cells.

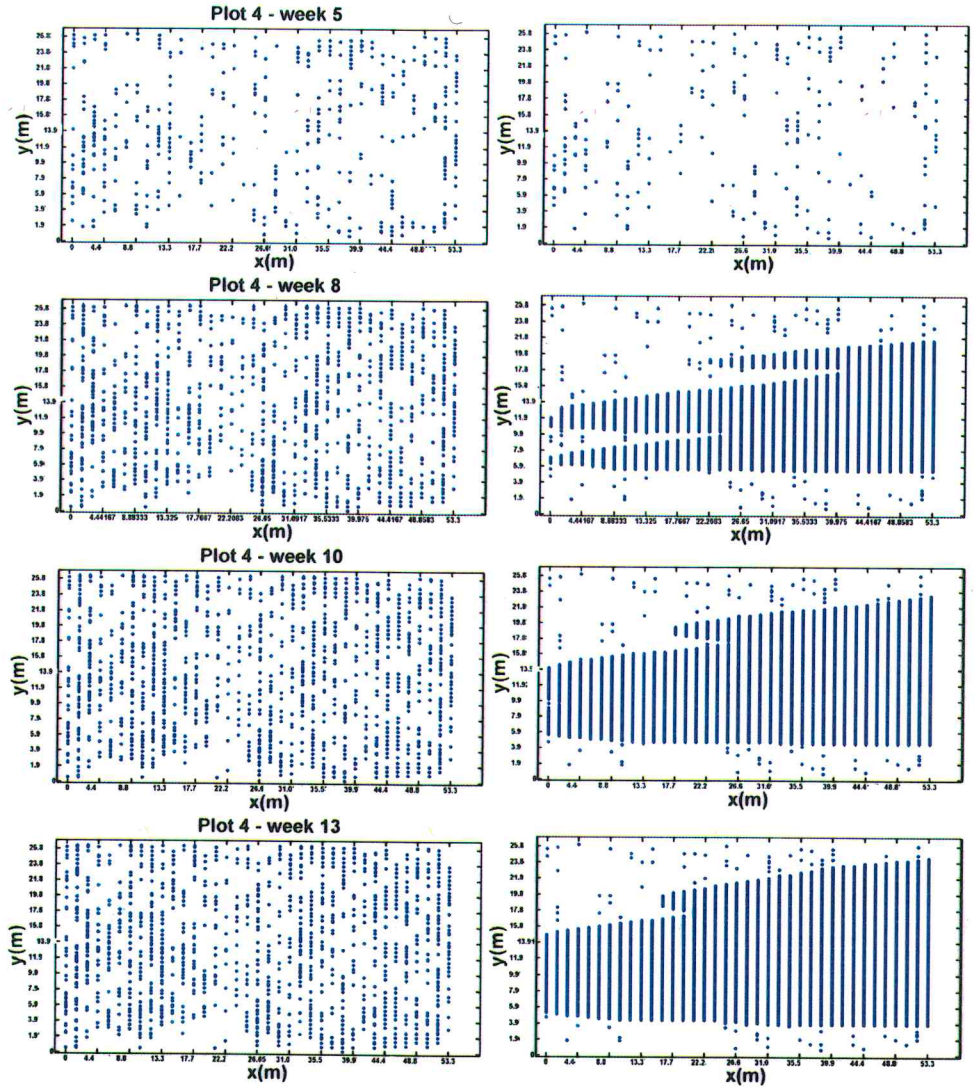

Figure A3: Representation of the spatial and temporal evolution of infested cells in plot 4. On the left are the collected data and at the right the simulated infestations. The blue dots represents the infested cells and the white cells are the non-infested cells

Appendix 3: Fuzzy processing of number of adult

The purpose of this section is to provide a concise explanation on the technicality related to the sub-component of the overall model handling the dynamical change of a neighbourhood. This was done by a fuzzy based representation of the adult number of *B. fusca* collected in pheromone-baited traps (*Na*) and the propagation index (*p*).

To determine the type of function, we referred to the expert knowledge. In the literature, the relationship between the abundance of insect males in pheromones baited traps and the damages incidences are usually linear [382–390]. Thus, piecewise linear functions were selected and used to characterize and classify *B. fusca* adult abundance. The triangular membership function has the analytical forms:

$$\mu^j(x) = \begin{cases} a_1^j & if \quad b_1^j < x, \\ \dfrac{x - b_1^j}{b_2^j - b_1^j} & if \quad b_1^j \le x \le b_2^j, \\ \dfrac{b_3^j - x}{b_3^j - b_2^j} & if \quad b_2^j \le x \le b_3^j, \\ a_2^j & if \quad x > b_3^j. \end{cases} \tag{64}$$

For the number of adults (*Na*) we selected five functions ($\mu^j(Na), j = 1\ to\ 5$) corresponding to five degrees of membership: "Very Small", "Small", "Medium", "Big", and "Very Big" respectively. The Maximal number of insects collected per week in the pheromone baited traps is divided to have four intervals separating the five peaks of the triangular function in Figure 8. The membership functions "Very small", "Medium" and "Very Big" do not overlap because they are considered as extreme cases. It is assumed in the model that the number of adults cannot be "Very Small" and "Medium", or "Medium" and "Very Big" at the same time. Thus, the probability of occurrence for theses combined states cases is null; reason why the overlapping of triangular is at $\mu = 0$. Finally, the parameters $a_i^j\,(i = 1,2)$ and $b_i^j\,(i = 1,2,3)$ of the membership functions are selected to satisfy previously mentioned conditions. The index of propagation p is assumed to belongs to the interval [0 1]; and associated membership functions $\mu^j(p)$ ($j = 1$ ("Low"), 2 ("$Medium$") *or* 3 ("$Strong$")) are assumed to be identical

and symmetrical. Parameters a_i^j and b_i^j for this membership are chosen in order to have three equally partitioned and symmetric functions.

The fuzzy rules are already mentioned in the methodology section. Here we explain how these rules are used to get the final membership function. The Mamdani and Assilian (MA) implication rules developed in the reference [391] have been applied here. The general aspect of the two fuzzy propositions is connected with the IF and THEN syntax:

R^k: IF (Na is j) THEN (p is i),

where k is the rule number ($k = 1\ to\ 5$); $i\ and\ j$ are the membership degrees of Na and p with the associated membership functions $\mu_{NA}^j(x)$, and $\mu_p^i(x)$ respectively. To apply a rule k, a specific value x_0 of Na is selected and $\mu_{NA}^j(x_0)$ is estimated. The resulting membership function $\mu^k(x)$ is obtained by applying the MA implication (*min* operator) [391]:

$$\mu^k(x) = \min[\mu_{NA}^j(x_0), \mu_p^i(x)]. \tag{65}$$

To obtain the final membership all the functions resulting from MA implication at each rule are aggregated. The aggregation has been done here by the max operator [496]:

$$\mu(x) = \max_{k\in[15]}(\mu^k(x)) \tag{66}$$

Once this function is obtained the output is deducted by the central-average-defuzzification formulae [392]:

$$\bar{x} = \frac{\int x \cdot \mu(x)dx}{\int \mu(x)dx} \tag{67}$$

The output of the fuzzy computing ($\bar{p}$) is a positive number that determines the type of Moore neighbourhood. If that number belongs to a certain interval (0-0.25, 0.25-0.75 or 0.75-1) then the corresponding Moore neighbourhood is 1,2 or 3

Appendix 4: Fuzzy processing of plant age

The purpose of this section is to provide a concise explanation on the technicality related to the sub-component of the overall model handling the dynamical change of the coupling between the crop and the pest. The link between the plant maturity and the regulation of the mass accumulation by the larvae.

To determine the type of function, we referred to the expert knowledge. In the literature, the qualitative change of food during the evolution of the age of the maize plant with time which increase the probability of diapauses in the larvae population [318,410]. Thus, piecewise linear functions were selected and used to characterize and classify age of the plant. The triangular membership function has the analytical forms:

$$\mu^j(x) = \begin{cases} a_1^j & if \quad b_1^j < x, \\ \dfrac{x - b_1^j}{b_2^j - b_1^j} & if \quad b_1^j \le x \le b_2^j, \\ \dfrac{b_3^j - x}{b_3^j - b_2^j} & if \quad b_2^j \le x \le b_3^j, \\ a_2^j & if \quad x > b_3^j. \end{cases} \tag{68}$$

For the number of weeks during the plant growth (WK) we selected five functions ($\mu^j(WK), j = 1\ to\ 5$)) corresponding to five degrees of membership: "Very Young", "Young", "Old", "Moderately Old", and "Very Old" respectively. The couple of membership functions "Very Young" - "Old", and "Young" - "Very Old" do not overlap because they are considered as extreme cases; it is assumed in the model that age of the plant cannot have both characteristics at the same time. Thus, the probability of occurrence for theses combined states cases is null; reason why the overlapping of triangular is at $\mu = 0$. Finally, the parameters $a_i^j (i = 1,2)$ and $b_i^j (i = 1,2,3)$ of the membership functions are selected to satisfy previously mentioned conditions. The index (k) representing the regulation of the mass accumulation by the larvae is assumed to belongs to the interval [0 1]; and associated membership functions

$\mu^j(k)$ (j=1 ("Low"), 2 ("Medium") or 3 ("High")) are assumed to be identical and symmetrical. Parameters a_i^j and b_i^j for this membership are chosen in order to have three equally partitioned and symmetric functions.

The fuzzy rules are already mentioned in the methodology section. Here we explain how these rules are used to get the final membership function. The Mamdani and Assilian (MA) implication rules developed in the reference [386] have been applied here. The general aspect of the two fuzzy propositions is connected with the IF and THEN syntax:

R^k: IF (WK is j) THEN (K is i),

where k is the rule number ($k = 1\ to\ 5$); $i\ and\ j$ are the membership degrees of WK and K with the associated membership functions $\mu_{WK}^j(x)$, and $\mu_K^i(x)$ respectively. To apply a rule k, a specific value x_0 of WK is selected and $\mu_{WK}^j(x_0)$ is estimated. The resulting membership function $\mu^l(x)$ is obtained by applying the MA implication (*min* operator) [386]:

$$\mu^l(x) = \min[\mu_{WK}^j(x_0), \mu_K^i(x)] \tag{69}$$

To obtain the final membership all the functions resulting from MA implication at each rule are aggregated. The aggregation has been done here by the max operator [494]:

$$\mu(x) = \max_{l\in[15]}(\mu^l(x)) \tag{70}$$

Once this function is obtained the output is deducted by the central-average-defuzzification formulae [387]:

$$\bar{x} = \frac{\int x \cdot \mu(x)dx}{\int \mu(x)dx} \tag{71}$$

The output of the fuzzy computing ($\bar{k}$) is a positive number that regulate mass accumulation by the larvae.

Appendix 4: List of publications

Appendix 4-1: Publications of this thesis

1. **Frank T. Ndjomatchoua**, Clément Tchawoua, Joël D.T. Tchinang, Bruno P. Le Ru and Henri E.Z. Tonnang (2015). Discrete Davydov's soliton in α-helical protein molecule with anharmonic hydrogen bond and thermal noise. *Communications in Nonlinear Sciences & Numerical Simulations*, vol. 25, 148-160. doi:10.1016/j.cnsns.2015.04.013
2. **Frank T. Ndjomatchoua**, Ndjomatchoua, Clément Tchawoua, Francois M. M. Kakmeni, Bruno P. Le Ru, and Henri E. Z. Tonnang (2016) Waves transmission and amplification in an electrical model of microtubules. *Chaos* Vol. 26, pp 053111-053118 (2016),doi: 10.1063/1.4952573
3. **Frank T. Ndjomatchoua**, Henri E.Z. Tonnang, Christophe Plantamp, Pascal Campagne, Clément Tchawoua, Bruno P. Le Ru (2016) Spatial and temporal spread of maize stem borer *Busseola fusca* (Fuller) (Lepidoptera: Noctuidae) damage in smallholder farms. *Agriculture, Ecosystems and Environment*, Vol. 235, pp 105-118, doi: 10.1016/j.agee.2016.10.01

Appendix 4-2: Others publications

1. Pedro SA, Abelman S, **Ndjomatchoua FT**, Sang R, Tonnang HEZ (2014) Stability, Bifurcation and Chaos Analysis of Vector-Borne Disease Model with Application to Rift Valley Fever. *PLoS ONE* 9(10): e108172. doi:10.1371/journal.pone.0108172
2. Ritter Y. A. Guimapi, Samira A. Mohamed, George O. Okeyo, **Frank T. Ndjomatchoua**, Sunday Ekesi and Henri E. Z. Tonnang (2016) Modeling the risk of invasion and spread of Tuta absoluta in Africa. *Ecological Complexity.* doi: 10.1016/j.ecocom.2016.08.001

Appendix 5: Workshop conferences and oral presentations

1. Octorber 2011: International School of Non-linear Dynamics in Complex Systems organized by International Center of Theoretical Physics (Trieste-Italy) at University of Yaoundé I, Cameroon
2. February 2012: International Conference on Solar Energy; ENSOLE day on the theme: Solar energy for Sustainable development, at University of Yaoundé I, Cameroon
3. May 2015: Training program on the Decision Support System for Agrotechnology Transfer (DSSAT): Assessing crop production, nutrient management, climatic risk and environmental sustainability with simulation models. Stuckey auditorium, Office of continuing education, The University of Georgia, Griffin, Georgia, USA.
4. September 2015: Regional Workshop on Climate Application for Food Security, Niamey, Niger. Organized by AGHYMET (Niamey-Niger) and International Center of Theoretical Physics (Trieste-Italy)
5. May 2016: The International Society for Ecological Modelling (ISEM) Global Conference 2016 from 8th to 12th MAY 2016, at Townson university, Baltimore, Maryland state, USA. First of all, I attended a pre-conference course on Agent-Based Modelling (ABM) the 7th of May 2016, and, I presented part of my Ph.D. study titled: Modelling plant damages spread induced by lepidopteran stem borer on maize farm. This presentation will be done during the general session of Tuesday, 10th May 2016. I have been granted two years membership in the ISEM.

Appendix 5: First pages of publications